PONTIFICIA UNIVERSIDAD CATOLICA DE CHILE
SCHOOL OF ENGINEERING

COPING WITH UNERTAINTY IN CLIMATE CHANGE: MERGING GENERAL CIRCULATION MODELS AND LOCAL CLIMATE TO SIMULATE THE FUTURE PERFORMANCE OF A RESERVOIR SYSTEM

CRISTIÁN CHADWICK

Thesis submitted to the Office of Graduate
Studies in partial fulfillment of the requirements
for the Doctor in Engineering Sciences

Advisor:
Jorge Gironás

Santiago de Chile, September, 2018

PONTIFICIA UNIVERSIDAD CATOLICA DE CHILE

SCHOOL OF ENGINEERING

COPING WITH UNERTAINTY IN CLIMATE CHANGE: MERGING GENERAL CIRCULATION MODELS AND LOCAL CLIMATE TO SIMULATE THE FUTURE PERFORMANCE OF A RESERVOIR SYSTEM

CRISTIÁN CHADWICK

Members of the Committee:

Jorge Gironás

Sebastián Vicuña

Francisco Meza

James McPhee

Amin Elshorbagy

Gustavo Lagos

Thesis submitted to the Office of Graduate Studies in partial fulfillment of the requirements for the Doctor in Engineering Sciences

Santiago de Chile, September, 2018

To my family who has always supported me.

ACKNOWLEGMENT

This research is the result of research projects Fondecyt Grant 1171133 and International Development Research Center (IDRC) Grant 107081-001. I also thank the support from grants CONICYT/FONDAP/15110017 and 15110020 (CIGIDEN and CEDEUS, respectively). Scholarships from CONICYT (21160861), Canada-Chile Leadership Exchange program, which allowed me to work in Saskatchewan University during 2014, Sociedad de Canal del Maipo and Vice-rectoría de Investigación at Universidad Católica de Chile are also acknowledged. I want to thank both the World Climate Research Programme's Working Group on Coupled Modelling, which is responsible for CMIP, and the climate modeling groups (Appendix D) for making available their model outputs. Chilean meteorological data for this study are publicly available from the Dirección General de Aguas, Chile (http://snia.dga.cl/BNAConsultas/reportes).

I want to thank the Centro de Cambio Global UC (CCG-UC) and their members for their support. I would also like to acknowledge the Departamento de Ingeniería Hidráulica of the Pontificia Universidad Católica de Chile, to all the staff, professors and students, for their help and companionship throughout these years. I would like to kindly acknowledge my advisor, Dr. Jorge Gironás, who has taught me so many things during the last years and with whom I expect to continue working in the future. I finally thank the members of the committee for their constructive suggestions and their participation throughout the thesis.

GENERAL INDEX

Page

LIST OF TABLES

Page

LIST OF FIGURES

Page

RESUMEN .

La simulación de variables hidro-climáticas y su impacto futuro implica usar Modelos de Circulación General (GCM) bajo distintos escenarios de gases de efecto invernadero o RCP (Representative Concentration Pathways). Cuantificar y tratar formalmente la incertidumbre asociada a estos modelos y escenarios es clave en estudios de impacto y adaptación al cambio climático. Este trabajo propone metodologías para enfrentar esta incertidumbre, particularmente en el análisis del desempeño de embalses, por medio de la transferencia de los estadísticos de los GCM al clima local. Inicialmente se demuestra la contribución relevante de los GCM y sus realizaciones a la incertidumbre total. Luego se propone un tratamiento de los GCM mediante la fusión de ensambles de estos y el clima local para generar series de clima estadísticamente compatibles con las proyecciones globales. La metodología es aplicada en tres cuencas Chilenas (Limarí, Maipo y Maule) simplificando el correcto tratamiento de los GCM y la generación de climas futuros asociados a probabilidades de ocurrencia para la modelación hidrológica. Esta metodología se utiliza para identificar el tiempo de emergencia (ToE) en el que el cambio en precipitaciones y temperaturas en estas cuencas aparece significativamente. Finalmente se evalúa una meta cambiante de entrega de agua como estrategia de adaptación del sistema de embalses Paloma (Limarí). Junto con las metodologías de generación de clima e identificación del ToE, otros resultados relevantes son: (1) sólo 5 percentiles de tendencia del ensamble de GCM replican las estadísticas obtenidas a partir de series individuales de clima para cada GCM; (2) el ToE ocurre antes del 2030 para las tres cuencas bajo escenarios RCP 6.0 y 8.5, siendo el Maule donde las precipitaciones futuras cambian mayormente; y (3) la reducción progresiva del agua distribuida por el sistema Paloma mantiene constante el número de fallas, pero reduce fuertemente la disponibilidad de agua.

Palabras Claves: cambio climático, incertidumbre, GCM, riego, precipitaciones y temperaturas, tiempo de emergencia, confiabilidad, resiliencia, vulnerabilidad, operación de embalses, estrategias de adaptación, tendencias futuras.

ABSRTACT .

Simulating hydro-climatic variables and their future impacts, require using General Circulation Models (GCMs) under different greenhouse-gases concentration scenarios, called RCP (Representative Concentration Pathways). Quantifying and explicitly coping with GCM and RCP uncertainty is a key issue in climate change impacts and adaptation studies. This work proposes methodologies to cope with these uncertainties, particularly in the reservoir performance, through merging the statistical attributes of GCM to local climate. First, the work shows the relevance of the uncertainty of the GCM and their realization to the overall uncertainty. This is followed by the proposal of a method that builds a GCM ensemble by merging their statistical attributes to local climate to generate climate time series that preserve both local and global statistics. The method is applied in three Chilean basins (Limarí, Maipo and Maule), and simplifies the GCM treatment to generate future climate associated with a certain probability of occurrence that can be used for hydrological modeling. This method is applied to identify significant changes in the Time of Emergence (ToE) of precipitation and temperature. Finally, a progressively changing water allocation goal is evaluated as an adaptation strategy to climate change for the Paloma reservoir system (Limarí). In addition to the methods for generating climate series and identify the ToE, other relevant results are: (1) only five trend percentiles are enough in the GCM ensemble to properly replicate the statistical attributes of using each GCM individually; (2) ToE is expected to happen before 2030 for the three basins under RCP 6.0 and 8.5, being the Maule basin the one that presents the earliest changes in precipitation; and (3) the progressive water allocation goal is able to maintain the number of failures of the Paloma system constant in time, but it has a big impact over the overall water allocation amount.

Keywords: climate change, uncertainty, GCM, risk, precipitation and temperature, time of emergence, reliability, resilience, vulnerability, reservoir operation, adaptation strategy, future trends.

1. CHAPTER 1: GENERAL INTRODUCTION

In water management practice decision makers used to assume stationarity to cope with uncertainty (Bras et al., 1983; Datta and Burgos, 1984; Datta and Houck, 1984). In recent years the stationarity assumption has been strongly questioned (Milly et al., 2008; Milly et al., 2015), as climate change is affecting the stationary behavior of hydro-climatic variables. Under a non-stationary future scenario, General Circulation Models (GCMs) are used to simulate future climate, information commonly used in studies to assess the impacts of climate change and provide the scientific basis for decision making. Several studies have focused on detecting and quantifying climate variability and changes in precipitation and temperature under future scenarios, and its potential effects over water resources and water infrastructure (e.g. Adeloye et al., 1999; Fowler et al., 2005; Giorgi and Bi, 2009; Mahlstein et al., 2011; Matonse et al., 2013; Mondal and Wasimi, 2007; Mondal et al., 2010).

Water systems are strongly dependent on the infrastructure, being water reservoir systems one of the key elements. In particular, several studies have evaluated the effects of climate change on reservoirs in general (Lettenmaier et al., 1999, Fowler et al., 2003, Steinschneider and Brown, 2012, Adeloye et al., 2016, Soundharajan et al., 2016) and their performance in particular (Steinschneider and Brown, 2012, Adeloye et al., 2016, Soundharajan et al., 2016). Vicuña et al. (2010) developed a reservoir operation rule that dynamically adapts trough time to changes in climate, whereas Adeloye et al. (2016) studied reservoir operation rules under a constant change, by using the delta change approach (Hay et al., 2000; Diaz-Nieto and Wilby, 2005; Minville et al., 2008). Nonetheless, to the best of our knowledge, a dynamical

adaptation in water allocation to climate change has not been addressed considering an uncertainty assessment using a special treatment that incorporates several GCMs and the four RCPs, as it would be required for a robust result (Chadwick et al., 2018a).

Climate change impact studies have several problems associated with the uncertainty, which according to the concept of *cascade of uncertainty* (Wilby and Dessai, 2010) increases as one moves from the definition of future greenhouse gas concentration (i.e. the Representative Concentration Pathway, RCP) up to the assessment of the impacts on the water or environmental system of interest produced by changes in the local climate. The first problem is that some studies do not consider or misunderstand the uncertainty of the processes; as Blöschl and Montanari (2010) argued, climate change impact studies tend to be too optimistic about their predictions. Important aspects are usually neglected, such as the uncertainty related to changes in climate variables and the differences in the strength of the emergence of temperature and precipitation. In fact, the changes in temperature emerge more clearly than for precipitation (Hawkins and Sutton, 2011). A second problem is that the bias correction or statistical downscaling methods to disaggregate locally the outputs of GCMs may lack of strong conceptual support, as they are mostly used to fulfill a specific need (Ehret et al., 2012). Moreover, even Regional Circulation Models (RCMs) are apparently not good enough to correctly simulate local conditions without bias correction (Teutschbein and Seibert, 2010). Thus, when a study focuses on the hydrological impacts, a large range of climate change projections obtained using several GCMs and downscaling methods is fundamental to investigate the spectrum of uncertainty (Chen et al., 2011). A final problem is that the uncertainty of the hydrological model used to simulate hydrological variables is also relevant, especially

when calibrated for certain climate conditions, but used for different ones under climate change (Merz et al., 2011). Overall, the assessment of the contribution to the uncertainty coming from the GCMs and their realization, as well as the RCP scenarios is not clear. Moreover, the local climate plays a significant role as it may hinder and affect not only the assessment of the uncertainty, but also the clear identification of the occurrence of climate change at the basin scale. Hence, identifying the time of emerge (i.e. the time at which climate change signal can be clearly identified from the climate noise) (Hawkins and Sutton, 2012) at the basin scale, and therefore, dependent of the local conditions, becomes an appealing idea that deserves to be explored. Such task has rarely been undertaken before, and only for the US (University of Washington, 2015; Leng et al. 2016).

Based on the background previously described, the following hypotheses are proposed for this research:

- The uncertainty induced by the GCMs and their realizations significantly alters the results of a climate change impact study.
- It is possible to generate climate with stochastic methods that preserves both the GCM and local precipitation and temperature statistics.
- It is possible to identify at a basin scale the time at which the climate change emerges, by using GCM projections and local climate statistics.
- A dynamic water allocation strategy yields better results in terms of maintaining a constant reliability than a single allocation objective in a dry basin under climate change.

The overarching objective of this study is to generate tools able to cope with the uncertainty on the different steps of a climate change impact study, which take into

consideration explicitly a wide range of GCMs and their realizations, as well as the local climate records. To address this objective, the following specific objectives have been defined according to the hypothesis abovementioned:

1. To analyze and understand the impact of climate change-induced uncertainty on the operation of large reservoirs, in order to assess and quantify the relative contribution of the GCM's, their realizations and RCP scenarios to this uncertainty.
2. To develop a GCM downscaling approach more suitable to cope with GCM uncertainty when dealing with climate change studies at the basin scale.
3. To propose a methodology to estimate time of emergence at local sclaes, considering GCMs outputs and local climatic conditions explicitly.
4. To evaluate the impact of progressive changes in climate over reservoir performance measured by using performance indexes, and possible adaptation strategies.

This document is organized in four main chapters, each corresponding to a self-contained investigation addressing the above highlighted objectives. The organization of this work is as follows:

Chapter 2 analyses the impact of choosing different GCM projections over the performance in the operation of a reservoir system, and the uncertainty associated with the GCMs and the RCPs. The Paloma reservoir system located in the Limarí river basin, a semiarid Mediterranean basin in central Chile, is used as a case study. The methodology uses several GCM projections and a quantile mapping bias correction (Wood et al., 2002; 2004; VanRheenen et al., 2004; Maurer, 2007; Maurer et al., 2009) as a downscaling method. The Water Evaluation and Planning (WEAP) system (Yates

et al., 2005a; b) was utilized to simulate the hydrology of the basin. Finally, the performance indexes proposed by Hashimoto et al. (1982) are used to measure the performance of the reservoir system.

Chapter 3 proposes a method more suitable to cope with GCM uncertainty when dealing with climate change studies. The method generates climate series by merging within a statistical framework the changes in precipitation and temperature from a group GCM and local climate statistics. The changes of annual precipitation and temperature obtained from the GCMs are statistically treated to produce trend percentiles, which are combined with local climate to generate climate time series that incorporate both the climate information from the CGM group as well as the local statistics. This methodology is evaluated against traditional downscaling and bias correction approaches, such as delta change, quantile mapping bias correction and the use of a subset of GCMs. The method is also compared against using individually each of the precipitation and temperature series, which are constructed by combining the local climate statistics with each individual GCM. In particular it is verified whether the proposed method reproduces the statistical attributes obtained from the post analysis of these series.

Chapter 4 proposes a methodology to identify, at a local scale, the time at which the climate change signal emerges from the climate noise, also known as Time of Emergence (ToE). ToE is commonly studied at large scales (Sui et al., 2014) or for the whole planet (Giorgi and Bi, 2009; Hawkins and Sutton, 2012). The methodology is implemented in three river basins in central Chile, and considers the method developed in Chapter 4 to generate future climate (precipitation and temperature) associated with different trend percentiles. These climate series are compared against series generated

to replicate the historical local climate, and the ToE is defined to be the time at which both sets of data are statistically different, using the statistical power of a Kolmogorov-Smirnov hypothesis test to assess the probability of certainty of this identification (i.e. the probability of being correct when accepting that the climate has statistically changed). As the trend percentiles from Chapter 3 are used, the power for different percentiles among a GCM group can be determined.

Chapter 5 evaluates through time different water allocation goal strategies for climate change adaptation. Just as in Chapter 2, the Paloma reservoir system in the Limarí river basin is used as case study, while the indexes proposed by Hashimoto et al. (1982) are considered in the performance assessment. However, in this Chapter the downscaling is done using the method developed in Chapter 3. Three alternative goals for the operation of the reservoir system are tested: (1) the current reservoir operation rule proposed by Ferrer et al. (1978), (2) a constant reduction of the water allocation goal, and (3) a progressive reduction of the water allocation goal. Particularly, alternatives (2) and (3) are designed to maintain the stationary historical reservoir reliability of the Paloma System.

This document closes with a summary, which highlights the most relevant conclusions of this work and proposes future research recommendations.

2. CHAPTER 2: ASSESSING THE ROLE OF GCM AND RCP SOURCES OF UNCERTAINTY IN THE PERFORMANCE OF CURRENT RESERVOIR OPERATION IN SEMIARID CHILE

2.1. INTRODUCTION

Different approaches are used to study optimal reservoir operation policies, such as linear programming (e.g. Yoo, 2009), nonlinear programming (e.g. Sinha et al., 1999) or dynamic programming (e.g. Stedinger et al., 1984). Typically, short and long-term horizons (Datta and Burges, 1984) are identified in reservoir operation policies. Commonly, stationarity is assumed for the long-term horizon; however, estimations of the inflows and demands are uncertain, particularly under the context of global change, and the effect of this uncertainty on the reservoir's performance is difficult to characterize. This is relevant, as the cost associated with inaccurate forecasting can be similar to the savings due to accurate forecasting (Datta and Burges, 1984).

Reservoir performance is typically evaluated using indexes, with reliability, resiliency and vulnerability (RRV) (Hashimoto et al., 1982) being widely used (Moy et al., 1986; Fowler, 2003; 2007; Goharian et al., 2017; Zhang et al., 2017; Alameddine et al., 2018). These indexes allow for quantitative comparison among different operation options, and describe water resource systems better than other metrics (e.g. mean, standard deviation), which often incompletely describe the system under failur (Hashimoto et al., 1982). The RRV approach is multivariate, although tradeoffs have been identified among these indexes (Moy et al., 1986; Bayazit and Ünal, 1990; Srinivasan and Philipose, 1996; 1998; Zhang et al., 2017). For example, short or

moderate failures instead of long or deep deficits are commonly preferred due the tradeoff between vulnerability and reliability (Hashimoto et al., 1982; Srinivasan and Philipose, 1996; 1998; Draper and Lund, 2004). This practice in reservoir operation is known as hedging (Srinivasan and Philipose, 1998).

Several studies have focused on quantifying climate variability and trends in precipitation and temperature under future scenarios, and their potential effects over water resources (e.g. Fowler et al., 2005; Mondal et al., 2010; Walton et al., 2017; Shi et al., 2018; Smitha et al., 2018). Other studies have assessed the impacts of these changes on water management systems and infrastructure (e.g. Fowler et al., 2007; Kim and Kaluarachchi, 2009). Climate change impact studies have several uncertainty problems. For example, temperature and precipitation changes are frequently treated equally, despite the fact that temperature trends emerge more clearly than precipitations' (Hawkins and Sutton, 2011), or that precipitation changes could even be considered as random processes (Sun et al., 2011). Second, the bias correction and statistical downscaling methods used over the General Circulation Models (GCMs) outputs for hydrological studies, may lack strong conceptual support (Ehret et al., 2012). Moreover, even Regional Circulation Models (RCMs) lack the skill to correctly simulate local hydrology without bias correction (Teutschbein and Seibert, 2010). Thus, when a study focuses on the hydrological impacts, a large range of projections obtained using several GCMs and downscaling methods is fundamental to investigate the spectrum of uncertainty (Chen et al., 2011). Third, the uncertainty of the variable(s) used to build hydrological models are also relevant but usually neglected, especially when calibrated and then used in different climate conditions (Merz et al., 2011).

Uncertainty has been incorporated in climate change studies in very different manners. The first studies did not perform uncertainty analysis (e.g. Fowler et al., 2003), nonetheless they acknowledged this limitation and recommended using future climate projections from different GCMs and ensemble members to estimate uncertainty. The consideration of just some GCMs is common as a result of the modeler's choice or to the fact that some specific GCMs have been identified locally to be suitable for climate change studies (Fowler et al., 2005). For example, Samadi et al. (2013) only used HadCM3 GCM with the A2 emission scenario, because they determined it to be the most appropriate GCM for the study area. Yung et al. (2011) adopted the most critical climate change scenarios, by using the largest reduction in precipitation and highest temperature increase. Buser et al. (2009) used four RCMs and one high resolution GCM with the A2 emission scenario, limiting the study to these five uncorrelated models because of the availability of GCMs with fine grids. In a more comprehensive study, Schaefli et al. (2007) studied the hydropower generation in the Swiss Alps under climate change using 19 RCMs. Nevertheless, uncertainty is usually quantified in terms of precipitation (Ouyang et al., 2014) or streamflow at most (Chen et al., 2011). Some studies have broadly analyzed different sources of uncertainty under climate change, by measuring reservoir operation's performance (Brekke et al., 2009; Georgakakos et al., 2012; Steinschneider et al., 2015a; 2015b; Whateley and Brown, 2016). Moreover, some studies recently evaluated the uncertainty of climate change on the reservoir performance using RRV indexes (Steinschneider and Brown, 2012; Adeloye et al., 2016; Schlef et al., 2017; Soundharajan et al., 2016). However, the following questions related to the impacts over reservoirs have not been fully addressed: (1) What is the relationship between

changes in climate and the performance of a current operation rule measured by RRV indexes? (2) Where does the greatest source of uncertainty come from: intra-GCMs (i.e. several realizations of the same GCM), inter-GCMs (i.e. across GCMs) or the Representative Concentration Pathways (RCPs)?

The objective of this chapter is to analyze and understand the impact of climate change-induced uncertainty on the operation performance of large reservoirs measured by RRV indexes, to assess and quantify the relative contribution of the GCMs and climate change scenarios to this uncertainty. The case study focuses on the long-term performance of a reservoir system under its current operation rule in the Limarí basin, Chile. Using a wide range of climate change scenarios, we analyze the range of RRV indexes performance, produced by the intra-GCM, inter-GCM and RCP.

2.2. THE LIMARÍ RIVER BASIN AND THE PALOMA RESERVOIR SYSTEM

The Limarí River basin is a snow dominated catchment with an area of 11,800 km^2 in north central Chile, whose outlet is located at 30º43’51’’S, 71º42’01’’W. It is a semi-arid basin with large spatial variation in precipitation, increasing from the Pacific coast to the Andes, and from north to south, with annual average between 100 and 300 mm. Precipitation occurs mostly during autumn and winter (May to August), and snow accumulates in the upper basin. The precipitation inter-annual variability is also high (i.e. coefficient of variation of 0.65 - 0.75 for different gauges) with a strong signal coming from the El Niño Southern Oscillation (ENSO) phenomenon (Montecinos and Aceituno, 2003). Streamflow is mostly produced by snow melt during spring and summer seasons (September to January). Hydro-meteorological

records for the basin are available from the Dirección General de Aguas (DGA, http://snia.dga.cl/BNAConsultas/reportes), the Chilean Water Agency. The streamflow gauges considered are listed in Table 2-1.

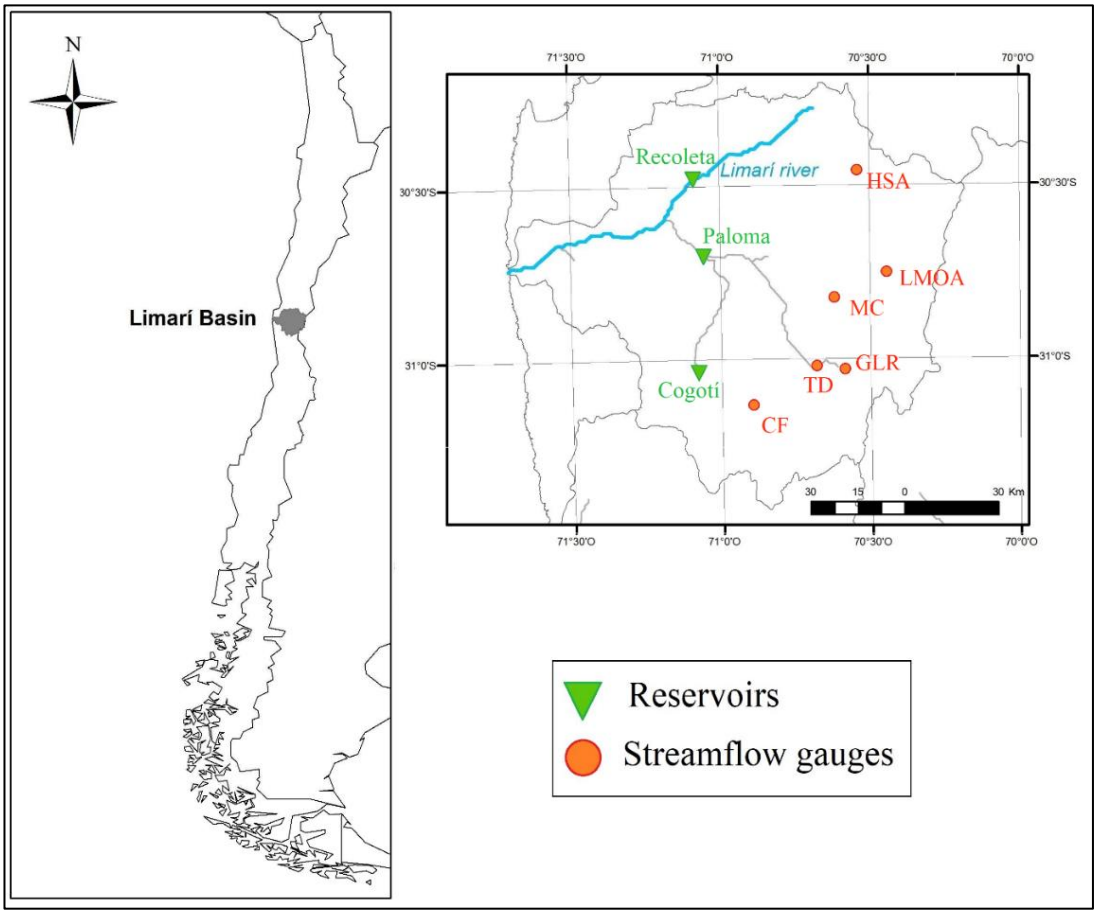

Figure 2-1: Map of the Limarí river basins and its location in Chile.

The Paloma reservoir system located in the basin supplies water to ~50,000 ha of irrigated land and drinking water to Ovalle city (110,000 inhabitants). The system is composed by the Paloma, Cogotí, and Recoleta reservoirs, whose capacities are 750, 150, and 100 Mm^3, respectively (Fig. 2-1). This capacity largely exceeds the average annual system inflow (i.e. 400 Mm^3), which allows coping with the inter-annual variability (Vicuña et al., 2012). The intra-annual streamflow variability is naturally regulated by snow accumulation and melting. Because future spring and summer flows

are expected to occur earlier in the season due to climate change (Vicuña et al., 2011; 2012), the reservoir system should participate more actively in regulating future flows.

Table 2-1: Streamflow gauges in the Limarí basin.

Station	Subcatchment	Area (km^2)	Years of record	Elevation (m)	Latitude	Longitude
San Agustín (HSA)	Hurtado	656	1969-2011	2,035	30º 27' 44" S	70º 32' 10" W
Ojos de agua (LMOA)	Los Molles	144	1969-2011	2,355	30º 44' 37" S	70º 26' 20" W
Cuestecita (MC)	Mostazal	353	1969-2011	1,250	30º 48' 46" S	70º 36' 46" W
Las Ramadas (GLR)	Grande	544	1969-2011	1,380	31º 00' 42" S	70º 34' 52" W
Desembocadura (TD)	Tascadero	238	1969-2011	1,370	31º 00' 43" S	70º 39' 52" W
Fragüita (CF)	Cogotí	475	1969-2011	1,065	31º 06' 43" S	70º 53' 06" W

The current operation rule of the system was developed by Ferrer et al. (1978), who used precipitation and streamflow data from 1944 to 1976 to simulate the inter-annual variability and various allocation scenarios. They estimated volumes of 138 and 220 Mm^3 for the 3- and 4-year moving average of the annual inflows to the system with 85% exceedance probability, and concluded that a wet year is expected to follow three dry years. Hence, a period of three years was considered critical for the long-term horizon operation of the reservoir system, leading to a single annual allocation decision (Ferrer et al., 1978). This operation rule has been valid for the last 40 years, and is consistent with Chilean water rights law, according to which annual water allocations can be given by DGA up to the volume with an 85% exceedance probability (DGA, 2008).

More formally the system operation is expressed as follows. The stored volume S (m^3) in reservoir j at the beginning of year t+1 is:

$$S_j^{t+1} = S_j^t - O_j^t + I_j^t - E_j^t - Sp_j^t \quad (2.1)$$

where *O*, *I* and *Sp* are the outflow, inflow and spilled water, respectively (m^3), and *E* is the net evaporation from the reservoir (m^3):

$$E_j^t = A_j^t \cdot \left(e_j^t - P_j^t\right) \quad (2.2)$$

where *e* is the evaporation (m), *P* is the precipitation (m), and *A* is the surface area (m^2), which is related to the water stored. *S* is restricted to the range defined by the reservoir maximum storage capacity MS (m^3) and the dead storage DS (m^3):

$$DS_j \leq S_j^t \leq MS_j \quad (2.3)$$

The water allocated in year *t*+1 (O_j^{t+1}) is a function of the stored water in the system composed of *M* reservoirs at year *t* ($S_T^t = \sum_{j=1}^{M} S_j^t$). If S_T^t overpasses a threshold or restrain bound (*RB*), a fixed amount α_j is allocated from reservoir *j*. Otherwise, the allocated water is a fraction *r* of the storage.

$$O_j^t = \begin{cases} \alpha_j & \text{if } S_T^t \geq RB \\ r \cdot S_j^t & \text{if } DS_j \leq S_T^t < RB \\ 0 & \text{if } 0 \leq S_T^t < DS_j \end{cases} \quad (2.4)$$

Ferrer et al. (1978) determined values of α = 240, 40 and 40 Mm^3 for the Paloma, Recoleta and Cogotí reservoirs respectively, as well as values of *RB* = 500 Mm^3 and *r* = 0.5. Thus, if the system storage exceeds 500 Mm^3, the maximum allowed annual water allocation is 320 Mm^3. Otherwise; half of the stored water is allocated.

2.3. METHODOLOGY

Several methods and tools were used to link climate, hydrology and the reservoir system and its performance. First, an already developed hydrological

climate-driven model implemented in the Water Evaluation and Planning (WEAP) system (Yates et al., 2005a; b) was calibrated using historical monthly runoff data. Then, precipitation and temperature data for the period 2011-2100 from 49 runs of GCMs (Appendix A) and the four RCPs (i.e. 149 climate projections) were downscaled to be used as input for the WEAP model to simulate streamflow series. Finally, the performance of the reservoirs' system under this set of streamflow scenarios was characterized through performance indexes. Details of these steps are presented in the subsections below.

2.3.1. HYDROLOGICAL MODELING

WEAP uses climate information as input to generate streamflow following a semi-distributed approach. In the model, elevation bands were used as hydrological units where climate, soil, topography and land use characteristics are specified. A WEAP model already set up for the Limarí Basin by Vicuña et al. (2011; 2012) was re-calibrated and used in this study. The re-calibration used the most recent years (1985 – 2011), leaving the period 1969-1984 for validation. This approach allows obtaining calibration parameter values closer in time to future climate projections, to avoid errors caused by a large lag time between the calibration and simulation periods (Merz et al., 2011). Overall, the simulated and observed hydrographs are similar, and satisfactory Nash-Sutcliffe efficiency (NSE) coefficient values (Nash and Sutcliffe, 1970) were obtained for the different streamflow gauges (Table 2-2); furthermore, observed and simulated average annual flows are very similar for the calibration period. The model tends to underestimate the annual flow for the validation period, while the coefficient of variation (CV) is underestimated for the entire period. When comparing the

validation and calibration periods, the NSE value improves for the San Agustín and Ojos de Agua gauges, is maintained for Cuestecita gauge and decreases for Las Ramadas, Desembocadura and Fragüita gauges (Table 2-2). The poorest performance of the model corresponds to San Agustin gauge (Fig. 2-2), which receives contributions from the highest elevations in the basin (> 5,000 m) where reliable meteorological measurements are scarce. Nonetheless, even at this gauge low flows (i.e. the most relevant flows for the long-term simulation of the basin) are well simulated. Moreover, the main tributaries contributing to the system (i.e. Las Ramadas, Fragüita and Cuestecita) are well simulated, and explain most of the inflows to Cogotí and Paloma reservoirs, which represent 90% of the system storage volume.

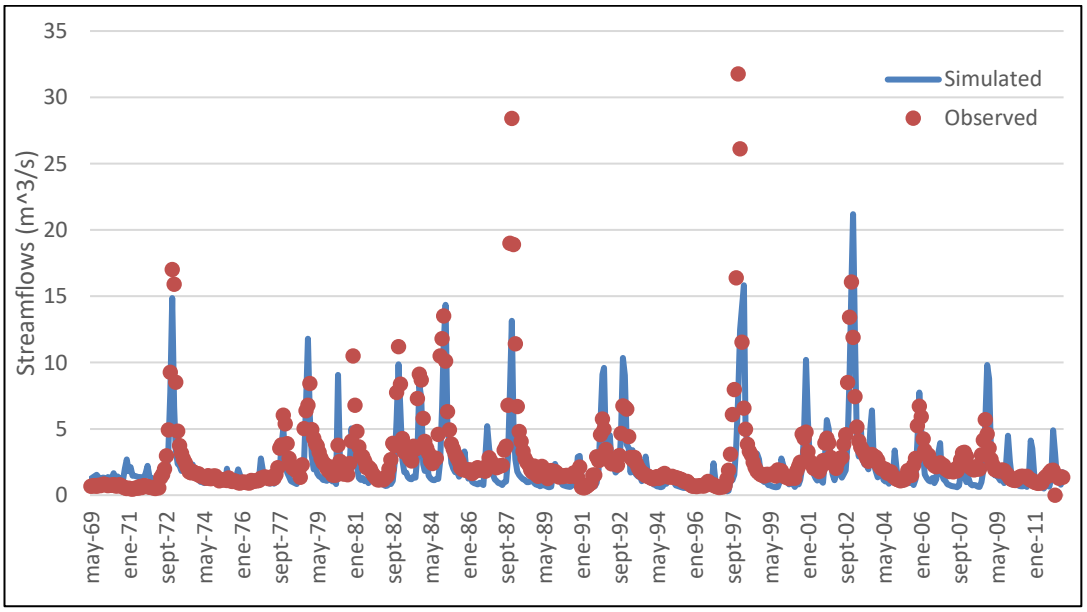

Figure 2-2: Observed vs. simulated monthly discharges for the period 1969-2011 at the San Agustin gauge in the Hurtado River.

Table 2-2: Comparison of observed (obs) and simulated (sim) streamflows both for calibration and validation periods.

	Calibration (1985-2011)					Validation (1969-1984)				
	NSE	Mean [m^3/s]		C.V.		NSE	Mean [m^3/s]		C.V.	
Station		Obs	Sim	Obs	Sim		Obs	Sim	Obs	Sim
San Agustín	0.45	2.79	2.77	0.82	0.53	0.63	2.74	2.57	0.71	0.40
Ojos de Agua	0.54	0.83	0.85	0.70	0.40	0.58	0.84	0.72	0.73	0.39
Cuestecita	0.63	1.60	1.66	0.92	0.70	0.63	1.79	1.32	1.02	0.77
Las Ramadas	0.72	3.93	3.97	0.92	0.77	0.67	4.72	3.29	0.80	0.71
Desembocadura	0.61	1.32	1.35	1.16	0.99	0.51	1.61	1.06	1.04	0.77
Fragüita	0.84	2.38	2.43	1.27	1.00	0.71	3.04	3.08	0.75	0.68

Note: C.V. Coefficient of variation = average/standard deviation, NSE Nash-Sutcliffe efficiency index; (Nash and Sutcliffe, 1970).

2.3.2. DEVELOPMENT OF CLIMATE CHANGE SCENARIOS

Under the premise that many GCMs are needed to characterize the uncertainty when analyzing climate change impacts, this study considered 49 GCMs realizations (Appendix A), and the RCPs 2.6, 4.5, 6.0 and 8.5 (Moss et al., 2010; Taylor et al., 2012). GCMs' projected precipitation and temperature series were downscaled using a quantile-mapping methodology, a bias-correction method developed for adjusting GCM's output for hydrological forecast (Wood et al., 2002), and subsequently used in other climate change impacts and uncertainty studies (e.g. Maurer et al., 2009; Walton et al., 2017; Shi et al., 2018). This method was successfully compared against other dynamic and statistical methods by Wood et al. (2004). In our work GCM outputs are interpolated using inverse square distance to the ground weather station location. These interpolated GCM data are then bias corrected against the historical records (1971-2005). Because precipitation in the study basin is highly seasonal and summer months (December-March) are mostly dry, a monthly precipitation quantile-mapping performs poorly. Thus, an annual quantile-mapping was used instead, whereas a k-

Nearest Neighbor (k-NN) method similar to the one used by Greene et al. (2012) was adopted to disaggregate annual precipitation into monthly data (Lall and Sharman, 1996; Rajagopalan and Lall, 1999). Following the heuristic approach adopted elsewhere (Lall and Sharman, 1996; Rajagopalan and Lall, 1999), a value of $k = \sqrt{L} = \sqrt{35} \approx 6$ was used in the implementation of the k-NN method, in which L is the number of years in the historical record. For temperature, the quantile-mapping approach was applied on a monthly scale, as originally proposed by Wood et al. (2002).

2.3.3. PERFORMANCE INDEXES

To assess the performance of the reservoirs system, the first step is to define a satisfactory and unsatisfactory state. The system is considered to be in a satisfactory state when the total demand (D) is met. If in a certain time step D is not satisfied, the system falls into an unsatisfactory state referred to as a failure. With this definition, the Paloma system is on failure when the water allocation is under $D = \sum_{j=1}^{M} \alpha_j = 320\ Mm^3$, i.e. when the demand is not fully satisfied. The Paloma system operation performance is evaluated under the future climate projections for the period 2011-2100. The performance criterion used are the reliability, resilience and vulnerability indexes proposed by Hashimoto et al. (1982), widely used in the literature (e.g., Bayazit and Ünal, 1990; Moy et al., 1986; Fowler et al., 2003; Kim and Kaluarachchi, 2009; Kjeldsen and Rosbejerg, 2004; Schaefli et al., 2007; Srinivasan and Philipose, 1996; 1998; Steinschneider and Brown, 2012).

Reliability (*Rel*) measures how often the system fails. For our purpose, it is calculated as the percentage of time that the system is able to meet the D, in the *n* years under evaluation.

$$Rel = 1 - \frac{\sum_{t=1}^{n} Z_t}{n} \tag{2.5}$$

where Z_t counts the number of years at failure:

$$Z_t = \begin{cases} 0 & \text{if} \sum_{j=1}^{M} O_j^t = D = 320\ Mm^3 \\ 1 & \text{if} \sum_{j=1}^{M} O_j^t < D = 320\ Mm^3 \end{cases} \tag{2.6}$$

where *t* is the year from 1 up to *n*, the last year of the analysis.

Resilience (*Res*) is a measure of how fast the system recovers once it has failed.

$$Res = \frac{\sum_{t=1}^{n} W_t}{\sum_{t=1}^{n} Z_t} \tag{2.7}$$

where W_t equals 1 each time step in which the system passes from failure to success and 0 if it stays on failure. Hence, $\sum_{t=1}^{n} W_t \leq \sum_{t=1}^{n} Z_t$, which ensures a *Res* range between 0 (no recovery from failure or always in failure) to 1 (immediate recovery from failure or never in failure).

Following the approach by Srinivasan and Philipose (1996; 1998), two indexes for vulnerability were used: (1) the maximum vulnerability or maximum water deficit ($MaxV$) as used by Moy et al. (1986), and (2) the average vulnerability or average water deficit ($AvgV$). Both indexes range between 0 and 1, and are:

$$MaxV = \frac{max(v^t)}{D} \tag{2.8}$$

where

$$v^t = D - \sum_{j=1}^{M} O_j^t \geq 0 \tag{2.9}$$

$$AvgV = \frac{\left(\frac{\sum_{t=1}^{n} v^t}{n}\right)}{D} \tag{2.10}$$

In Eq. (2.8) and (2.10), vulnerability values are standardized by D.

Finally, the Standardized Average Outflows (*OF*) was used as an additional index in the analysis:

$$OF = \frac{\left(\frac{\sum_{t=1}^{n} \sum_{j=1}^{M} O_j^t}{n}\right)}{D} \tag{2.11}$$

hence, *OF* ranges between 0 and 1, and measures the mean percentage of water allocated by the system compared to D.

2.4. RESULTS AND ANALYSIS

The changes in the reservoir system's performance for the period 2011-2100 is analyzed under the different GCMs and RCPs. The uncertainty is characterized by relating the range of the RRV indexes and the climate on three possible categories: inter-GCM, intra-GCM and RCP contribution to the overall uncertainty. Fig. 2-3 compares the values of the Reliability, Resilience and Standardized Average Outflow for all the GCMs and RCPs, whereas Fig. 2-4 presents the same for both vulnerability indexes. Both Figures show the historical simulated RRV performances as a dashed line. The reliability range (Fig. 2-3a) varies with the climate change scenario. For example, for GCM 2 (see Appendix A), the reliability is slightly above 0.4 for RCP

8.5, whereas it reaches a value over 0.7 for RCP 2.6 (i.e. more than a 30% difference in the time under failure). Other GCMs lead to clustered reliability values regardless of the RCP (for instance Rel = 0.2 for the GCM 17). Overall, the inter-GCM reliability range is wider than the RCP reliability range. Note for example that under RCP 4.5, the reliability goes from almost zero (GCM 16) to one (GCM 11.5). The standardized outflow (Fig. 2-3c) follows the same pattern. Reliability and standardized outflow perform worse in the future, even under RCP 2.6. On the other hand, the intra-GCM reliability range of some GCMs is clustered around a single value across all their realizations while others have a wide range (Fig. 2-3a). For example, the three realizations of GCM 13 under RCP 4.5 produce reliabilities values of 0.09 (GCM 13.2 and 13.3) and 0.1 (GCM 13.1). Under RCP 4.5, GCM 6 has an intra-GCM reliability range of 0.63, going from 0.1 (GCM 6.3) to 0.73 (GCM 6.2). The wider range of the intra-GCM reliability for GCM 6 as compared to GCM 13, is not explained by the higher number of realizations (i.e. 10 and 3 realizations, respectively), as almost any subgroup of three realizations from GCM 6 would produces a reliability range of 0.3 or more.

A similar range of results is observed for resilience (Fig. 2-3b). For example, the GCM 2 produces a resilience value of 0.18 for RCP 4.5, and above 0.5 for RCP 2.6. Interestingly, the resilience for this GCM under RCP 8.5 is almost the same as for RCP 6.0 (*Res* = 0.3) and higher than for RCP 4.5. Similar to the reliability, the inter-GCM range is wider than the RCP range. The range of results is similar to the reliability range because a couple of GCM and RCP combinations produce high resilience values (i.e. GCM 9, RCP 6.0; GCM 34, RCP 4.5), but most of the resilience values tend to be grouped between 0 and 0.4. These values indicate that the expected

duration of a failure is slightly longer than 2 years. The resilience index presents the same intra-GCM pattern as reliability, with a wide range for some GCMs (e.g. GCM 6), while for others similar index values are produced across their realizations (e.g. GCM 13). Compared to the historical situation, resilience index performs worse for 146 of the 149 future projections analyzed. Higher reliability and resilience values tend to be related, although this does not always hold. For instance, the best resilience of GCM 4.5 (realization r5i1p1 of GCM CCSM4, Table A1) results from RCP 2.6, while its best reliability results from RCP 4.5.

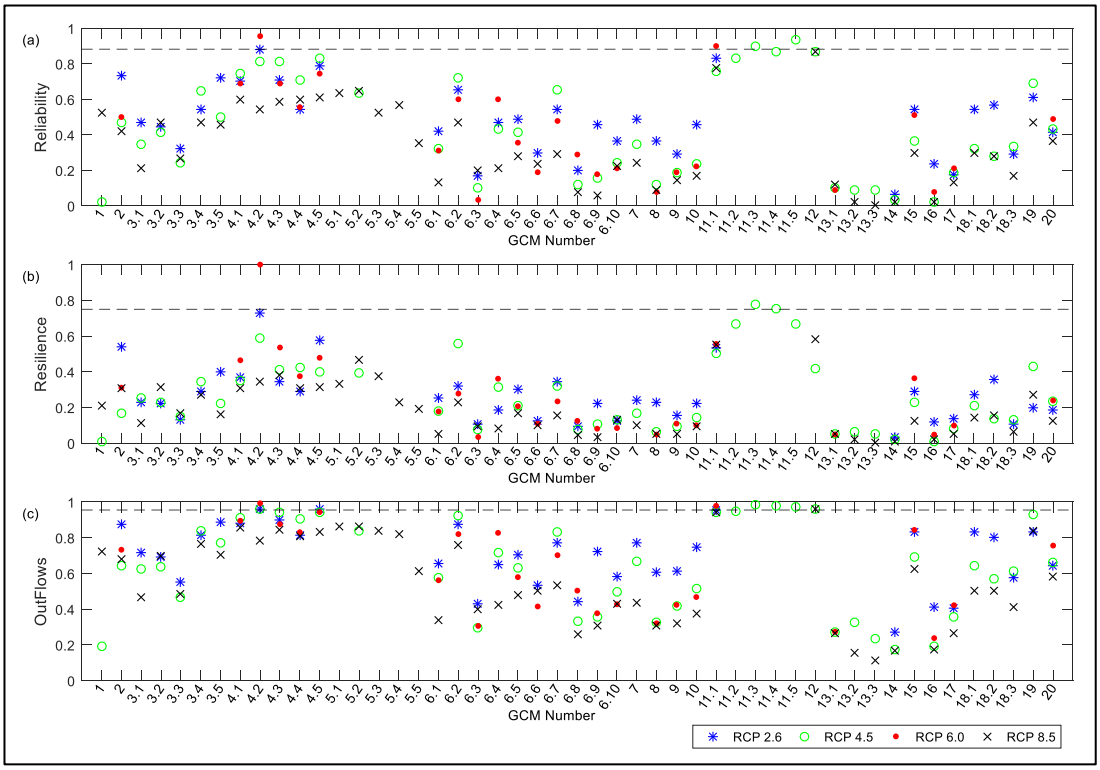

Figure 2-3: Reliability (a), resilience (b) and standardized outflow (c) for the different RCPs and GCMs. The simulated mean historical performance (years 1971-2005) is presented with a dashed line.

Maximum water deficit values for most of the GCMs and RCPs combinations are larger than 0.8 (Fig. 2-4a). However, the issue of inter-GCM dispersion already

discussed for the other indexes, still holds. Low vulnerability values are obtained for the GCMs and RCPs combinations that produce high reliability and resilience. Again, the pattern of higher uncertainty due to GCMs is noticeable in Fig. 2-4b. More specifically a wide range of $AvgV$ is produced among the GCMs (inter-GCM); such a range is also produced by most of the realizations for a given GCM (intra-GCM), just as for other indexes. The intra-GCM range of $MaxV$ is small for most of the GCMs, because at least one extremely severe drought appears as part of the future climate projection (Fig. 2-4a). Nevertheless, results spread is wider considering different GCMs than that resulting from different RCPs. As expected, both vulnerability indexes show a worsening future performance.

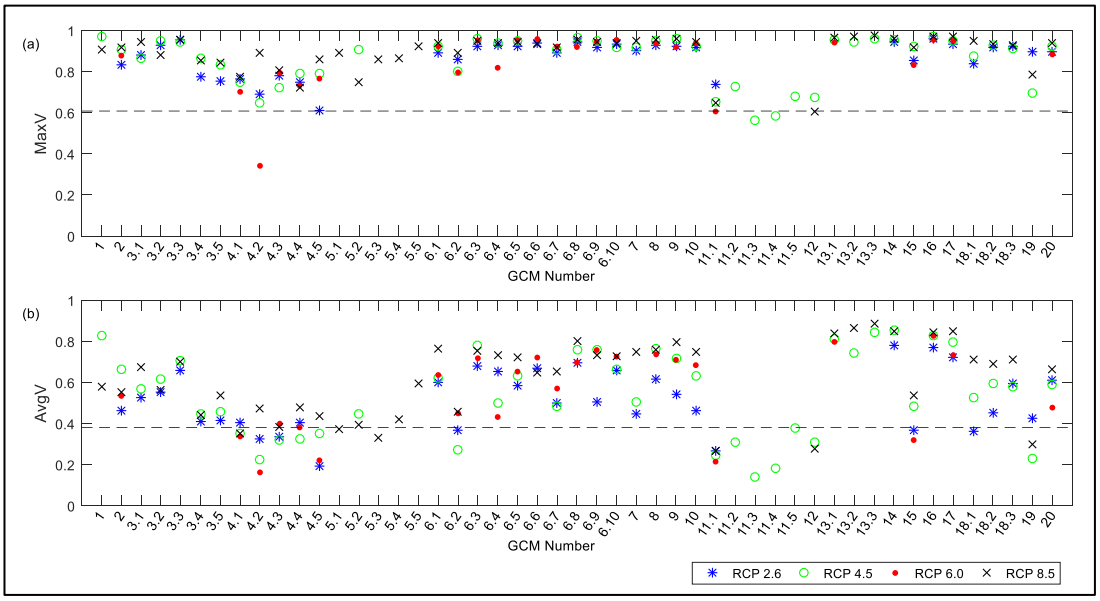

Figure 2-4: *MaxV* (a) and ***AvgV*** (b) for the different RCPs and GCMs. The simulated mean historical performance (years 1971-2005) is presented with a dashed line.

Overall, results reported in Fig. 2-3 and Fig. 2-4 show that the performance indexes are subject to higher inter-GCM induced uncertainty, followed by intra-GCM

induced uncertainty, with the RCP-induced uncertainty being the least significant source. This contribution of GCMs and their realizations to the uncertainty can be further seen in the boxplots significant overlapping in Fig. 2-5. Despite this overlapping, the system's performance tends to be slightly worse for more severe RCPs. For example, the median reliability decreases from around 0.5 (RCP 2.6) to 0.3 (RCP 8.5), while the median standardized average outflows decrease from 0.7 to 0.5. Interestingly, the interquartile ranges of the boxplots are wider for the RCPs 4.5 and 6.0, especially for reliability and standardized outflow. The big overlap of the indexes in Fig. 2-5 emphasizes that GCMs contribute the biggest portion of the uncertainty. This is a significant result, as the reservoir operators would make similar decision under any of these RCPs, although decisions can be quite different based on different GCMs, or even based on different realizations of the same GCM (Fig. 2-3 and 2-4). If the current reservoir system's operation rule is not modified, future scenarios where performance metrics worsen compared to the historical ones are very likely.

To evaluate the temporal dynamics of the GCM and RCP induced uncertainty over the performance of the system operation, the simulation period is divided into time windows 2011-2045 and 2046-2100. The future is unpromising even for the 1st period, with few GCMs' projections producing performances similar to the historical one (Fig. 2-6). Furthermore, there is a significant performance's worsening in the 2nd period, especially under RCP 8.5, as the medians become more different among RCPs in this period (e.g. the difference in reliability medians between RCP 2.6 and 8.5 goes from 0.1 in the 1st period to 0.3 in the 2nd period). However, the overlap of the boxplots is still big for the 2nd period, emphasizing that, despite the increase in RCP uncertainty, the portion of uncertainty related to the GCMs is still larger. The overlapping is caused

by an increase in the uncertainty of the GCMs, which is seen in the interquartile range of the boxplots (e.g. the RCP 8.5 standardized outflow boxplot goes from 0.47-0.80 in the 1st period to 0.20-0.74 in the 2nd period).

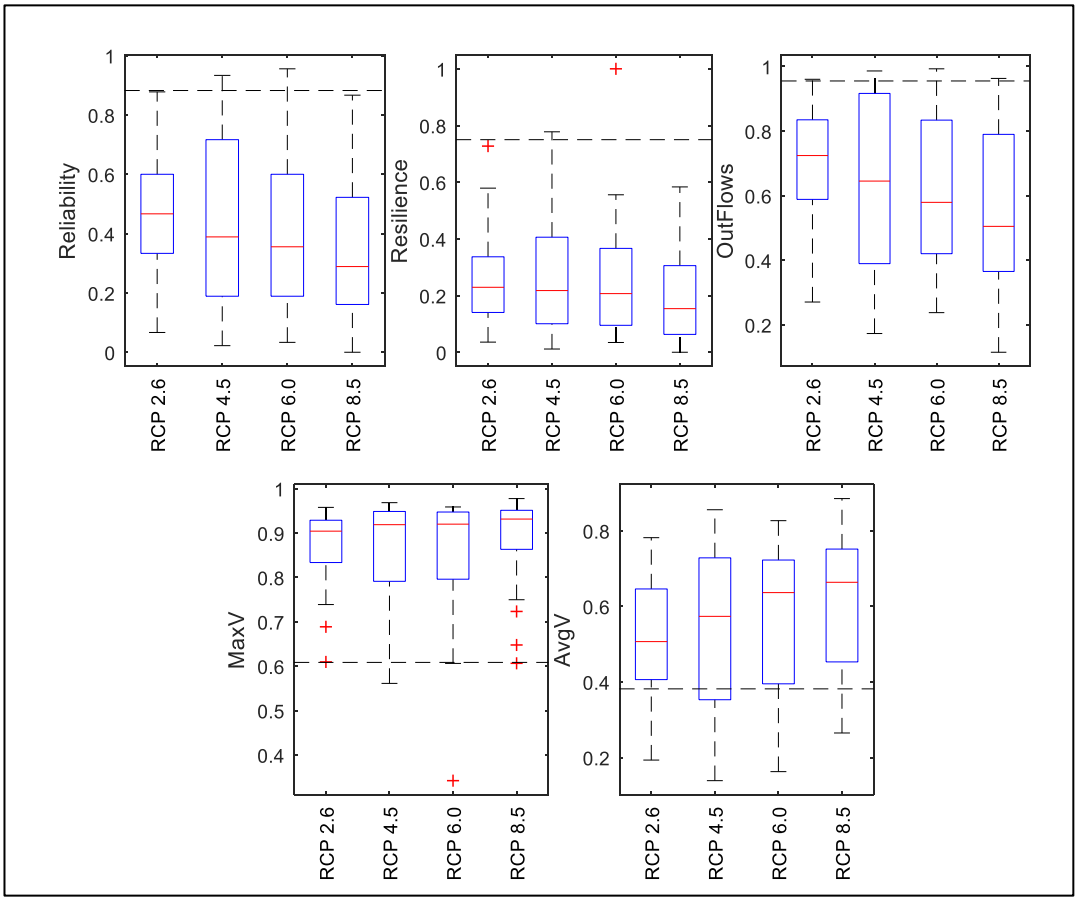

Figure 2-5: Boxplot for indexes of reliability, resilience, standardized outflows, ***MaxV***, and ***AvgV***. The simulated historical performance (years 1971-2005) is presented with a dashed line.

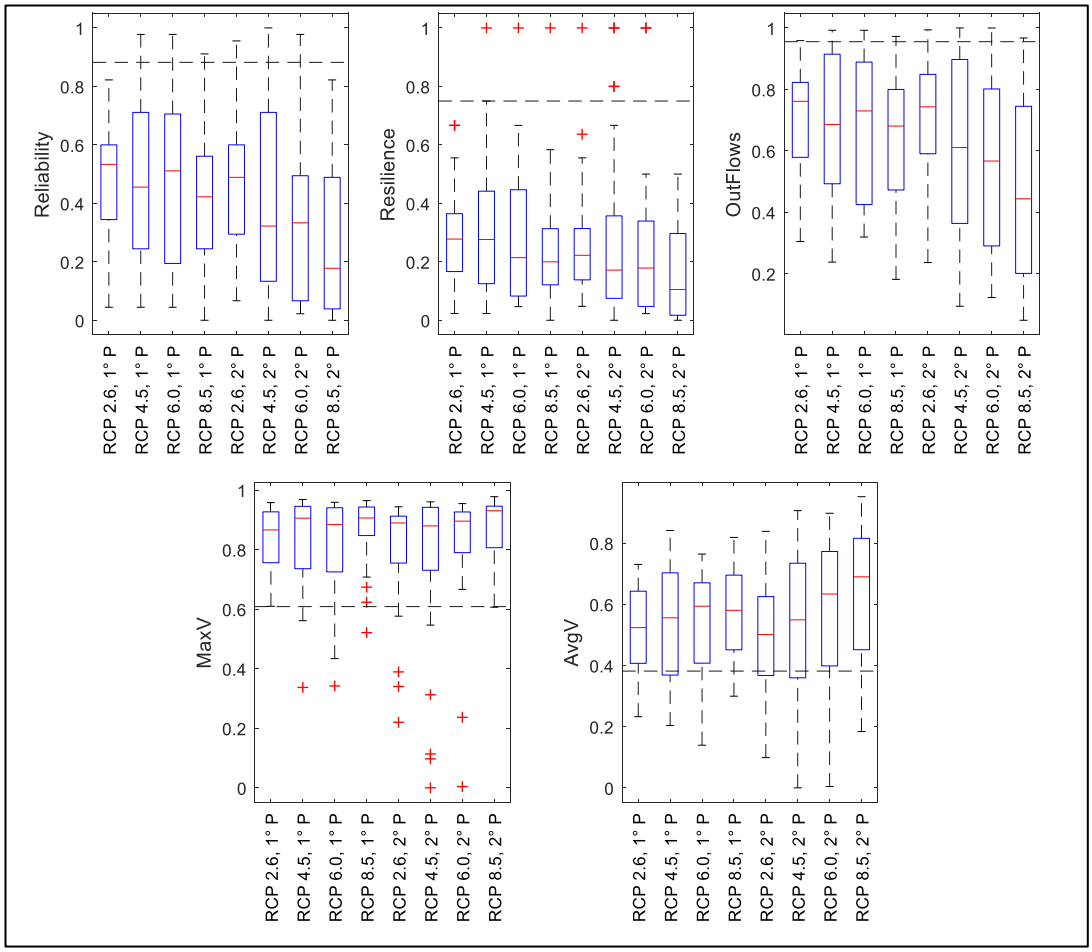

Figure 2-6: Boxplot for indexes of reliability, resilience, standardized outflows, ***MaxV***, and ***AvgV***, for the 1st (years 2011-2054, 1° P) and 2nd (years 2055-2100, 2° P) period. The simulated historical performance (years 1971-2005) is presented with a dashed line.

Some studies evaluated the tradeoff among the RRV indexes under the same climate conditions and different reservoir operations (Moy et al., 1986; Bayazit and Ünal, 1990; Srinivasan and Philipose, 1996; 1998; Zhang et al., 2017). Here the reservoir system operation is constant and the relationship among RRV indexes and changes in climate, measured by the percentage of change (PC) in precipitation, is evaluated. *PC* is calculated from the raw GCMs before downscaling:

$$PC = \frac{AFPP - ACPP}{ACPP} \tag{2.12}$$

where $AFPP$ and $ACPP$ are the average future annual precipitation between 2011 - 2100 and over the control period (1971 - 2005) respectively. Appendix A presents *PC* values for all the GCMs and RCPs.

Table 2-3: Pearson (Spearman) correlation coefficients between different performance indexes.

	Reliability	Resilience	$MaxV$	$AvgV$	Outflows	PC
Reliability	1.00 (1.00)	0.93 (0.97)	-0.84 (-0.91)	-0.94 (-0.95)	0.97 (0.99)	0.93 (0.93)
Resilience	0.93 (0.97)	1.00 (1.00)	-0.90 (-0.90)	-0.90 (-0.94)	0.88 (0.97)	0.85 (0.90)
$MaxV$	-0.84 (-0.91)	-0.90 (-0.90)	1.00 (1.00)	0.85 (0.94)	-0.78 (-0.93)	-0.79 (-0.89)
$AvgV$	-0.94 (0.95)	-0.90 (-0.94)	0.85 (0.94)	1.00 (1.00)	-0.97 (-0.98)	-0.90 (-0.91)
Outflows	0.97 (0.99)	0.88 (0.97)	-0.78 (-0.93)	-0.97 (-0.98)	1.00 (1.00)	0.92 (0.93)
PC	0.93 (0.93)	0.85 (0.90)	-0.79 (-0.89)	-0.90 (-0.91)	0.92 (0.93)	1.00 (1.00)

Fig. 2-7 and Table 2-3 illustrate the strong correlation between the performance indexes and *PC* values. *PC* reaches the highest Person or linear correlation values with reliability and standardized outflow (0.93 and 0.92, respectively), which are similar to the Spearman or rank correlation (0.93 and 0.93, respectively), i.e., the correlation is strongly linear. The index with the lowest Pearson correlation coefficient against *PC* is $MaxV$ (r = -0.79), which can be attributed to the non-linear relationship between both variables observed in Fig. 2-7. In fact, the differences between Pearson and Spearman correlation identify non-linear relationships. For example, these two coefficients clearly differ when comparing *PC* and $MaxV$, resilience and outflows, and $MaxV$ and outflows (Table 2-3). Both resilience and $MaxV$ have an apparent threshold

after which the linear relationship with *PC* does not hold (Fig. 2-7). Moreover, they have a non-linear relationship with most of the other indexes (Table 2-3), except among them. These non-linear correlations among the indexes support the necessity of using more than one RRV index, as they cannot be reduced to a single index. The outflow is the most redundant index, because it highly correlates with reliability and $AvgV$ (Table 2-3). *PC* values from the four RCPs significantly overlap for the performance indexes; nevertheless, higher RCPs tend to produce greater negative changes in precipitation (Fig. 2-7).

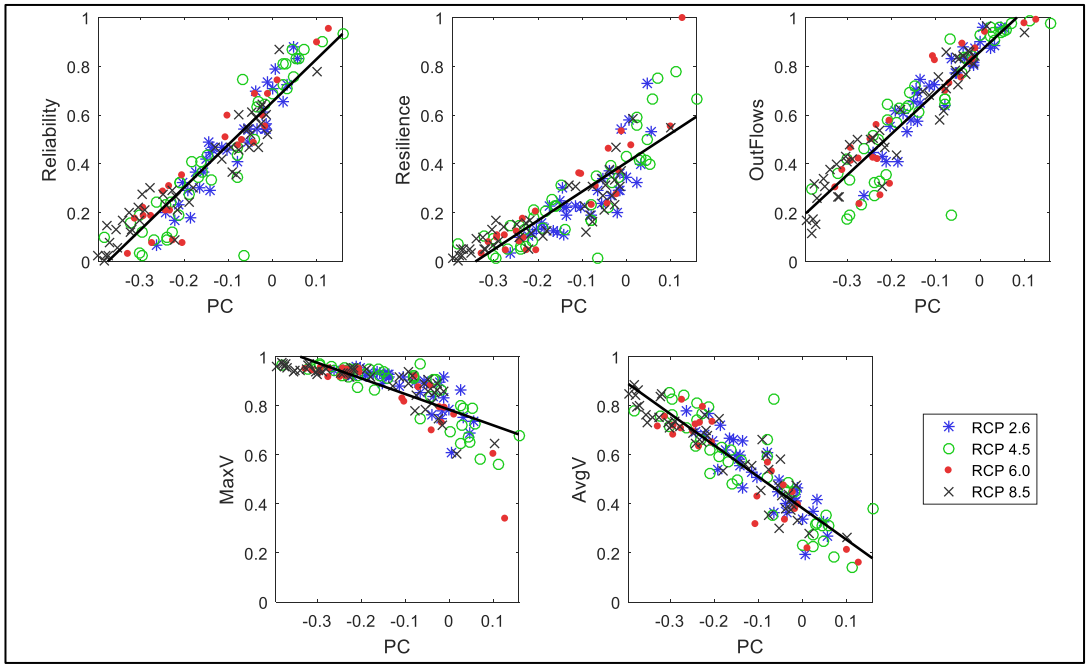

Figure 2-7: Reliability, resilience, standardized outflows, $\boldsymbol{MaxV}$, and $\boldsymbol{AvgV}$ vs percentage of change in precipitation ($\boldsymbol{PC}$) of the raw GCMs.

2.5. CONCLUSION

This chapter evaluates the uncertainty associated with the GCMs, their realizations and the RCP scenarios over the performance of the current operation of the Paloma reservoir system, in the Limari River basin, Chile, under climate change

for the period 2011-2100. This assessment was conducted by downscaling the GCMs temperature and precipitation outcomes with a quantile-mapping bias correction approach, which in turns served as input to a WEAP hydrological model. Modeled flows were used to simulate the operation of a reservoir system under the current operation rule, whose performance was characterized using RRV indexes. Our main conclusions are:

- The overall uncertainty in the performance increases in time, both due to larger GCM and RCP uncertainties later in the century. The main contribution to this uncertainty comes from the GCMs, particularly for the early future. This can cause significant changes in the assessment of the reservoir performance.
- For most of the GCMs, the intra-GCMs (i.e. several realizations of a single GCM) uncertainty is comparable to the inter-GCM uncertainty, as few GCMs present the same performance for several realizations. This is relevant as multiple GCM realizations are generally not considered when studying climate change impacts on water systems.
- The uncertainties associated with GCMs differ for different RCPs. Overall, there is more uncertainty associated with RCP 4.5 and RCP 6.0, while the uncertainty for RCP 2.6 was the lowest. More studies are needed to determine whether this result will hold for other locations.
- The performance measured by every index worsens in time when compared to the historical situation, even for an early period.
- As expected, a strong correlation between the performance indexes and the percentage of change of precipitation simulated by the GCMs (*PC*) was found.

Hence, to reduce the uncertainty of the reservoir system performance, the *PC* uncertainty must be reduced.

- Given the non-linear relationships among the indexes, they provide complementary and relevant information about the current operation rule under different climate conditions. Only the standardized average outflow can be ignored, due to its strong correlation with reliability and average vulnerability.

The strong correlation between the changes in climate and the performance indexes may allow the assessment of the future climate conditions that will take the reservoir system to not satisfy the demand under the current operation rule. Moreover, our results suggest the modification of this rule to better regulate water allocation. Such rule should consider the new reservoir under construction in the upper basin, known as Valle Hermoso. Finally, future studies considering other downscaling methods and different hydrological models should be carried out, to quantify the uncertainty associated with these components in the assessment of the system's performance.

3. CHAPTER 3: USING A STATISTICAL PRE-ANALYSIS APPROACH AS AN ENSEMBLE TECHNIQUE FOR THE UNBIASED MAPPING OF GCM CHANGES TO LOCAL STATIONS

3.1. INTRODUCTION

Uncertainty is inherent to water resources planning and management. Typically, this planning has considered stationarity to characterize and quantify uncertainty. In particular, the design and operation of water infrastructure uses historical hydro-meteorological records that are assumed to be representative of the future. Such approach is used to assign costs and benefits to decisions and projects, as well as to estimate the involved system performance (Bras et al., 1983; Datta and Burgos, 1984; Datta and Houck, 1984). But decision making should no longer rely completely on the assumption of stationarity (Milly et al., 2008; Milly et al., 2015), as global change in general, and climate change in particular, are altering the behavior of hydro-climatic variables.

A widely used approach to cope with uncertainty in water resources management under stationarity has been probabilistic risk assessment, in which exceedance probabilities are given to different possible outcomes. Risk assessment has also been used in non-stationary extreme flood evaluation (Stedinger and Griffis, 2011; Vogel et al., 2011; Salas et al., 2012; Obeysekera and Salas, 2013; Salas and Obeysekera, 2013; Read and Vogel, 2015), and serves as an alternative to evaluate changes and variability in climate. Although a non-stationary risk assessment is challenging (Serinaldi and Kilsby, 2015), and a probabilistic projection of climate

change could mislead decision-makers by under-evaluating the real range of possible futures (Clark and Pulwarty, 2003), risk assessment under deep uncertainty, such as climate change, is possible (Shortridge et al., 2017).

Climate change and its impacts on the hydrological regime and water systems, have been widely studied by several authors (i.e., Downing et al., 1997; Adeloye et al., 1999; Lettenmaier et al., 1999; Fowler et al., 2005; Mondal and Wasimi, 2007; Giorgi and Bi, 2009; Mondal et al., 2010; Hagemann et al., 2011; Mahlstein et al., 2011; Matonse et al., 2013). These climate change impact studies typically follow a top-down approach that starts form the climate projections identified from General Circulation Models (GCMs) for different greenhouse gases (GHG) scenarios. These projections are downscaled to a regional or local scale, and used to run models to simulate specific impacts over different sectors, activities or components of the environment, such as infrastructure, crops, cities, ecosystems, etc. (Wilby and Dessai, 2010; Kiparsky et al., 2012).

Unfortunately, the approach depicted above is associated with an increasing cascade of uncertainty (Wilby and Dessai, 2010), which makes decision making very difficult (Hallegatte, 2009). Indeed, the top-down studies that use insufficient GCMs, lack the ability to quantify their contribution to the total uncertainty explained by this cascade. The consideration of just some of the GCM is commonly due to simplicity or to the fact that some specific GCM have been identified locally to be suitable for climate change studies (Fowler et al., 2005). For example, Yung et al. (2011) evaluated 11 scenarios in the assessment of municipal water supply risk using only two GCMs (i.e. the most extreme ones) in addition to population forecasts and a variety of demand management programs and possible system expansions. Kim and Kaluarachchi (2009)

used six GCMs to estimate an average future change when studying the impacts of climate change in the Blue Nile River. However, other studies consider a larger number of GCMs and GHG scenarios to analyze a wider range of possible future outcomes (Schaefli et al., 2007; Maurer et al., 2009). Typically, a large contribution to the uncertainty comes from the downscaling methods (Chen et al., 2011; Ouyang et al., 2014) and the GHG scenarios. In fact, the uncertainty coming from this last factor becomes more dominant in a distant future (Hawkins and Sutton, 2011). Nonetheless, several authors have identified large uncertainties associated with the GCM choice (Minville et al., 2008; Hawkins and Sutton, 2011; Chen et al., 2011; Teng et al., 2012; Ahmadalipour et al., 2017). Using a large number of GCMs improves the characterization of the impacts of climate change and its variability, by allowing for example, the estimation and assessment of risk or the relative probability of future scenarios, both concepts commonly used to deal with uncertainty in water management. Yet, considering a large number of GCMs to produce the different possible climate series may be beyond the capabilities of most water resource practitioners and decision-makers, thus the development of simple approaches to treat multiple GCM projections becomes essential. Such approaches must not compromise the correct representation of both local climate and GCMs projections.

In the attempt of having a suitable alternative to cope with GCM uncertainty when dealing with climate change, this chapter develops an ensemble technique for the mapping of GCM changes to local stations, in which both the local climate variability and the GCMs' statistics are preserved (i.e. the technique is unbiased). The approach extracts future changes from annual precipitation and temperature time series derived from multiple GCM runs. A statistical framework combining these changes

allows using the needed trend percentiles to represent the range of future climate conditions. Finally, climatic variability is added to these trends to produce future scenarios coherent with local conditions. The methodology is applied to three different river basins located in the Mediterranean regions of Chile using 45 future climate projections run under the scenario RCP 8.5. In these applications, we extensively assess the results of our method against those obtained from considering individually each possible GCM output. We also compare its ability to preserve GCM and local statistics against that of more traditional approaches such as delta change, bias correction and the use of a subset of GCMs. The chapter is organized as follows: section 3.2 describes the approach that is able to manage GCM uncertainty for climate variability and climate change studies, whereas section 3.3 describes the study area and the climate time series. In section 3.4 the method is applied to the different case study basins, while in section 3.5 the main conclusions are presented.

3.2. METHODOLOGY

The proposed methodology is based on a statistical pre-analysis of the GCM described in Fig. 3-1. This pre-analysis is used to build climate time series that incorporate both trends from the GCM and natural variability. The GCM pre-analysis approach is tested against the conventional analysis of all GCM runs in which each possible GCM is considered individually to produce the corresponding climate series. These series are treated statistically to estimate future climate conditions and their corresponding probability of occurrence. The ability of the proposed method to map GCM changes to local stations is also tested against other three commonly used methods (i.e. quantile mapping bias correction, the use of a subset of representative

GCMs and delta change). Further details of the climate time series generation upon the conventional analysis of all GCM runs, the pre-analysis of the GCMs and the commonly used methods are provided in subsections 3.2.1, 3.2.2 and 3.2.3 respectively

3.2.1. CONVENTIONAL ANALYSIS OF ALL GCM RUNS

The conventional analysis of all GCM runs combines two components: (1) The extraction of changes in precipitation and temperature data from the GCM, and (2) the generation of annual climate series around these changes. This analysis is performed for each GCM *G* under scenario RCP 8.5 (Moss et al., 2010), although any other radiative forcing scenario can eventually be used.

3.2.1.1. GCM CLIMATE CHANGE EXTRACTION

In this step, the three or four closest grid points of the GCM precipitation and temperature outputs (Fig. 3-1a) are interpolated to the gauge location using the inverse square distance method (Myers, 1994). Then, the normalized moving averages in precipitation ($NMAP_{t,G}$) is obtained for the GCM for a moving time window (e.g. 25 or 30 year window) whose last year is *t* (Fig. 3-1b). $NMAP_{t,G}$ measures the change in precipitation and is defined as the ratio between the GCM precipitation output moving averages ($MAP_{t,G}$) and the average from the control period of the GCM adopted up to the last year of this control period t_o ($AP_{t_o,G}$):

$$NMAP_{t,G} = \frac{MAP_{t,G}}{AP_{t_o,G}} \qquad , (t_o < t < t_f) \tag{3.1}$$

where t_f is the last year of the output from GCM.

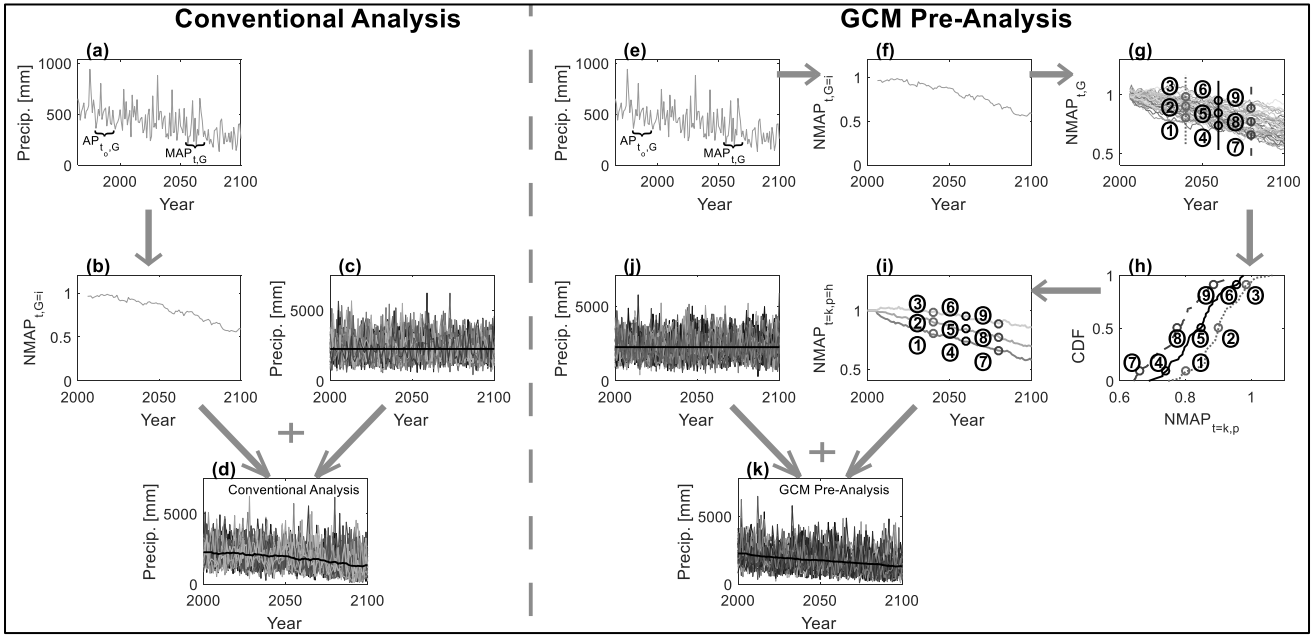

Figure 3-1: Schematic representation of GCM pre-analysis and conventional analysis of all GCM runs approaches. From the GCM precipitation (a and e) the normalized moving average ($\boldsymbol{NMAP_{t,G}}$) is obtained by the ratio between the moving averages ($\boldsymbol{MAP_{t,G}}$) and the control period average ($\boldsymbol{AP_{t_o,G}}$) (b and f). $\boldsymbol{NMAP_{t,G}}$is used in the annual time series generator (c) to obtain the precipitation series with the conventional analysis approach (d). Several percentiles of $\boldsymbol{NMAP_{t,p}}$(g and h) are used to build the GCM trends (i). These trends are used in the annual time series generator (j) to obtain the precipitation series with the GCM pre-analysis approach (k).

On the other hand, the temperature difference for a given GCM ($DMAT_{t,G}$) is obtained by the difference between the GCM temperature output moving average ($MAT_{t,G}$) and the average from the control period ($AT_{t_o,G}$):

$$DMAT_{t,G} = MAT_{t,G} - AT_{t_o,G} \qquad ,(t_o < t < t_f) \tag{3.2}$$

An analogous process is used to extract the change in the standard deviation of precipitation from the GCM group. In the case of precipitation, the normalized moving standard deviation ($NMSDP_{t,G}$) is defined for each GCM as the ratio between the GCM precipitation output moving standard deviation ($MSDP_{t,G}$) and the standard deviation from the control period ($SDP_{t_o,G}$):

$$NMSDP_{t,G} = \frac{MSDP_{t,G}}{SDP_{t_o,G}} \qquad ,(t_o < t < t_f) \tag{3.3}$$

The temperature standard deviation difference ($DMSDT_{t,G}$) is obtained for each GCM by the difference between the GCM temperature output moving standard deviation ($MSDT_{t,G}$) and the standard deviation from the control period ($SDT_{t_o,G}$):

$$DMSDT_{t,G} = MSDT_{t,G} - SDT_{t_o,G} \qquad ,(t_o < t < t_f) \tag{3.4}$$

3.2.1.2. ANNUAL CLIMATE TIME SERIES GENERATOR

The second step is the generation of annual series of temperature and precipitation that incorporate local variability using a probability density function (PDF) (Fig. 3-1c). These series are generated considering the changing climate according to the statistics of the GCMs. For each gauge of interest, the process starts by obtaining the moments (mean μ, standard deviation σ and skewness) of the annual precipitation and temperature records. These moments, or the future expected ones obtained using the historical moments and the rates of change calculated in Eqs. (3.1-

3.4), are used to estimate the parameter set θ of any PDF $f_Y(y,\theta)$ of the variable Y (temperature or precipitation). Thus, θ will change in time according to the outcome from the GCMs, either if they are used individually to generate the climate series (subsection 3.2.1.3), or if they are considered jointly using the proposed ensemble approach (subsection 3.2.2). Note that for precipitation we only used strictly non-negative distributions. The PDF $f_Y(y,\theta)$ is chosen by minimizing the Kolmogorov-Smirnov (KS) statistic of the KS test (Ayyub and McCuen, 2011). Note also that the generation of temperature and precipitation series may eventually need considering and preserving the correlation between them if significant, as well as possible correlations among locations. This was not needed in the case study here presented. As an alternative, the series can be normalized to generate correlated numbers which can then be transformed back to the original variables domain using the inverse of their cumulative distribution function (Ayyub and McCuen, 2011). In Appendix B we propose a method for this purpose, which is applied to one of the river basins of our case study.

3.2.1.3. INCORPORATING GCM CHANGES INTO NON-STATIONARY ANNUAL CLIMATE SERIES GENERATOR

We now combine the GCM precipitation and temperature changes obtained in Eq. (3.1) through (3.4) with the annual climate series generator depicted in subsection 3.2.1.2 for each year *t*. Thus, the resulting precipitation and temperature series incorporate both the GCM precipitation and temperature mean and standard deviation changes, as well as the natural variability coming from the standard deviation (Fig. 3-1d). Note that other potential sources of annual natural variability not captured by the

standard deviation are not considered. Under this approach, the value of the climatic variable at any time *t* for the GCM is obtained as:

$$Y_{t,G} = F_Y^{-1}(u, \theta) = F_Y^{-1}\left(u, \mu^*(t,G), \sigma^*(t,G)\right) \quad (3.5)$$

where u is a random uniform number [0-1]. Note that the values of the parameter set θ change with time, as both the mean (μ^*) and standard deviation (σ^*) vary according to the GCM changes, while the skewness, if needed, is assumed to be constant. This approach was also adopted by Vogel et al. (2011) to incorporate trends in the return period of floods. The value of μ^* and σ^* in Eq. (3.5) at any year *t* for precipitation are calculated from the historical mean (μ) and standard deviation (σ) and the normalized change rates calculated in Eq. (3.1) and Eq. (3.3):

$$\mu^*(t,G) = \mu \cdot NMAP_{t,G} \quad (3.6)$$

$$\sigma^*(t,G) = \sigma \cdot NMSDP_{t,G} \quad (3.7)$$

For temperature, μ^* and σ^* are obtained using the changes rates from Eq. (3.2) and Eq. (3.4):

$$\mu^*(t,G) = \mu + DMAT_{t,G} \quad (3.8)$$

$$\sigma^*(t,G) = \sigma + DMSDT_{t,G} \quad (3.9)$$

Note that Eq. (3.5) allows the generation of annual climate variables. If intra-annual climate series were needed, disaggregation methods such as the k-Nearest Neighbor, k-NN, (Rajagopalan and Lall, 1999) or the stochastic temporal disaggregation method (Thober et al., 2014) can be used. In fact, Greene et al. (2012) applied k-NN to disaggregate annual precipitation and temperature data into finer time-scales.

3.2.2. GCM PRE-ANALYSIS

The GCM pre-analysis considers the following steps: (1) Extraction of changing rates of precipitation and temperature associated with each GCM (Fig. 3-1 e and f); (2) grouping the changes from each GCM (Fig. 3-1g); (3) calculation of the empirical cumulative distribution functions (CDF) of the GCM changes for each year (Fig. 3-1h); (4) construction of GCM trends using the CDFs (Fig. 3-1i), and (5) generation of annual climate series around each GCM trend (Fig. 3-1k).

To identify the long-term trends in precipitation and temperature, the resulting $NMAP_{t,G}$ and $DMAT_{t,G}$ time series calculated from Eq. (3.1) and Eq. (3.2) are grouped (Fig. 3-1g). For each year *t*, empirical cumulative distribution functions (CDF) for the values of $NMAP_{t,G}$ and $DMAT_{t,G}$ are calculated (Fig. 3-1h). The trend in time associated with a given percentile or non-exceedance probability p (i.e. $NMAP_{t,p}$ or $DMAT_{t,p}$, Fig. 3-1i) is given by the values of $NMAP_{t,G}$ (or $DMAT_{t,G}$) with the same probability p calculated from the CDF of each year. Hence, several trends (e.g. 25th, 50th, 75th percentiles) could be extracted and considered to analyze different possible future scenarios explicitly, in order to represent the dispersion among the group of GCM results.

An analogous process is done for the standard deviation. Thus, empirical CDF for changes in the standard deviation of precipitation and temperature ($NMSDP_{t,G}$ and $DMSDT_{t,G}$) calculated from Eq. (3.3) and Eq. (3.4) are obtained. Again, different percentiles are chosen, which allows the definition of continuous trends with percentile p ($NMSDP_{t,p}$ and $DMSDT_{t,p}$). To avoid producing climate data whose trends in average and variability are inconsistent with the GCM output, the value of p is chosen

for the trend of the normalized moving average in precipitation ($NMAP_{t,p}$) and it is randomly generated for the trend of the normalized moving average in standard deviation ($NMSDP_{t,p}$) after considering the average correlation between $NMAP_{t,G}$ and $NMSDP_{t,G}$. The same procedure is applied to temperature ($DMAT_{t,p}$ and $DMSDT_{t,p}$). Note that we focus the subsequent assessment of our method on an independent analysis of temperature and precipitation. Were a joint analysis of these variables needed, one could also consider the correlation among the average and standard deviation of precipitation and temperature when assigning the values of *p*. This could be done by choosing the value of p for the $NMAP_{t,p}$, and randomly generating the value of p for $NMSDP_{t,p}$, $DMAT_{t,p}$ and $DMSDT_{t,p}$. This process must consider the matrix with the correlations among $NMAP_{t,G}$, $NMSDP_{t,G}$, $DMAT_{t,G}$ and $DMSDT_{t,G}$.

The trends estimated from the GCM output are used on the annual climate series generator (Fig. 3-1j). Thus, the resulting climate series (Fig. 3-1k) is a GCM ensemble that incorporates the natural variability. The climatic variable at any year *t* for a trend percentile in μ (p_1) and in σ (p_2 correlates with p_1), is obtained as:

$$Y_{t,p_1,p_2} = F_Y^{-1}(u,\theta) = F_Y^{-1}\left(u,\mu^*(t,p_1),\sigma^*(t,p_2)\right) \quad (3.10)$$

note that Eq. (3.10) is the same as Eq. (3.5), but it uses the GCM ensemble trends instead of the changes of a single GCM. The values of the parameter set θ change with time, as both the mean (μ^*) and standard deviation (σ^*) change with $NMAP_{t,p}$, $DMAT_{t,p}$, $NMSDP_{t,p}$ and $DMSDT_{t,p}$.

3.2.3. BIAS CORRECTION AND DOWNSCALING METHODS

The GCM pre-analysis capability to reproduce the raw GCM projection changes over the mean and the standard deviation of annual precipitation is also tested against a quantile mapping bias correction (Wood et al., 2002), the sub-set of representative GCM projections (Whetton et al., 2012) and the delta change approach (Hay et al., 2000). These three approaches are some of the most widely used to incorporate GCM statistics to climate change studies.

The quantile mapping bias correction (QMBC) was originally developed by Wood et al. (2002), and subsequently used elsewhere (e.g. VanRheenen et al., 2004; Maurer, 2007; Maurer et al., 2009; Shi et al., 2018; Walton et al., 2017). Wood et al. (2004) successfully compared this method against other dynamic and statistical methods. In our work, the QMBC is applied to annual precipitation data by using a gamma-gamma transformation (Sharma et al., 2007).

The sub-set of GCM projections is a selection of a few raw GCMs projections that are more likely and/or have a more severe impact (Whetton et al., 2012). We selected five raw GCM projections to represent the quantiles of the GCM precipitation projection changes. The most extreme GCM mean precipitation changes (i.e. 1% and 99% percentiles) and the inter-quartiles (i.e. 25%, 50%, 75%) between the near future (2036-2063) and the control period (1978-2005) were selected as representative of the entire group of GCM projections. This five GCM projections are not bias corrected.

The delta change approach, also called change factor, consists in applying the changes in the raw GCM projections to the historical climate data (Hay et al., 2000; Diaz-Nieto and Wilby, 2005; Minville et al., 2008). For precipitation, the delta change

method multiplies the historical precipitation series by the change factor associated with the mean precipitation of the raw GCM projections.

3.3. STUDY AREA AND CLIMATE TIME SERIES

The methodology is applied to three basins located in central Chile (Fig. 3-2): (1) the Limarí River basin, a semiarid Mediterranean basin in north central Chile whose outlet is located at 30º43'51''S, 71º42'01''W; (2) the Maipo River Basin, a Mediterranean basin in central Chile whose outlet is located at 33º 36' 40'' S, 71º37' 50'' W; and (3) the Maule River Basin, another Mediterranean basin in central south Chile whose outlet is located at 35º 19' 00'' S, 72º 24' 30'' W. All these basins are bordered on the west by the Pacific Ocean and on the east by the Andes Mountains.

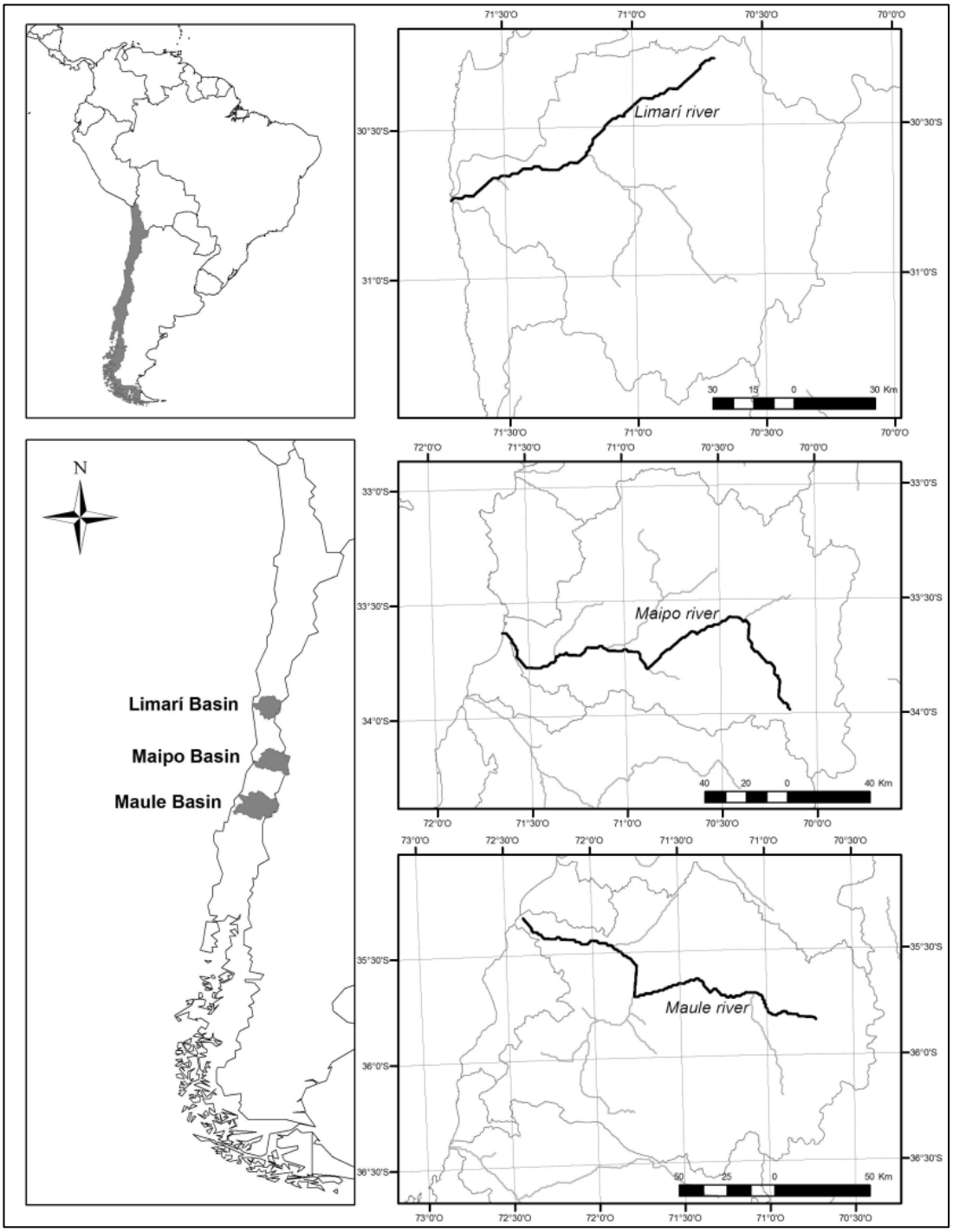

Figure 3-2: Limarí, Maipo and Maule river basins and their geographic location.

Table 3-1: Annual mean, standard deviation and coefficient of variation (CV) of precipitation and temperature recorded at Las Ramadas, Cerro Calán and Armerillo gauges.

Basin	Station	Years	Latitude	Longitude	Elevation [m]	Mean Precip. [mm]	Std. Dev. Precip. [mm]	C.V. Precip.	Mean Temp. [°C]	Std. Dev. Temp. [°C]	C.V. Temp.
Limarí	Las Ramadas	(1978-2005)	31º 01' 11" S	70º 35' 11" W	1,380	341.5	209.8	0.61	16.3	0.54	0.033
Maipo	Cerro Calán	(1978-2005)	33º 23' 42" S	70º 32' 12" W	848	452.2	201.0	0.44	16.3	0.40	0.025
Maule	Armerillo	(1978-2005)	35º 42' 04" S	71º 04' 38" W	492	2397.2	807.2	0.34	14.0	1.12	0.080

These three basins are representative of the Mediterranean climate conditions in central Chile. Differences in annual precipitation regime are observable in basic rainfall statistics obtained from rain gauges in each basin (Table 3-1). Annual rainfall increases from north to south, while the annual temperature tends to decrease (Table 3-1). On the other hand, the value of the coefficient of variance for precipitation decreases with latitude, reflecting a less variable inter-annual precipitation in the south. The historical control period used in our study goes from 1978 to 2005. The duration of this period was restricted on the one side by the availability of data and the existence of a shift of the Pacific Decadal Oscillation that took place between 1975 and 1976 that affects the stationarity assumption (Trenberth, 1990; Rosenblüth et al., 1997; Trenberth and Stepaniak, 2001; Giese et al., 2002; Boisier and Aceituno, 2006; Bown and Rivera, 2007). On the other hand, year 2005 corresponds to the end of historical control period of the GCM (Taylor et al., 2012).

For this study we considered 45 climate projections of 20 GCMs and their realizations from the fifth Coupled Model Intercomparison Project (CMIP5) (Taylor et al., 2012) listed in the Appendix C. A weighting factor corresponding to the inverse of the number of realizations of each GCM is used for each one of the 45 GCM projections (e.g. each one of the five CanESM2 projections have a weighting factor of $1/5$). Other alternative weighting criteria could be used.

3.4. RESULTS AND DISCUSSION

In this section we evaluate the effectiveness of the GCM pre-analysis strategy. For this purpose, we first validate the conventional analysis of all GCM runs as the best method to reproduce both the local climate and GCMs' statistics (subsection

3.4.1). We then use this approach as the reference to assess the ability of the GCM pre-analysis to reproduce the statistical moments of precipitation and temperature (subsection 3.4.2). Finally, in subsection 3.4.3 we compare future precipitation and its recurrence probabilities over several years estimated using the GCM pre-analysis and the conventional analysis of all GCM runs. Furthermore, we evaluate the error between both approaches by varying the number of trends considered on the GCM pre-analysis.

3.4.1. REPRODUCTION OF GCM PRECIPITATION CHANGE

The ability of the GCM pre-analysis to reproduce both the precipitation from the Limarí basin and the changes of the GCM projections is compared in Fig. 3-3 against the results from the conventional analysis, QMBC, the subset of five GCM and the delta change method. The GCM pre-analysis uses 45 trend percentiles of the mean, and the standard deviation trends are randomly selected after considering the correlation among them. To avoid producing results that are bias toward the GCMs with more realizations, each GCM realization is repeated *n* times, where *n* is the ratio between the least common multiple of the number of realizations of each GCM and the number of realizations of that specific GCM (i.e. each CanESM2 realization is considered six times, because the least common multiple of the number of realizations of each GCM is 30 and CanESM2 has five realizations).

The historical mean precipitation is well reproduced by all the methods, except the raw GCMs and the subset of five GCMs, which has not gone through bias correction (Fig. 3-3 a). Because it uses the historical record, the delta change always reproduces the historical mean. The percentage of change of the mean precipitation for the near period (2036-2063) according to the raw GCMs is well reproduced by all the

methods, except the QMBC (Fig. 3-3 b), whereas for the late period (2066-2093) is well reproduced by the delta change and both the conventional analysis and the GCM pre-analysis (Fig. 3-3 c). The subset of five GCMs partially reproduce the percentage of change in the late period, while QMBC tends to overestimate the negative changes. The best method in reproducing the mean precipitation and its change is the delta change, followed closely by both the conventional analysis and the GCM pre-analysis, which do not capture the exact range of change from the raw GCMs. This is explained by the fact that trend is assigned the last year of the moving window when built, which causes a time lag between the changes from the raw GCM and both methods. The subset of GCMs performs correctly in the near period, because the selection was done in this period, but in the late period its performance decreases. As noted also by Pierce et al. (2015), the QMBC method may significantly alter the changes projected by the raw GCMs.

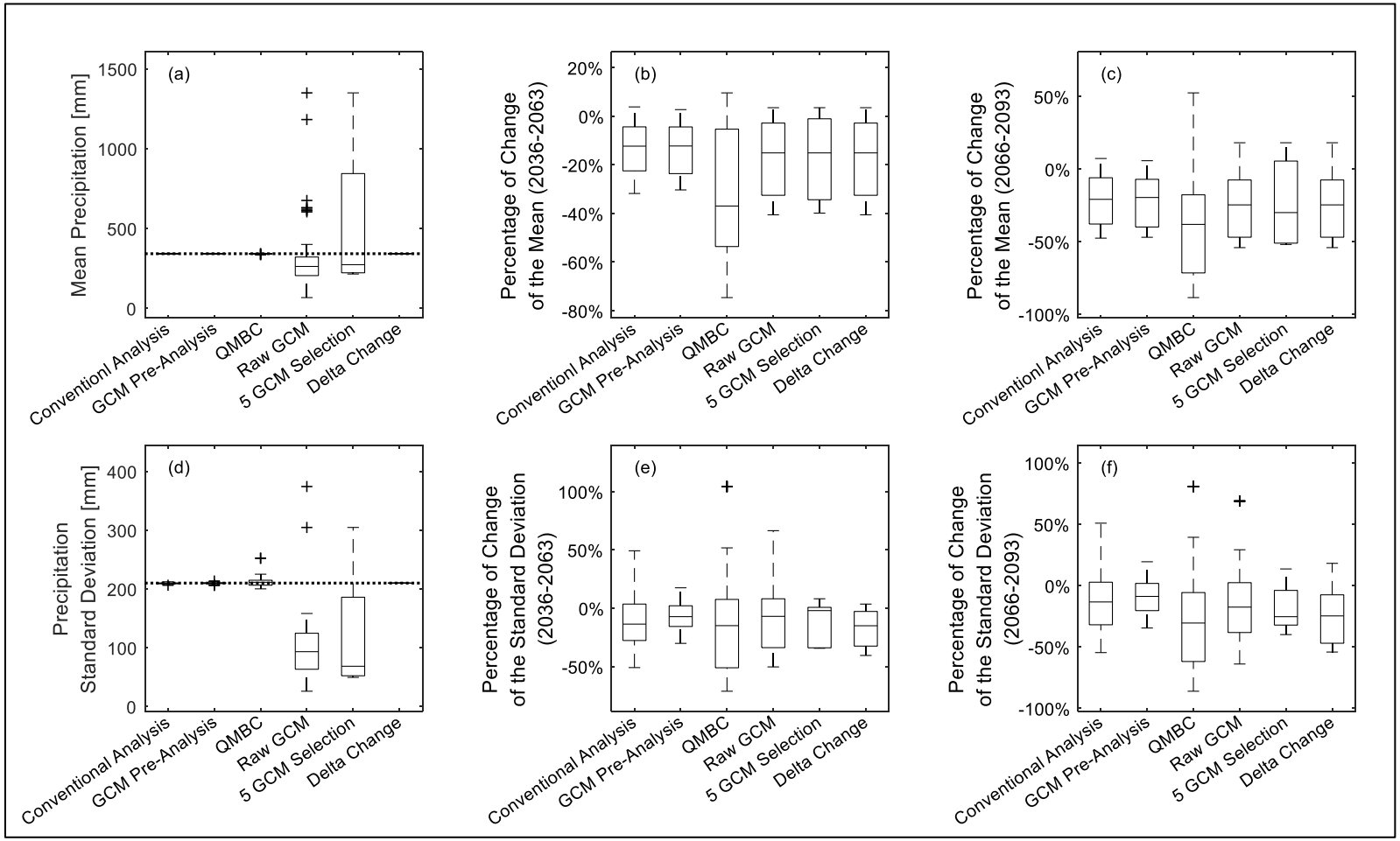

Figure 3-3: Performance of different downscaling or bias correction methods in reproducing the mean and standard deviation of historical precipitation (dotted lines) and its future change (%) for the Limarí basin.

The historical precipitation standard deviation is perfectly reproduced both by the conventional analysis, the GCM pre-analysis and by delta change, and very well reproduced by the QMBC (Fig. 3-3 d). The raw GCM and the GCM subset significantly underestimate the standard deviation. The percentage of change of the standard deviation for the near future (2036-2063) is best reproduced by the conventional analysis followed by QMBC (Fig. 3-3 e). Although the GCM pre-analysis is not able to correctly represent the range of the standard deviation changes, it represents the median change very well. Finally, both the GCM subset and the delta change perform poorly. For the late period (2066-2093) the conventional analysis is the best in representing the standard deviation changes (Fig. 3-3 f). Again, the GCM pre-analysis reproduce the median change well, but cannot capture the range of values correctly. All the other methods have trouble in reproducing the changes in the standard deviation.

Overall, the conventional analysis is the best method to both reproduce local climate and GCMs' statistics, followed by the GCM pre-analysis. Although the GCM pre-analysis does not perform as expected on the standard deviation changes, it represents the median change very well. The rest of the downscaling and/or bias correction methods have different problems in preserving the raw GCMs' changes.

3.4.2. REPRODUCTION OF THE CLIMATE TIME SERIES MOMENTS

Fig. 3-4 compares GCM percentiles of the first three moments obtained from the conventional analysis and the GCM pre-analysis (i.e. mean μ, standard deviation σ/coefficient of variation CV and skewness) of the future climate data (precipitation and temperature) for the three basins (Limarí, Maipo and Maule). This comparison

uses the simplest alternative for the percentiles of the trends, which is adopting the same percentiles for μ and σ trends on the GCM pre-analysis. Nonetheless this alternative may over-simplify the representation of the future climate. Note that climate data generated by using the conventional analysis has three dimensions: a GCM dimension, number of annual random realizations and time. In this case, the moments are calculated over the random realizations and then, for each year, percentiles are estimated by building the empirical CDF over the GCMs (Fig. 3-4). Because in the GCM pre-analysis percentiles are chosen while building trends, they are known before generating the climate data. Hence, in this case moments are estimated over the random realization for each year (Fig. 3-4). The selection of trend percentiles for μ and σ in the GCM pre-analysis before generating climate values, allows by construction to reproduce the same percentiles of the conventional analysis.

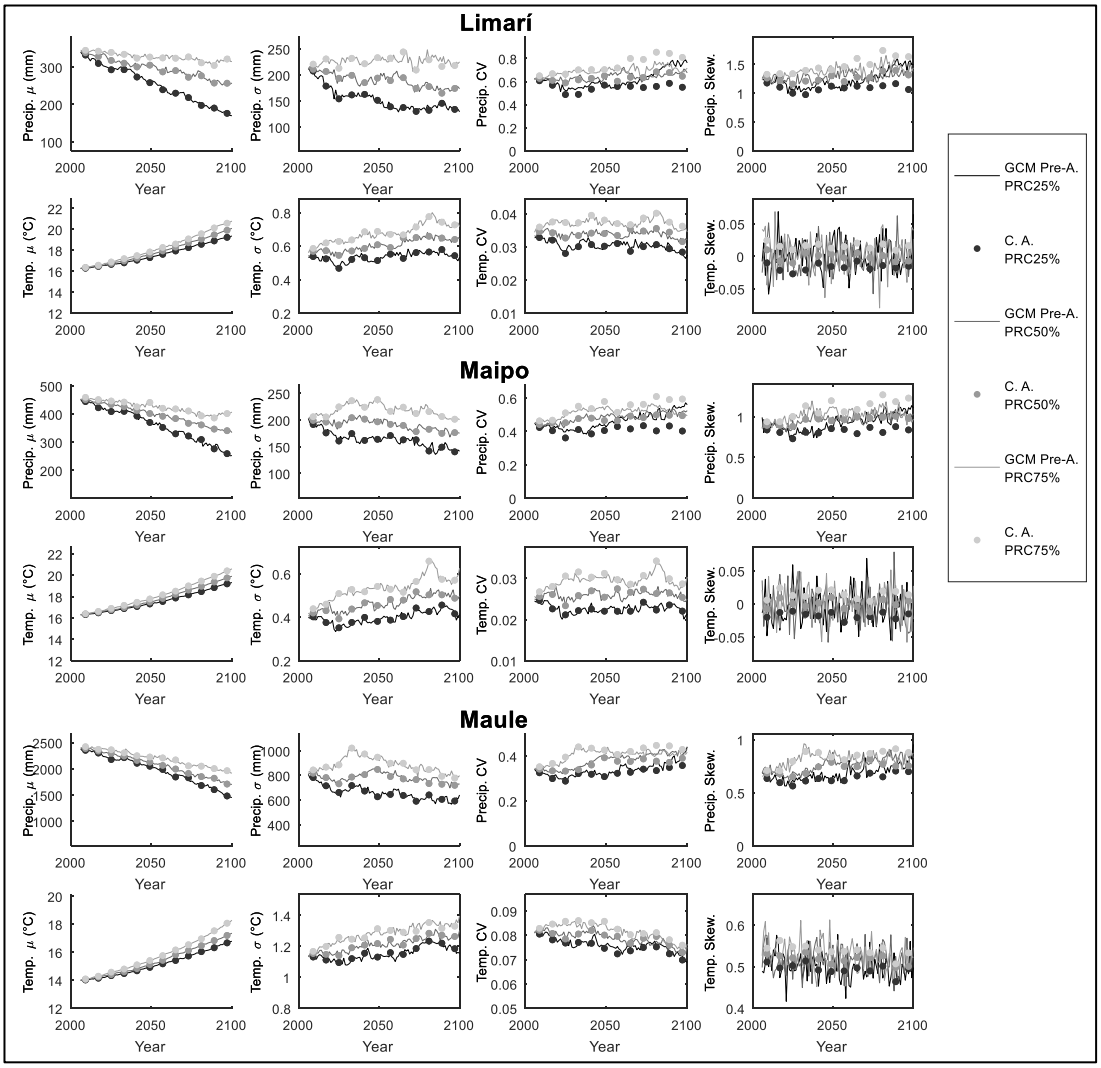

Figure 3-4: Comparison of the 25th, 50th and 75th GCM percentiles of the mean (first column), standard deviation (second column), coefficient of variation (third column) and skewness (forth column) obtained with the GCM pre-analysis and the conventional analysis (C. A.) approaches. The analysis is performed for precipitation (first, third and fifth row) and temperature (second, fourth and sixth row) in the Limarí (first and second row), Maipo (third and fourth row) and Maule (fifth and sixth row) basins. The same percentiles for the mean and the standard deviation were used in the GCM pre-analysis.

The mean and standard deviation of precipitation and temperature for the three basins (Fig. 3-4, first and second column) of GCM pre-analysis are the same as conventional analysis for the 25^{th}, 50^{th} and 75^{th} percentile. Hence, not only future values of μ and σ are the same, but also GCM percentiles can be chosen at the beginning, which simplifies the analysis when using the GCM pre-analysis. The CV and the skewness of the 50^{th} percentile of precipitation are the same for GCM pre-analysis and conventional analysis (Fig. 3-4, third and fourth column). Such level of agreement was not obtained for the 25^{th} and 75^{th} percentiles, especially after year 2050. For temperature, the behavior of CV produced by GCM pre-analysis and conventional analysis is very similar (Fig. 3-4, third column), with minor differences being observed for the Maule basin. Finally, temperature skewness obtained from the GCM pre-analysis and conventional analysis are similar although more variability is produced in the pre-analysis case (Fig. 3-4, fourth column). Overall, the moments obtained from GCM pre-analysis are quite close to the moments obtained from conventional analysis.

Because the same trend percentiles for μ and σ were used in the GCM pre-analysis shown in Fig. 3-4, the reproduction of moments obtained from conventional analysis is the best possible we could obtain. In reality however, these percentiles are not necessarily the same, although they are correlated (i.e. a GCM producing a big change in the mean, tends to produce a larger change in the standard deviation as well). Fig. 3-5 presents same results as Fig. 3-4, but GCM pre-analysis takes into account these differences between the trends for μ and σ. In this case, GCM pre-analysis uses 45 equally spaced percentiles of the mean, while percentiles for the standard deviation trends are randomly selected after considering the correlation among them. GCM pre-analysis moments are estimated along the dimension of the random realizations, and

then the percentiles are estimated from empirical CDF over GCMs for each year (Fig. 3-5). Note that results from conventional analysis in Fig. 3-4 and 3-5 are the same.

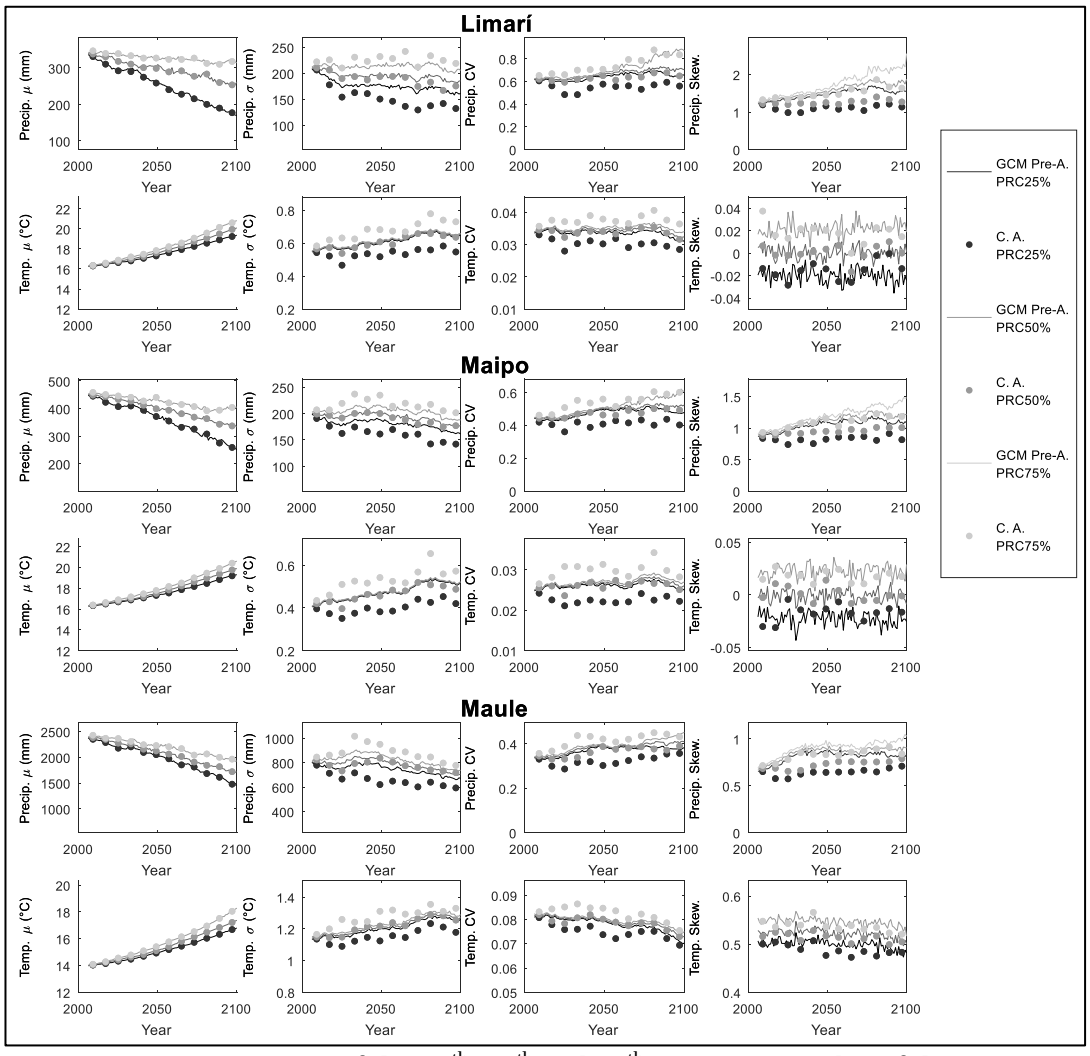

Figure 3-5: Comparison of the 25th, 50th and 75th GCM percentiles of the mean (first column), standard deviation (second column), coefficient of variation (third column) and skewness (forth column) obtained with the GCM pre-analysis and the conventional analysis (C. A.) approaches. The analysis is performed for precipitation (first, third and fifth row) and temperature (second, fourth and sixth row) in the Limarí (first and second row), Maipo (third and fourth row) and Maule (fifth and sixth row) basins. Randomly correlated percentiles for the mean and the standard deviation were used in the GCM pre-analysis.

For the three river basins, the 25th, 50th and 75th percentiles of μ for precipitation and temperature of climate generated with GCM pre-analysis and conventional analysis are the same (Fig. 3-5, first column). The skewness in temperature is also quite similar for all three basins (Fig. 3-5, fourth column), whereas for precipitation, they are not alike (i.e. the values from the conventional analysis are overestimated by the pre-analysis values). The pre-analysis and conventional analysis σ and the CV for both precipitation and temperature also differ, though in some cases the medians are similar (Fig. 3-5, second and third columns). The differences in σ are partially due to random selection of trend percentiles on the GCM pre-analysis, making comparison not completely fair. Note that mean is the only moment clearly changing across all three basins (Fig. 3-4 and 3-5), with reductions in precipitation and increases in temperature.

3.4.3. REPRODUCTION OF FUTURE PRECIPITATION

In the previous subsection the effectiveness of GCM pre-analysis was tested by its performance on the reproduction of the main statistical properties. We now test the ability of the method to reproduce future precipitation and the recurrence of different magnitudes and durations. We assess GCM pre-analysis approach by comparing future consecutive number of years with precipitation under a threshold by year 2070 for the Limarí, Maipo and Maule river basins against those estimated by the conventional analysis approach (Fig. 3-6). In particular, we count the number of time windows of 3, 6 and 10 consecutive years with precipitation under a certain value. In the case of conventional analysis, we counted the number of time windows in a 10,000 year realization of what is predicted for year 2070 by each of the 45 GCM projections.

The average number of time windows from the 45 series is then reported in Fig. 3-6 and compared against result from the GCM pre-analysis case. In the latter, the number of time windows was also obtained after averaging the number of time windows identified from each of the 10,000 simulations of year 2070 using 45 and 5 equally spaced trend percentiles of μ. The 45 trend percentiles were used to have the same number of trends and GCM projections, while using 5 trend percentiles implies a simplified version adopted to better understand the capacity of the proposed method to deal with uncertainty using a reduced number of trend percentiles. Note than in this case the percentiles of σ trend were randomly selected considering the correlation with the μ trend.

The difference (in percentage) between the results from both GCM treatment approaches when using the 45 trend percentiles decreases with the number of time windows being identified. The maximum percentage error decreases from -100% (Fig. 3-6e) to 12.2% (Fig. 3-6i) up to 3.3 % (Fig. 3-6a) as the average number of detected time windows goes from ~1 to 35 or more, up to 200 or more respectively. Overall the number of time windows for the three basins is similar regardless the length of the time window adopted, showing the effectiveness of GCM pre-analysis method to deal in a simple manner with a wide range of GCM climate projections. Interestingly, GCM pre-analysis with only 5 trend percentiles is remarkably similar to that using 45 trends, with maximum percentage errors a slightly larger than the ones previously mentioned.

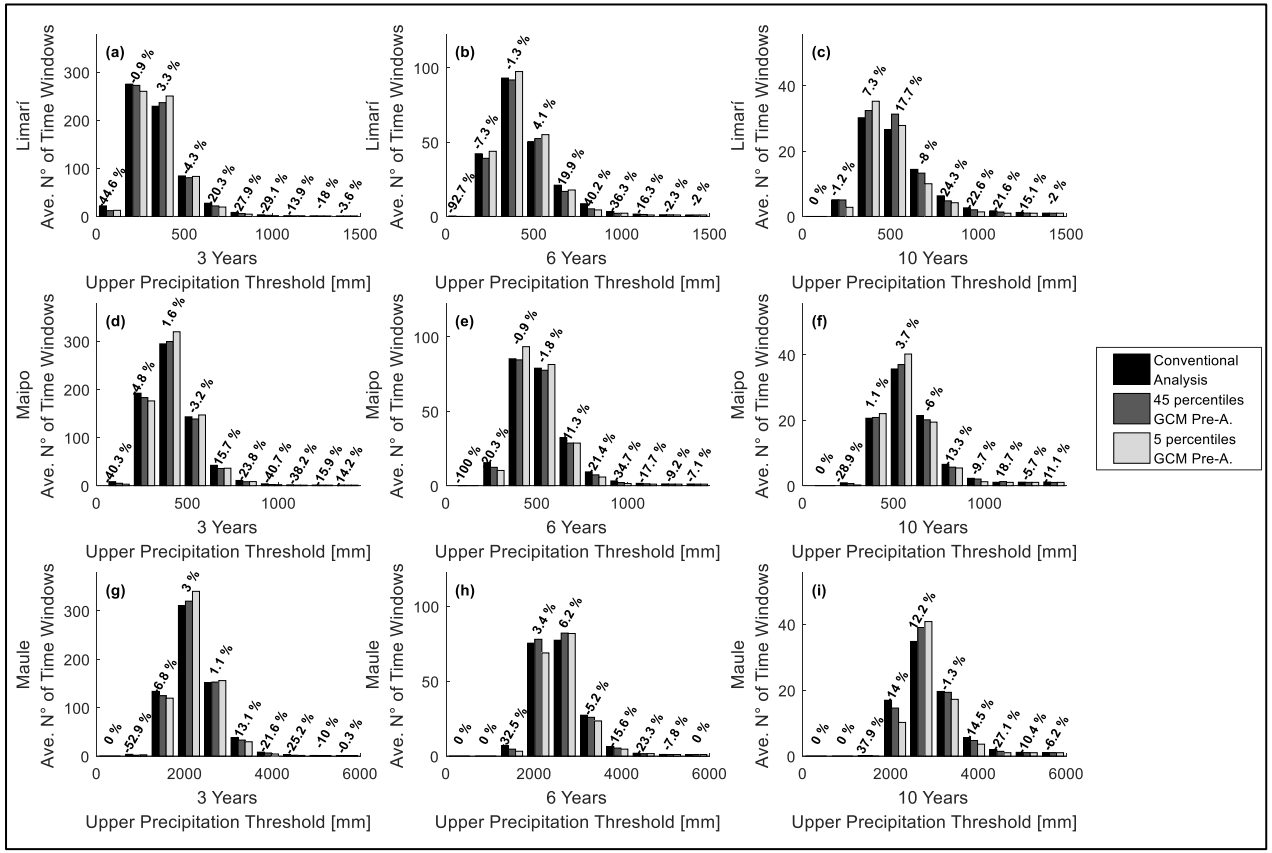

Figure 3-6: Average number of series with exactly 3, 6 and 10 consecutive years with precipitation under a certain value from 10,000 years of simulation with the 45 GCMs (conventional analysis), 45 percentiles and 5 percentiles for the climate series generator (GCM pre-analysis). The comparison is performed for the year 2070 for the three river basins. The difference in percentage between the 45 percentiles of GCM pre-analysis and conventional analysis is presented above the bars.

Future water scarcity is a big concern in Mediterranean regions, especially in those Chilean locations where a drier and warmer climate is expected (Vicuña et al., 2011; Meza et al., 2012; Vicuña et al., 2012; Demaria et al., 2013). Future precipitation conditions on Limarí, Maipo and Maule basins can be analyzed by estimating the probability of 3- 6- and 10-year precipitation falling below a certain threshold magnitude, regardless of what happens the years before or after. For this purpose, using conventional analysis approach, we simulated 10,000 years realizations of the future climate projections of years 2050 (mid-term) and 2090 (long-term). We used each of the 45 future GCM projections, and counted the number of times in which the above mentioned condition was identified. This number, divided by the total number of years of simulation is what was used to estimate the probability. For pre-analysis approach, we only used 5 equally spaced trend percentiles of μ. Again, the total count divided by the number of years in the simulation corresponded to the probability. Later on, we explain the rationale behind the selection of 5 percentiles.

The above-mentioned probabilities for the three basins and the two future years (2050 and 2090) are shown in Fig. 3-7. For example, for the year 2050, there is a 36% probability that the following 3 years will have less precipitation than the average of 341.5 mm in the Limarí basin (Fig. 3-7a). Note that these probabilities combine the effect of both climate uncertainty (i.e. that related to the standard deviation of the stationary precipitation) and uncertainty related to the discrepancy among the GCMs under RCP 8.5. To complement results in Fig. 3-7, Table 3-2 lists the probabilities of having 3, 6 and 10 consecutive years with less precipitation than the historical average reported in Table 3-1 for the study basins. Table 3-2 also has the probabilities of having 3, 6 and 10 consecutive years under the average for the stationary historical scenario.

For the stationary scenario, the current probability of having 3 consecutive dry years in the Limarí is 23%, which is similar that of Maipo (24%) and slightly higher than the one of Maule (20%). By year 2050 these probabilities increase in the Maipo to 40%, in Maule 38% and Limarí 36%. By 2090 the probability of having 3, 6 and 10 consecutive dry years for Maule basin (i.e. 59%, 38% and 24%, respectively) will be higher than the probabilities expected for the Maipo basin (54%, 33% and 20%) and the Limarí basin (49%, 29% and 17%).

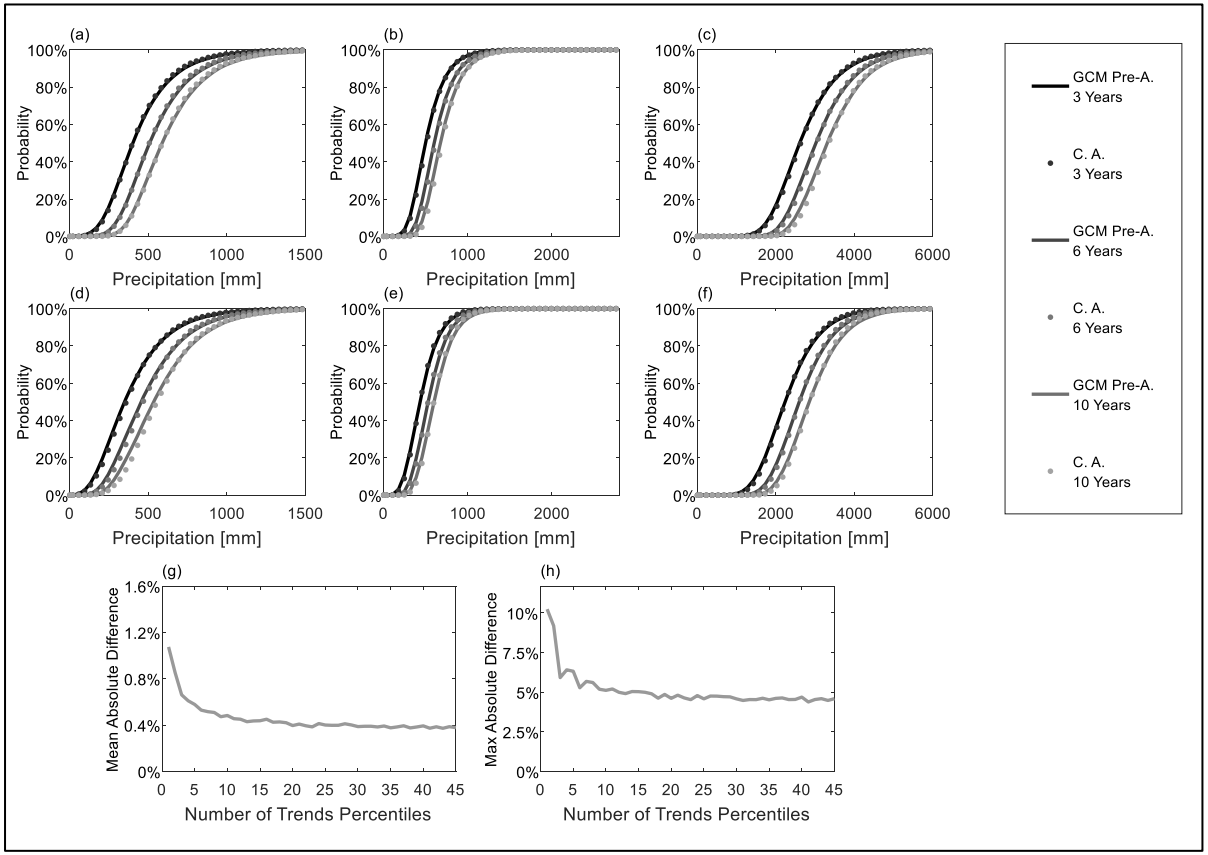

Figure 3-7: Probability of having 3, 6 and 10 consecutive years with precipitation lower than a certain value for the Limarí (a and d), Maipo (b and e) and Maule (c and f) basins, using GCM pre-analysis and conventional analysis (C. A.). The analysis is performed for year 2050 (a, b and c) and 2090 (d, e and f). The overall mean absolute (g) and maximum absolute (h) difference of the comparison of both approaches for several numbers of trend percentiles of the GCM pre-analysis.

Fig. 3-7g and Fig. 3-7h show the mean and maximum absolute difference of the probability of consecutive years below different precipitation thresholds between conventional analysis and GCM pre-analysis for different numbers of equally spaced mean trend percentiles. Note that plots consider all the basins, two future years of evaluation and several realizations for smoothing the curve. With 5 or more trends used for the GCM pre-analysis, differences with respect to the results from conventional analysis are significantly reduced. For example, by using only one trend in the GCM pre-analysis differences with conventional analysis are more than double the one obtained when using 5 or more trends. Fig. 3-7g and 3-7h support the use of the GCM pre-analysis approach for two reasons. First, using 5 to 10 trends significantly reduces the error compared to using a GCM single trend. Second, the difference between the GCM pre-analysis and conventional analysis is fairly small. Note that a GCM single trend is equivalent to the widely used single GCM ensemble (Kim and Kaluarachchi et al., 2009; Greene et al., 2012).

Table 3-2: Probability of observing 3, 6 and 10 consecutive years with precipitation lower than the historical mean for the Limarí, Maipo and Maule basins. Three cases are considered: a stationary scenario (S.S.) assuming historical values, and a mid-century (2050) and end of century (2090) year.

Basin	Station	3 consecutive years			6 consecutive years			10 consecutive years		
		S.S.	Year 2050	Year 2090	S.S.	Year 2050	Year 2090	S.S.	Year 2050	Year 2090
Limarí	Las Ramadas	23%	36%	49%	6%	15%	29%	1%	5%	17%
Maipo	Cerro Calán	24%	40%	54%	6%	18%	33%	1%	8%	20%
Maule	Armerillo	20%	38%	59%	4%	17%	38%	1%	7%	24%

To evaluate the severity of the future reductions in precipitation over the study basins, we defined the changes in annual precipitation ($CAP_{j,i}$) index, which is similar to the well-known Standard Precipitation Index (SPI) (McKee et al., 1993; Bhuiyan et al., 2006; Burke and Brown, 2008; Khan et al., 2008):

$$CAP_{j,i} = \frac{PP_{j,i} - \mu_i}{\sigma_i} \tag{3.11}$$

The $CAP_{j,i}$ index is computed for each year j using the moving average of i years. It corresponds to a standardized moving average annual precipitation obtained by subtracting the mean of the annual historical precipitation moving average (μ_i) from the i years moving average annual precipitation $(PP_{j,i})$ and dividing by the standard deviation of the annual historical precipitation moving average (σ_i).

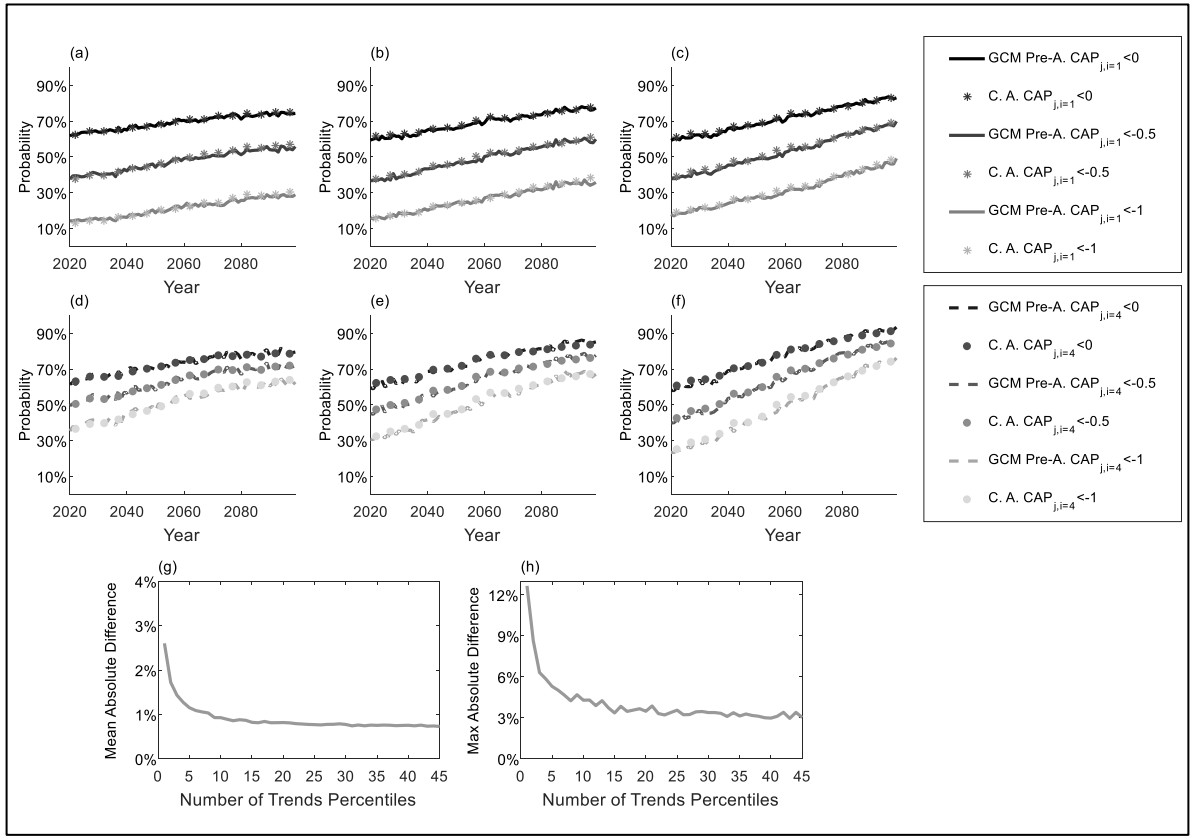

Figure 3-8: Probability of having $\boldsymbol{CAP_{j,i=1}}$ (a, b and c) and $\boldsymbol{CAP_{j,i=4}}$ (d, e and f) under 0, -0.5 and -1 for the Limarí (a and d), Maipo (b and e) and Maule (c and d) river basins, using GCM pre-analysis and conventional analysis (C. A.). The overall mean absolute (g) and maximum absolute (h) difference of the comparison of both approaches for several numbers of trend percentiles of the GCM pre-analysis.

Fig. 3-8 shows the continuous temporal change of the probability of having values of the $CAP_{j,i}$ index under 0, -0.5 and -1 in the three basins, for two values of moving average window (i.e. i = 1 and 4 years). Again, the results obtained from both the GCM pre-analysis and conventional analysis are compared, although in this case the continuous change is evaluated. These probabilities also combine the effect of both the climate uncertainty and the uncertainty related to the discrepancy among the GCMs under RCP 8.5. Only 5 equally spaced mean trend percentiles are used for GCM pre-analysis, while conventional analysis uses the 45 future GCM projections (Fig. 3-8 a through f). To assess the impact of the number of trend percentiles chosen for the pre-analysis approach, we used different numbers of equally spaced mean trend percentiles to calculate the mean difference and maximum absolute difference of the probability of having $CAP_{j,i}$ under 0, -0.5 and -1 between the conventional analysis and the GCM pre-analysis (Fig. 3-8g and Fig. 3-8h). Just as in Fig. 3-7g and 3-7h, the difference between having GCM pre-analysis and conventional analysis can be significantly reduced by considering 5 or more trends on the GCM pre-analysis, instead of the single median GCM ensemble. Again, the GCM pre-analysis allows reducing the error of not using a GCM group by using a multiple trend GCM ensemble, instead of a single median GCM ensemble.

The probability of $CAP_{j,i=1}$ being under 0 for year 2020 and 2100, goes from 62%, 59% and 59% to 74%, 77% and 83% for the Limarí (Fig. 3-8a), Maipo (Fig. 3-8b) and Maule (Fig. 3-8c) basins, respectively. The probability of having $CAP_{j,i=1} < -1$ for years 2020 and 2100 worsens for Limarí (i.e. going from 14% to 29%, Fig. 3-8a), Maipo (i.e. going from 16% to 36%, Fig. 3-8b) and Maule (i.e. going from 18% to 49% Fig. 3-8c) river basins. The Maule is the most affected basin, because the

probability of having more negative values of $CAP_{j,i=1}$ increases the most. The probability of $CAP_{j,i=4}$ being under 0 for year 2020 and 2100, also worsens significantly for the Limarí (i.e. from 61% to 80%, Fig. 3-8d), Maipo (i.e. from 60% to 85%, Fig. 3-8e) and Maule (i.e. from 58% to 93%, Fig. 3-8f) basins. Again, the probability of $CAP_{j,i=4}$ being under -1 for year 2020 and 2100 worsens for the Limarí (i.e. going from 35% to 63%, Fig. 3-8d), Maipo (i.e. going from 31% to 67%, Fig. 3-8e) and Maule (i.e. going from 23% to 76%, Fig. 3-8f) basins. Once more, the most affected basin is the Maule basin, showing a steeper slope of $CAP_{j,i}$, which indicates grater changes in its precipitation through the century.

3.5. CONCLUSION

In this chapter we propose an ensemble technique for the unbiased mapping of GCM changes in precipitation and temperature to local stations, based on both the statistical pre-analysis of the GCMs and the inclusion of natural climate variability. The method was implemented in three Mediterranean basins in Chile (Limarí, Maipo and Maule), and evaluated against a conventional analysis method in which each GCM is individually used to build future climatic scenarios from which percentiles are computed. This evaluation included the assessment of the ability to reproduce statistical moments, and to estimate the length, severity and probability of occurrence of precipitation under different thresholds. Moreover, the pre-analysis approach was also compared against commonly used downscaling and/or bias correction approaches (quantile mapping bias correction, a GCM subset selection and delta change). The following conclusions are emphasized:

- The best approach to reproduce both local climate and incorporate the changes from the raw GCM projections is the conventional analysis, followed by the GCM pre-analysis. Both methods outperform other commonly used downscaling and/or bias correction approaches.
- Results obtained using GCM pre-analysis and conventional analysis are very similar. On average there is less than a 0.4% difference between the probabilities of future years below different precipitation thresholds estimated with both methods.
- Using 5 to 10 trend percentiles obtained from the GCM pre-analysis is clearly better than using the single trend of the median GCM ensemble, as in the last case the uncertainty or discrepancy among the group of GCMs is not formally considered. The GCM pre-analysis has the advantage of building GCM ensembles that incorporate not only the mean or median, but also the entire range of climate projections of a group of GCMs.
- The GCM pre-analysis is able to simulate accurately the percentiles of the mean and the standard deviation of the temperature and precipitation of a group of GCMs. The percentiles of the skewness and coefficient of variation are less well represented.

Despite its good performance, the GCM pre-analysis is an ensemble technique that does not allow the preservation of the physical internal consistency of an individual GCM. If such consistency were crucial, the conventional analysis is recommended. Thus, the method here proposed must be understood as an ensemble-type approach that successfully preserves the local climate while incorporating the GCMs' statistical attributes.

Considering that the GCM percentiles can be chosen at the beginning of the GCM pre-analysis, the proposed method becomes an attractive alternative to assess climate change uncertainty and perform impact studies. Furthermore, the application of the approach to other river basins is quite auspicious due to its good performance in challenging basins with high annual precipitation variability. As the method incorporates both the local climate and the GCM changes, it allows the identification of the most vulnerable basins to climate change in a certain region or country, and the eventual prioritization of investments. From the three basins here studied, the Maule basin is the one for which we identified the highest probability of being drier in the future. Nevertheless, one should also consider the magnitude of changes in precipitation and the socioeconomic and environmental impacts of these drier conditions, before making any decision or taking action.

4. CHAPTER 4: WHEN SHOULD WE ADAPT? ASSESSING THE LOCAL TIME OF EMERGENCE FOR PLANNING ADAPTATION DECISIONS

4.1. INTRODUCTION

Hawkins and Sutton (2012) define Time of Emergence (ToE) as the time at which the signal of climate change emerges from noise of natural variability. ToE studies not only focus on precipitation (Giorgi and Bi, 2009; Hawkins and Sutton, 2011; Lee et al., 2016; Nguyen et al., 2018) and temperature (Diffenbaugh and Scherer, 2011; Hawkins and Sutton, 2012; Mahlstein et al., 2011; Mora et al., 2013), but also heat waves and extreme temperatures (Harrington et al., 2016; King et al., 2015; King et al., 2016; Lopez et al., 2018), sea level (Carson et al., 2016; Lyu et al., 2014), current system upwelling (Brady et al., 2017), and different ocean properties (Keller et al., 2014; Henson et al., 2017). Finding ToE allows decision-makers to plan the implementation of adaptation plans and the incorporation of GCM projections in the design of new infrastructure.

ToE is most commonly detected by a General Circulation Model (GCM) signal-to-noise ratio exceeding a certain threshold (Giorgi and Bi, 2009; Hawkins and Sutton, 2012; Keller et al., 2014; Lee et al., 2016; Lyu et al., 2014; Sui et al., 2014), although other alternatives have been proposed. For example, Muir et al. (2013) find the time at which the signal permanently exceeds the pre-industrial simulated control variability. Other studies detect significant difference in climate using the Kolmogorov-Smirnov test (King et al., 2015; Mahlstein et al., 2011; Mahlstein et al.,

2012a; Mahlstein et al., 2012b), although the statistical power of the test is neither reported nor used to identify the ToE year with a given probability.

ToE has been estimated almost exclusively for the entire world (Giorgi and Bi, 2009; Hawkins and Sutton, 2012), or at large scales including China, (Sui et al., 2014) and India (Akhter et al., 2018). Nevertheless, management decisions and adaptation strategies are implemented locally, where climate variability can differ considerably from that of the GCM projections. Moreover, a probabilistic approach in the identification of ToE is needed to incorporate its uncertainty in decision-making. Lehner et al. (2017) analyze different sources of uncertainty and demonstrated that GCM biases in variability significantly impact ToE detection. To the best of our knowledge the work of Akhter et al. (2018) is the only one considering these biases to estimate ToE using a Quantile Mapping Bias Correction.

At the current time, we have only found two works that estimate local ToE over streamflow. The first one corresponds to the initiative CIG - Time of Emergence (http://toe.cig.uw.edu) developed by the Climate Impacts Group and the Center for Data Science of the University of Washington (University of Washington, 2015). This initiative designed several tools -at the prototype level- to determine the ToE for 35 climatic variables using Variable Infiltration Capacity model (VIC) (Liang et al., 1994, 1996). Streamflow is one of the ToE variables estimated during different times of the years across counties, watersheds and major rivers of the Pacific Northwest in the USA. The second study in which ToE was computed for streamflow is that of Leng et al., (2016), who also analyzed streamflow projections from the VIC driven by 97 downscaled and bias-corrected CIMP5 climate projections over the conterminous United States (Reclamation 2014). Both studies were developed in north hemisphere,

particularly the USA, local hydroclimate ToE for the south pacific region of Latin America yet needs to be estimated.

From our literature review, we detected three important issues that should be better addressed, especially for the pacific coast of the southern hemisphere: (1) accounting for GCM biases in variability by considering both local climatic conditions and GCM projections when identifying the ToE; (2) determining the local ToE at a basin scale; and (3) determining the probability of certainty in the identification of the ToE. To cope with these issues, this chapter proposes a methodology to identify ToE for precipitation and temperature at a local scale. This methodology uses the statistical power to identify significant differences between climate series with natural variability and series that also incorporate GCM trend percentiles. We evaluated the methodology on the southern hemisphere pacific coast, by using three Chilean river basins under four representative concentration pathway (RCP) scenarios.

4.2. METHODOLOGY

4.2.1. CLIMATE TIME SERIES GENERATION

We use the climate time series generator method proposed by Chadwick et al. (2018a), which considers (1) the extraction of long-term trends from a GCM group, and (2) the generation of two sets of annual climate time series: a stationary one and another one incorporating these trends. The trends are extracted from the changes of a GCM group for each RCP. Precipitation mean changes from the GCM projection *G* (Fig. 4-1a) are obtained by the ratio between the moving averages of the GCM precipitation ($MAP_{t,G}$) and the average from the GCM control period ($AP_{t_o,G}$), where t and t_o are the last year of the moving window and the control period, respectively.

This ratio is called normalized moving average ($NMAP_{t,G}$) (Fig. 4-1d). The trends are built using all the $NMAP_{t,G}$ from each RCP (Fig. 4-1b). For each year *t* an empirical cumulative distribution function (CDF) of all the $NMAP_{t,G}$ is fitted (Fig. 4-1c). Finally, the trend percentile with a non-exceedance probability p_1, $NMAP_{t,p_1}$, is obtained from the CDFs of each year (Fig. 4-1f). Note that $NMAP_{t,p_1}$ corresponds to a statistical mapping of the changes from a GCM group, and several trend percentiles can be used to map the dispersion among the group of GCM results.

An analogous process is undertaken for precipitation standard deviation. The trend percentile of the standard deviation ($NMSDP_{t,p_2}$) with a non-exceedance probability p_2 is randomly generated considering the average correlation with the trend percentile p_1 of the mean, which is chosen. For temperature, a similar process for extracting the trends is applied, but the normalized moving difference between moving average of temperature and the average of the control period of the GCM is used instead.

For the generation of annual climate series of data (Fig. 4-1e), in each station of interest probability distribution functions (PDFs) $f_Y(y,\theta)$ are fitted to the observed annual records of the variable *Y* (temperature or precipitation) through the estimation of the parameter set θ using the mean μ and standard deviation σ. These PDFs are used to generate stationary time series of precipitation and temperature (Fig. 4-1g):

$$Y_i = F_Y^{-1}(u,\theta) = F_Y^{-1}(u,\mu,\sigma) \quad (4.1)$$

where u is a random uniform number [0,1], and Y_i is the i^{th} annual precipitation or temperature value randomly generated for the stationary set of climate.

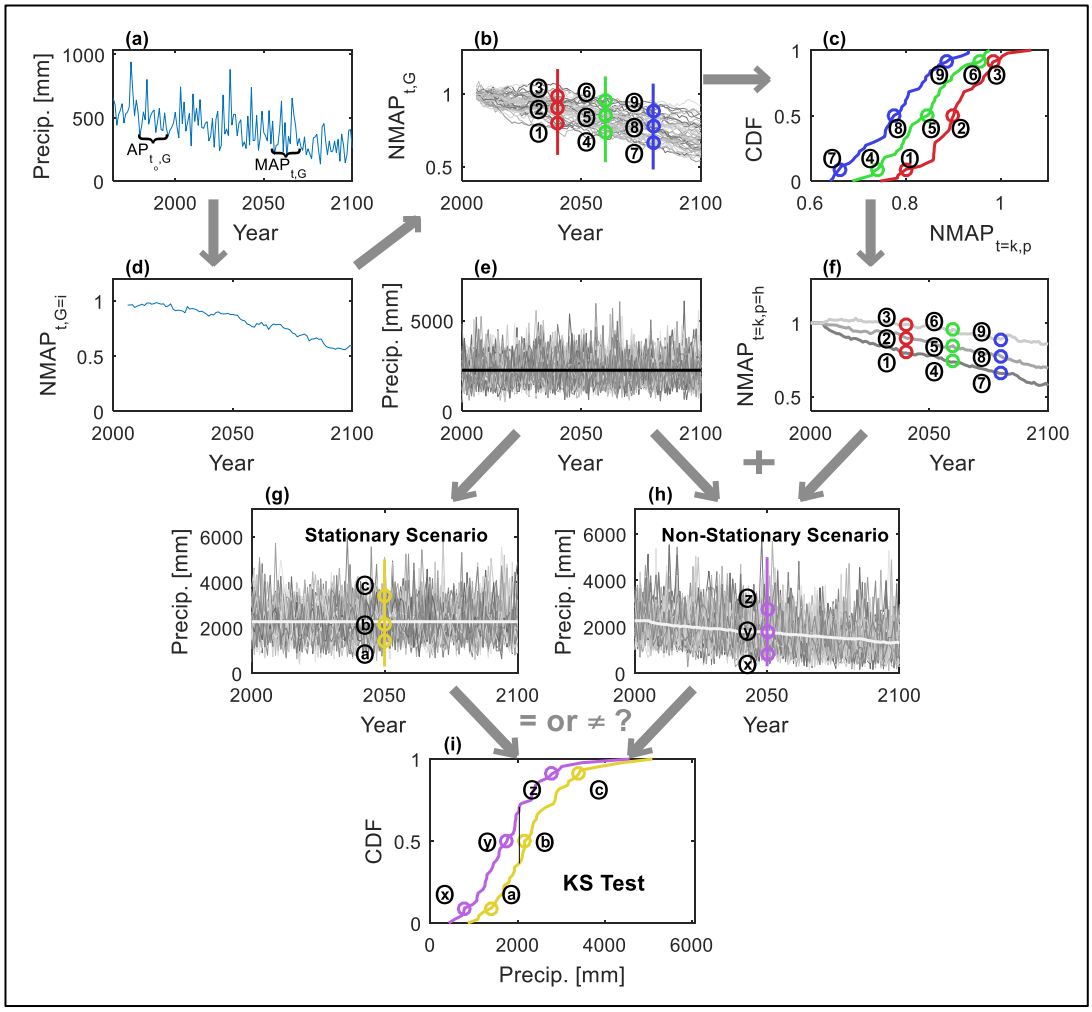

Figure 4-1: Representation of the future climate generation. From each GCM´s precipitation series (a) the normalized moving average is obtained (d). Several percentiles of the normalized moving average (b and c) are used to build the GCM trends associated with different percentiles (f). The annual time series generator (e) is used to obtain the stationary set of climate (g), and is also combined with the trends to obtain the non-stationary set of climate (h). Finally, the KS-test is applied each year to compare both sets of climates (i) and assess whether they belong to the same population.

A second set of annual climate data combines the GCMs trend percentiles and the local climate PDFs $f_Y(y,\theta)$ (Fig. 4-1h), case in which the parameter set θ change in time according to the GCMs. Hence, this set is a GCM ensemble that incorporates

the natural variability. Under this approach, the value of the climatic variable at any time for a given p_1 and RCP is the value obtained from the PDF, but with mean μ^* and standard deviation σ^* that change through time according to the trends:

$$Y_{t,i,p_1} = F_Y^{-1}(u,\theta) = F_Y^{-1}\left(u,\mu^*(t,p_1),\sigma^*(t,p_2)\right) \quad (4.2)$$

where Y_{t,i,p_1} is the i^{th} annual precipitation or temperature value randomly generated, using the trend percentile p_1 of the mean, for the non-stationary set of climate. The value of μ^* and σ^* in Eq. (4.2) at any particular year *t* for precipitation are calculated from the historical mean (μ) and standard deviation (σ) and the multiplicative normalized change rates:

$$\mu^*(t,p_1) = \mu \cdot NMAP_{t,p_1} \quad (4.3)$$

$$\sigma^*(t,p_2) = \sigma \cdot NMSDP_{t,p_2} \quad (4.4)$$

For temperature, μ^* and σ^* are obtained using the additive changes rates:

$$\mu^*(t,p_1) = \mu + DMAT_{t,p_1} \quad (4.5)$$

$$\sigma^*(t,p_2) = \sigma + DMSDT_{t,p_2} \quad (4.6)$$

4.2.2. IDENTIFYING TOE

To identify the ToE, the Kolmogorov-Smirnov test (KS-test) is used to evaluate whether or not the two sets of climate data generated for each year belong to the same population (null hypothesis H_o) (Fig. 4-1i). A value of 1 is assigned if the hypothesis is rejected and 0 otherwise:

$$KS_{t,j} = \begin{cases} 1 & \text{if } H_o \text{ is rejected} \\ 0 & \text{if } H_o \text{ is not rejected} \end{cases} \quad (4.7)$$

where *KS* is the result of the hypothesis test for year *t* of the repetition *j* of the test. Thus, the ToE corresponds to the year when the GCM trend makes the two sets of climate generated with Eq. (4.1) and (4.2) significantly different. Such difference is assessed by means of the statistical power (hereafter denoted power) of the KS-test (i.e. the probability of rejecting the null hypothesis when the alternative hypothesis is correct:

$$1 - \beta = \frac{\sum_{j=1}^{R} KS_{t,j}}{R} \tag{4.8}$$

where the power $(1 - \beta)$ is empirically estimated as the percentage of time the hypothesis H_o is rejected. A mean power larger than a threshold value *K* (e.g., *K* = 0.6) implies the identification of the ToE with probability *K* of making the correct assessment.

To reduce computational time and obtain the power from several KS-tests, a bootstrapping approach is implemented. A large number of climate series (i.e. 3000, corresponding to the total size N_1) are produced for each set of generated climate (i.e. the stationary climate and for each of the GCM trend percentiles). Through the bootstrapping, *R* samples of size N_2 are randomly selected from each set of generated climate, for which the KS-test is applied with a significance level $\alpha = 1\%$. A value of $N_2 = 1{,}062.76 \approx 1{,}000$ is determined by restricting the maximum difference between the cumulative distribution function of the two sets of climate data to 0.05 (i.e. $d_{0.01} = 1.63/\sqrt{N_2} = 0.05$) (Massey, 1951), whereas *R* = 100 to obtain a power value with 2 significant digits. Hence, over two repetitions, only $N_2/N_1 = 1/3$ of the sample size is

expected to be repeated. Nonetheless, a sensitivity analysis evaluating different values of α, N_1, N_2, and R is presented in the results section.

4.3. STUDY AREA AND CLIMATE SERIES

The methodology was applied to three Mediterranean basins in Chile, ranging from semi-arid to humid (Fig. 4-2): the Limarí, the Maipo and the Maule river basins (i.e. average precipitations of 341, 452 and 2397 mm, respectively). These basins have the Pacific Ocean to the west and the Andes Mountains to the east and are representative of climate conditions in central Chile (Table 4-1). Annual rainfall increases from north to south, while the temperature tends to decrease. Conversely, the values of the coefficient of variation (CV) reflect a decreasing inter-annual precipitation with latitude, having values of 0.61, 0.44 and 0.34 for Limarí, Maipo and Maule, respectively. The historical record used is restricted on one side by year 1976 to avoid the effect of a shift in the Pacific Decadal Oscillation that occurred between 1975 and 1976 (Boisier and Aceituno, 2006; Bown and Rivera, 2007; Giese et al., 2002; Rosenblüth et al., 1997; Trenberth, 1990; Trenberth and Stepaniak, 2001) and, on the other end, by year 2005, the historical control period of the GCMs (Taylor et al., 2012).

We considered 49 realizations of 20 GCMs (Table D1, from Appendix D) from the fifth Coupled Model Intercomparison Project (Taylor et al., 2012) under RCP scenarios 2.6, 4.5, 6.0 and 8.5 (Moss et al., 2010). Because each one of the GCMs was assumed to have the same weight, the inverse of the number of realizations of each GCM is used as weighting factor for each one of the 45 GCM projections (Chadwick et al., 2018).

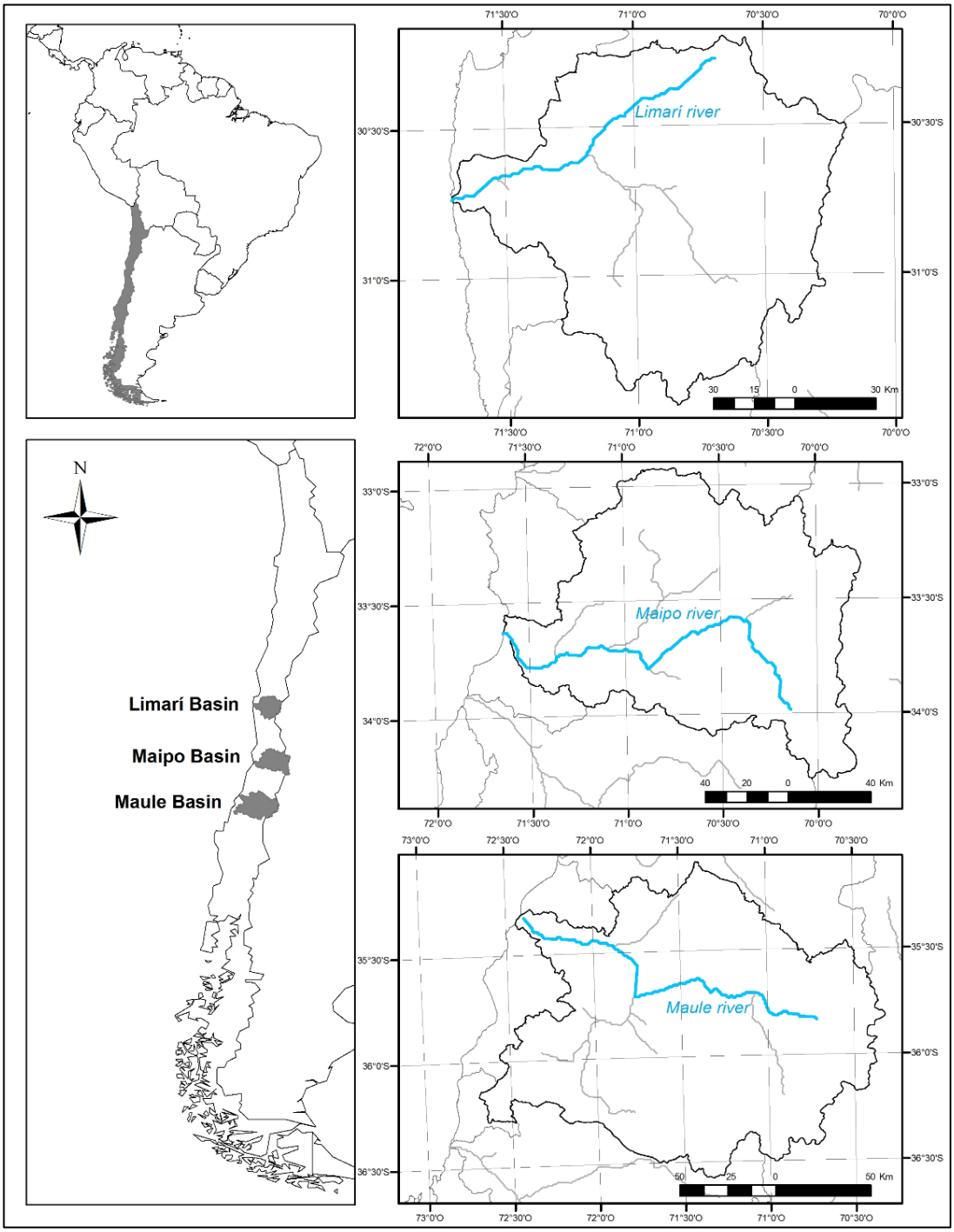

Figure 4-2: Case study basins and their locations in central Chile.

Table 4-1: Annual mean, standard deviation and coefficient of variation (CV) for precipitation and temperature recorded at rain gauges in the case study basins.

Basin	Station	Years	Latitude	Longitude	Elevation [m]	Mean Precip. [mm]	Std. Dev. Precip. [mm]	CV Precip.	Mean Temp. [°C]	Std. Dev. Temp. [°C]	CV Temp.
Limarí	Las Ramadas	(1978-2005)	31° 01' 11" S	70° 35' 11" W	1,380	341.45	209.81	61%	16.25	0.542	3.3%
Maipo	Cerro Calán	(1978-2005)	33° 23' 42" S	70° 32' 12" W	848	452.17	200.98	44%	16.30	0.401	2.5%
Maule	Armerillo	(1978-2005)	35° 42' 04" S	71° 04' 38" W	492	2397.18	807.24	34%	13.98	1.124	8.0%

4.4. RESULTS AND DISCUSSION

4.4.1. TIME OF EMERGENCE

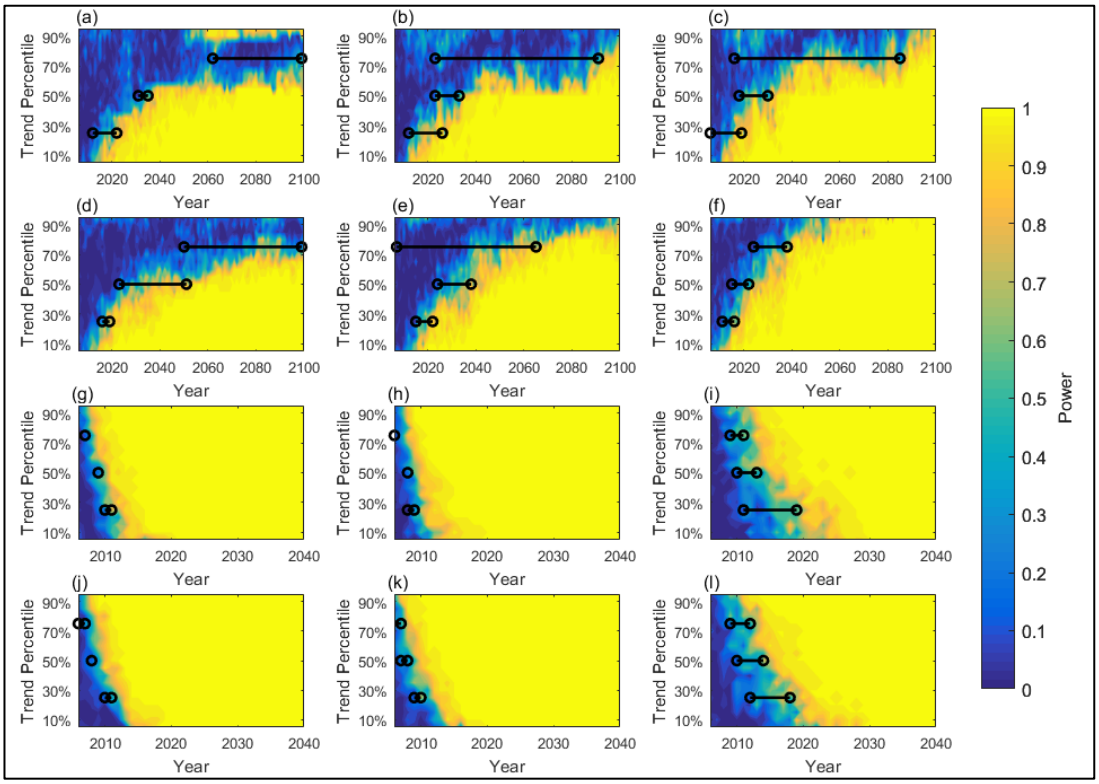

Figure 4-3: Power of the hypothesis test resulting over time and for different GCM trend percentiles of the mean, which represent the ToE of precipitation (a to f) and temperature (g to l) for the Limarí (first column), Maipo (second column) and Maule (third column) basins under RCPs 6.0 (first and third row) and 8.5 (second and fourth row). Black lines indicate the first and last year with power of 0.25 and 0.75 for the GCM 25th, 50th and 75th percentiles.

Fig. 4-3 shows the KS-test power for precipitation and temperature for each year under RCPs 6.0 (first and third row) and 8.5 (second and fourth row) for the three study basins. We used nineteen trend percentiles of the mean (5%, 10%,…, 95%) to characterize the GCM uncertainty (Fig. 4-3, y-axis). Black lines indicate the transition

zone of the ToE, identifying the first and last year with power of 0.25 and 0.75 for the 25th, 50th and 75th percentiles of the GCM trends. If the 0.75 threshold is never exceeded during the entire period, the transition zone is assumed to be beyond 2100.

Under RCP 6.0, changes in precipitation for approximately 20% and 10% of the GCMs do not emerge by 2100 in the Limarí (Fig. 4-3a) and the Maipo basin (Fig 4-3b) respectively, whereas for the Maule basin (i.e. the basin with the least inter-annual precipitation variability) the ToE takes place before 2100 for all the GCMs (Fig. 4-3c). Note also the sensitivity of the power to different trend percentiles, as the ToE associated with a power of 0.75 delays more than 60 years when considering the 75th trend percentile instead of the 25th one. Under RCP 8.5 the ToE for precipitation has not completely emerged by 2100 only for the Limarí basin (Fig. 4-3d), as the last computed ToE occurs close to 2100 in the Maipo basin (Fig. 4-3e), and between years 2050-2060 in the Maule basin (Fig. 4-3f). Again, the trend percentile impacts considerably the ToE identification, although the location also plays a significant role. Indeed, the ToE associated with a power of 0.75 delays more than 80 years for the Limarí basin when comparing the 25th and 75th percentile; this delay is reduced to ~20 years for the Maule basin. This difference among basins is most likely due to their different CV values (Table 4-1). Under RCP 6.0, the ToE manifests before 2100 in the Limarí basin for the highest percentiles of precipitation produced by a few of the GCM projections predicting increasing precipitation, as opposed to most of the GCM projections that predict future reductions. Shorter transitions of 10 years or less tend to be associated with the GCMs predicting higher precipitation reductions (below 30th percentile). Overall, the basin with the shortest transition zone is the Maule river basin (Fig. 4-3c and 4-3f). Finally, the transition zone for temperature occurs before 2020

for the three basins under RCPs 6.0 and 8.5 (Fig. 4-3g to 4-3l). Moreover, after 2030 there is a complete certainty (i.e. power of 1) that temperature differs from the historical one for all the GCMs in all the basins, with the ToE of the Maule basin being the last one. The impact of the trend percentile over ToE for temperature is much smaller than that for precipitation.

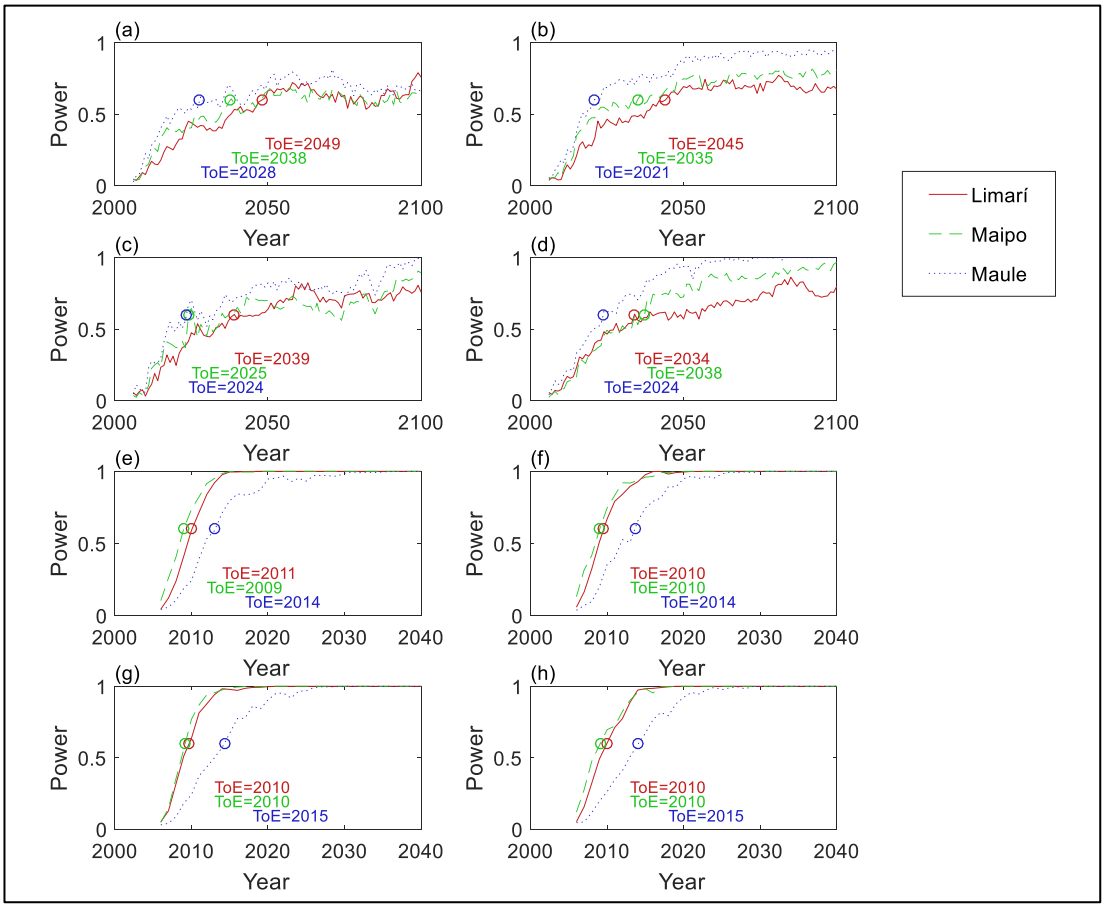

Figure 4-4: Average power trough time representing the ToE of precipitation (a to d) and temperature (e to h) for the Limarí, Maipo and Maule basins under RCPs 2.6 (a and e), 4.5 (b and f), 6.0 (c and g) and 8.5 (d and h). The circle marker indicates the ToE associated with a power of 0.6.

Fig. 4-4 shows the annual power average for each basin and RCP, which combines the 19 trend percentiles. For all the RCPs, the ToE of precipitation (Fig. 4-4a to 4-4d) occurs first in the Maule basin (dotted blue line) and last in the Limarí

basin (solid red line). If 0.6 is adopted as the threshold power value, under RCP 2.6 the ToE of precipitation would occur in years 2049, 2038 and 2028 for the Limarí, Maipo and Maule basins, respectively (Fig. 4-4a), while under RCP 8.5, these years are 2034, 2038 and in 2024 (Fig. 4-4d). None of the basins reach the power of 0.9 under RCP 2.6 (Fig. 4-4a), while only the Maule basin reaches a power value of 0.9 under RCP 4.5 (Fig. 4-4b). By 2100, Maule is the only basin with a power value of 1 under RCP 6.0 (Fig. 4-4c), while under RCP 8.5 the Maule and the Maipo basins reach a power of 1 by year 2070 and 2100, respectively (Fig. 4-4d). Limarí is the only basin that has a power below 0.9 under the four RCPs. Overall, for more pessimistic RCP scenarios ToE occurs earlier with a greater degree of certainty.

ToE for temperature occurs at the beginning of the century regardless of the RCP or basin (Fig. 4-4e to 4-4h). By the year 2020 both Limarí and Maipo basins have reached power values of 1 for temperature regardless the RCP, whereas the Maule basin reaches power values of 1 for temperature by year 2025 under all four RCPs. These results suggest that temperature changes significantly for all the GCMs and RCPs.

4.4.2. SENSITIVITY ANALYSIS

An analysis was performed to study the sensitivity of the transition zone (i.e. first and last year with power of 0.25 and 0.75) to changes in the parameters values involved in the approach (i.e. N_1, N_2, R and α). The analysis is performed for precipitation in the Maipo basin under RCP 8.5, although the results are similar for the other basins and RCPs. Changing N_1 does not have a clear impact on the ToE year (Table 4-2), while the ToE is detected sooner when increasing N_2. Furthermore, R does

not impact the results, although a minimum number of repetitions is required for the identification of the years with power values of 0.25 and 0.75. Lastly, as expected, increasing α reduces the ToE year. In fact, as α and, to a larger extent, N_2 affect the results by changing the value of the KS-test statistic, they must be selected carefully. Overall, we emphasize the relevance of a sensitivity analysis like the one presented.

Table 4-2: Sensitivity analysis of the first and last years in the transition zone (i.e power of 0.25 and 0.75), for the precipitation in the Maipo basin under RCP 8.5. Parameters used in subsection 4.4.1 are marked in gray.

	Total Size (N_1)					
Power	1500	3000	5000	8000	12000	17000
0.25	2014	2016	2016	2016	2017	2016
0.75	2044	2042	2043	2042	2045	2044
	Sample Size (N_2)					
Power	50	100	250	500	1000	2000
0.25	2059	2048	2032	2022	2016	2010
0.75	>2100	>2100	2085	2059	2043	2031
	Number of Repetitions (R)					
Power	25	50	100	250	500	1000
0.25	2016	2016	2016	2015	2016	2015
0.75	2044	2043	2046	2040	2045	2040
	Level of Significance (α)					
Power	1%	2%	3.5%	5%	7.5%	10%
0.25	2016	2013	2012	2011	2008	2007
0.75	2047	2041	2035	2035	2032	2031

4.5. CONCLUSIONS

This work proposes a method to detect the emergence of climate change at a basin scale using trend percentiles of the GCMs projections and local climate information. By means of the statistical power, the method identifies differences between stationary historical climate and the non-stationary local climate generated

using these projections. Thus, the method enables the comparison of the ToE at different locations under a specific RCP scenario with an uncertainty assessment of a large group of GCMs. Moreover, it provides information to prioritize the implementation of local risk assessment and adaptation measures.

From the analysis of three Mediterranean basins in Chile (i.e. Limarí, Maipo and Maule), the precipitation ToE occurs later for higher values of the local coefficient of variation (CV). Thus, climate change signal emerges from the local climate first in the Maule basin, and then in the Maipo and Limarí basins. Nevertheless, the relationship between ToE and CV among different locations may not hold for other cases, as the ToE also depends on the strength of the GCMs signal. Furthermore, the chosen GCM trend percentile significantly impact the ToE detection due to differences in the strength of the climate signal. Thus, the ToE associated with a given power can be delayed in several decades when considering different trend percentiles.

As expected, the implementation of the statistical test to differentiate the changing climate from the stationary climate affects the ToE identification. The parameters impacting this implementation are those affecting the acceptance or rejection of the KS-test (i.e. the sample size and the level of significance α).

Overall, under a continuous change the emergence cannot be assigned to a single year, unless threshold values of those evolving metrics (statistical power for this study) reflecting the climate dynamics are defined. Nevertheless, there will not be a total certainty that the change has taken place by exceeding the defined threshold values.

5. CHAPTER 5: COPING WITH WATER SCARCITY IN A DRYING BASIN: A PROGRESSIVE REDUCTION OF WATER ALLOCATION AS A RESERVOIR OPERATION STRATEGY UNDER CLIMATE CHANGE SCENARIO

5.1. INTRODUCTION

Water management has been interested in optimal reservoir operation policies for a long time. Optimal operation has been studied by using different approaches and techniques, such as linear programming (e.g. Datta and Houck 1984; Yoo 2009), nonlinear programming (e.g. Lall and Miller 1988; Simonovic and Marino 1982; Sinha et al. 1999), or dynamic programming (e.g. Bras et al. 1983; Stedinger et al. 1984). The reservoir operation performance is typically evaluated trough performance indexes, with reliability, resiliency and vulnerability (RRV) (Hashimoto et al. 1982) being the most widely used (Moy et al. 1986; Kjeldsen and Rosbejerg 2004; Kundzewicz and Kindler 1995; Fowler 2003; 2007; Goharian et al., 2017; Zhang et al., 2017; Alameddine et al., 2018). The RRV approach implies a multi objective problem, having a tradeoff among the indexes that are correlated to a certain extent (Moy et al. 1986; Bayazit and Ünal 1990; Srinivasan and Philipose 1996, 1998; Zhang et al., 2017). Water management attempts to avoid extreme failures, which are typically worse than several minor failures (Draper and Lund 2004; Hashimoto et al. 1982; Shih and ReVelle 1994, 1995; Srinivasan and Philipose 1996, 1998). Increasing the storage by holding water to reduce future larger losses, although compromising immediate benefits, is known in reservoir operation as hedging (Srinivasan and Philipose 1998). This concept has been extensively addressed in the literature (Eum et

al. 2011; Jain 2014; Shiau 2009, 2011; Shih and ReVelle 1994, 1995), and its optimal value is obtained when the marginal benefit of water release is equal to the marginal benefit of storage (Damper and Lund 2004).

Costs and benefits analysis tools are fundamental for designing and operating water infrastructure projects, as well as estimating the involved system performance (Bras et al. 1983; Datta and Burgos 1984; Datta and Houck 1984). Such analyses must consider uncertainty, a key challenge in water resources planning and management. Typically, uncertainty in water management has been characterized and quantified by assuming stationarity. Nonetheless, hydro-climatic variables are changing due to climate change, and thus decision making should no longer assume a stationary future (Milly et al. 2008; Milly et al. 2015). Several studies have focused on quantifying climate variability and trends in precipitation and temperature under future scenarios, and their potential effects over water resources (e.g. Fowler et al., 2005; Mondal et al., 2010; Walton et al., 2017; Shi et al., 2018; Smitha et al., 2018). Other studies have assessed the impacts of these changes on water management systems and infrastructure (e.g. Fowler et al., 2007; Kim and Kaluarachchi, 2009). Typically, these studies adopt a top-down approach starting with the climate projections from General Circulation Models (GCM) for different representative concentration pathways (RCP) scenarios. These projections are downscaled to the domain of interest, and used to simulate specific impacts over different sectors, activities or components of the environment, such as infrastructure, crops, cities, ecosystems (Wilby and Dessai 2010; Kiparsky et al. 2012). Unfortunately, this approach is associated with an increasing cascade of uncertainty (Wilby and Dessai 2010), which makes decision making very difficult (Hallegatte 2009).

Some studies have broadly analyzed different sources of uncertainty under climate change, by measuring reservoir operation's performance (Brekke et al., 2009; Georgakakos et al., 2012; Steinschneider et al., 2015a, 2015b; Whateley and Brown, 2016). Moreover, some studies recently evaluated the uncertainty of climate change on the reservoir performance using RRV indexes (Steinschneider and Brown, 2012; Adeloye et al., 2016; Schlef et al., 2017; Soundharajan et al., 2016; Chadwick et al. 2018b). Adeloye et al. (2016) studied the impact of hedging under climate change. To the best of our knowledge, only Chadwick et al. (2018b) and Soundharajan et al. (2016), who deepened the initial assessment by Adeloye et al. (2016), have evaluated the variability of reservoir performance indexes under climate change impact assessment. Because Soundharajan et al. (2016) and Adeloye et al. (2016) used a delta change approach (e.g. Vicuña and Dracup 2007; Hay et al. 2000; Diaz-Nieto and Wilby 2005; Minville et al. 2008) to incorporate climate change, the impacts of a continuously changing climate was not evaluated. In fact, an assessment of a reservoir performance through time in which this continuously changing climate is considered, would allow evaluating an adaptation strategy based on a continuously varying water allocation goals. Such task has been performed before (Vicuña et al. 2010), to the best of our knowledge, it has not been addressed considering an uncertainty assessment using a special treatment that incorporates several GCMs and the four RCPs, as would be required for a robust result, as discussed by Chadwick et al. (2018a).

The objective of this chapter is to evaluate the performance of two different reservoir water allocation strategies under an uncertain and continuously changing climate, which are restricted to maintain historical levels of reliability. The strategies are compared against the historical water allocation goal, and include a (1) single and

permanent reduction (i.e. constant), and (2) a progressive reduction in time of the water allocation goal. In the assessment we use RRV indexes to evaluate the reservoir performance within a probabilistic framework, which considers both local variability and the uncertainty induced by several GCMs. The method is applied to the Paloma Reservoir System, located in the Limari river basins in the Semiarid Mediterranean region of Chile. The outline of this chapter is as follows: section 5.2 describes the study area and its reservoir system; section 5.3 explains the details of the different methods involved in the evaluation; section 5.4 shows the results and the discussion; and section 5.5 presents the main conclusions.

5.2. THE LIMARÍ RIVER BASIN AND THE PALOMA RESERVOIR SYSTEM

The Limarí River basin is a semiarid snow dominated basin with an area of 11,800 km^2 and is located in north central Chile, with its outlet at 30º43’51’’S, 71º42’01’’W. The available monthly records of precipitation and temperature for period 1971-2005 (i.e. historical period) shows a large spatial variation in precipitation, increasing from the coast to the Andes, and from north to south, with annual average ranging from 100 to 300 mm. Precipitation occurs mostly during autumn and winter (May to August), and snow accumulates in the upper half of the basin. The inter-annual variability of precipitation is high (i.e. coefficient of variation of 0.65 - 0.75 for different gauge) due mostly to the El Niño Southern Oscillation (ENSO). Stream flow from melting is significant during spring and summer (September to January).

The Limarí basin has the Paloma reservoir system, which supplies water to approximately 500 km^2 of irrigated land and drinking water to the city of Ovalle (110,000 inhabitants). The system is composed of the Paloma, Cogotí, and Recoleta reservoirs, whose capacities are 750, 150, and 100 Mm^3 respectively (i.e. a total of 1000 Mm^3 for the system) (Fig. 5-1). This capacity exceeds largely 400 Mm^3, the average annual inflows to the system, which allows the control of the inter-annual variability caused by ENSO. The intra-annual stream flow variability is naturally regulated by the snow accumulation and melting processes. Because of climate change, spring and summer flows are expected to shift into the winter (Vicuña et al., 2011; 2012). Thus, the reservoir system should participate more actively in controlling this variability in the future.

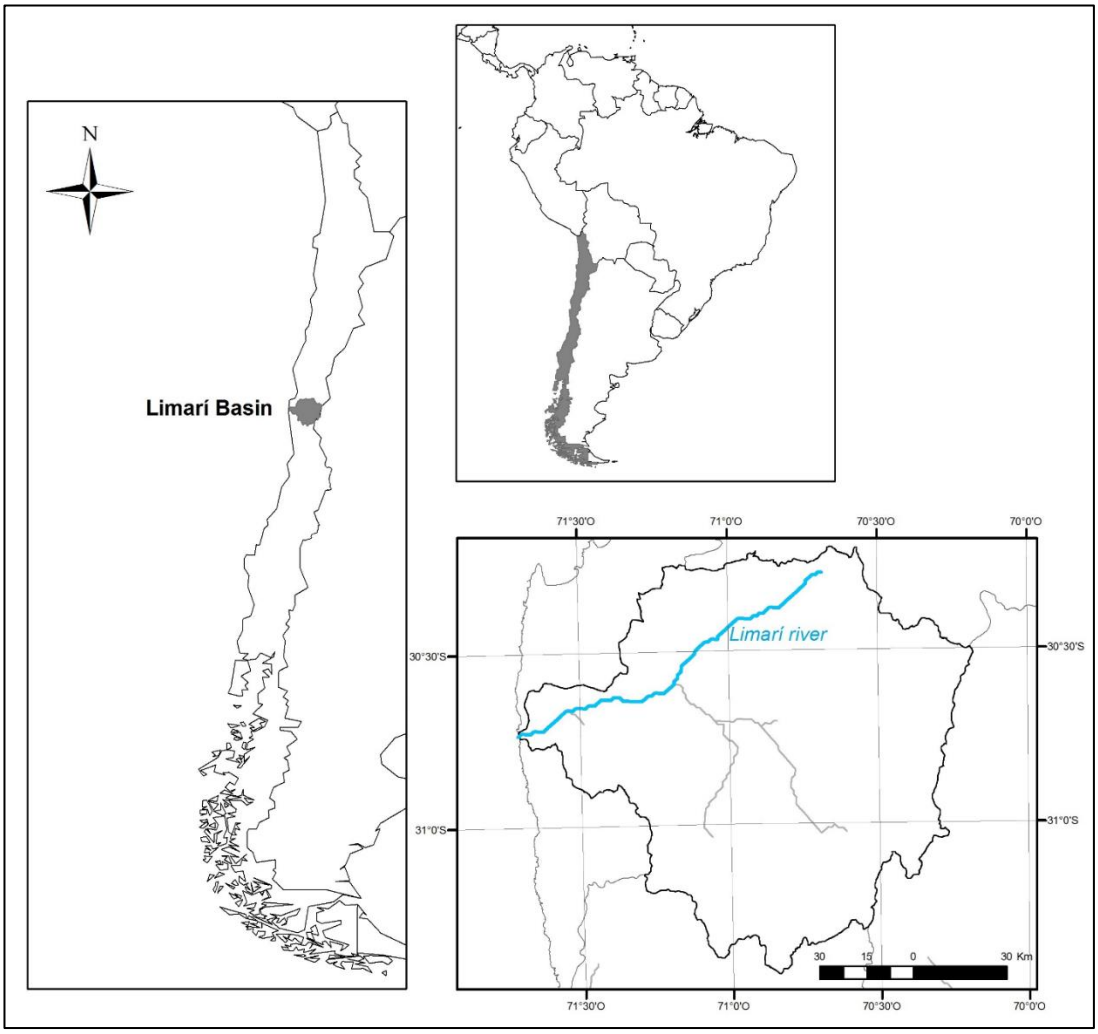

Figure 5-1: The Limarí river basin and its location in central Chile.

The current operation rule of the reservoir system was developed by Ferrer et al. (1978), who simulated the inter-annual variability and various allocation scenarios based on precipitation and streamflow data from 1944 to 1976. They estimated annual volumes of 138 and 220 Mm^3 for the 3- and 4-year moving average of the annual inflows to the system with 85% of exceedance probability. The large difference between these two values led them to conclude that a wet year is expected to follow three dry years. Hence, three years was considered to be the critical period for the inter-

annual planning of the reservoir system, leading to a single annual allocation decision that works on the long-term horizon (Ferrer et al., 1978).

The stored volume S (m^3) in reservoir j at a year t+1 is given by:

$$S_j^{t+1} = S_j^t - O_j^t + I_j^t - E_j^t - Sp_j^t \quad (5.1)$$

where O , I and Sp are the outflow, inflow and spilled water, respectively (m^3), and E is the net evaporation from the reservoir (m^3), given by:

$$E_j^t = A_j^t\left(S_j^t\right) \cdot \left(e_j^t - P_j^t\right) \quad (5.2)$$

Where e is the evaporation (m), P is the precipitation (m), and A is the surface area (m^2), which is related to the water stored. S is restricted to the range defined by the maximum storage capacity MS (m^3) and the dead storage DS (m^3):

$$DS_j \leq S_j^t \leq MS_j \quad (5.3)$$

The annual allocated water in year t+1 (O_j^{t+1}) is function of the stored water in the system composed of M reservoirs at year t ($S_T^t = \sum_{j=1}^{M} S_j^t$). If S_T^t exceeds a threshold or restrain bound (RB), a fix amount α_j^t is allocated from reservoir j. Otherwise the allocated water is a fraction r of the total storage.

$$O_j^{t+1} = \begin{cases} \alpha_j^t & \text{if } S_T^t \geq RB \\ r^t \cdot S_j^t & \text{if } DS_j \leq S_T^t < RB \\ 0 & \text{if } 0 \leq S_T^t < DS_j \end{cases} \quad (5.4)$$

Ferrer et al. (1978) determined constant values of α = 240, 40 and 40 Mm^3 for the Paloma, Recoleta and Cogotí reservoirs respectively, as well as values of RB = 500 Mm^3 and r^t = 0.5. Thus, if the system storage exceeds 500 Mm^3, the maximum allowed annual water allocation is 320 Mm^3. Otherwise; half of the stored water is

allocated. To evaluate the impact of the constant and progressive reduction of the water allocation goals, the values of α and r will be altered on this study.

5.3. METHODOLOGY

A suite of methods and tools were used in this study to link climate, hydrology, the reservoir system and its performance under different water allocation goal strategies. First, local climate records as well as precipitation and air temperature outputs from several GCMs runs under the four different RCPs were used to generate synthetic climate data. These climate data were used as input to a hydrologic model of the Limarí River basin to obtain the corresponding stream flow series. The performance of the reservoirs system under these stream flow scenarios is characterized through different performance indexes. Finally, we use these stream flow scenarios to assess and compare the performance of the adaptation strategies to climate change defined according to two goals, i.e., a constant and a progressive reduction of the water allocation.

5.3.1. GCM, GREENHOUSE GASES CONCENTRATION SCENARIOS, DOWNSCALING METHOD AND CLIMATE TIME SERIES

A wide range of GCMs and greenhouse gases concentration scenarios are needed to study and characterize the uncertainty induced by them. This study uses the RCPs 2.6, 4.5, 6.0 and 8.5 (Moss et al. 2010) and 49 realizations of the GCMs (Appendix D), defined according to the 5th phase of the Climate Model Intercomparison Project (Taylor et al. 2012). We adopted the ensemble technique for the unbiased mapping of GCM changes to local stations proposed by Chadwick et al. (2018a), in which both the local climate variability and the GCMs' statistics are

preserved. In the method trend percentiles are extracted from the GCM group and combined with annual local precipitation and temperature data generated from the empirical cumulative distribution function (CDF) fitted to historical records, to generate non-stationary local climate series for the respective percentiles. To maintain the historical spatial correlation and the correlation between temperature and precipitation, a Vector Autoregressive Model VAR(0) is used as explained in Chadwick et al. (2018a).

In this study five scenarios are evaluated: a reference historical scenario (here after denoted stationary), and four RCPs scenarios (2.6, 4.5, 6.0 and 8.5). For the stationary scenario the historical climate from the period 1971-2005 is used to generate 200 synthetic realizations of the future climate (2011-2100). For each RCP scenario, 200 realizations of the future climates are generated using trend percentiles mapping the dispersion of the outcomes from the results of the group of GCM runs for each RCP and the local climate information. Ten equally spaced trend percentiles for the changes of the precipitation mean are adopted, as recommended by Chadwick et al. (2018a), while the trend percentiles of the precipitation standard deviation, temperature mean, and standard deviation are randomly selected considering the correlation among them (for more detail see Chadwick et al. 2018a). For each trend percentile 20 synthetic realizations are generated, adding a total of 200 synthetic future realizations for each RCP scenario.

The annual data are disaggregated at a monthly scale through the resampling of historical data with a modify version of the k-NN method (Greene et al. 2012; Rajagopalan and Lall 1999), which preserves the intra-annual historical climate structure. This method compares the value of the standardized annual precipitation or

temperature generated for year *a* to be disaggregated ($y_{g,a}$) against the standardized historical annual value ($x_{g,b}$) of year *b* for the record *g* (note that a record is any of the series of precipitation or temperature data recorded within the study area). Furthermore, the standardization consists in subtracting the historical mean and dividing by the historical standard deviation. The weighted Euclidean distance ($d_{b,a}$) is then given by:

$$d_{b,a} = \sqrt{\sum_{g=1}^{m} w_g \left(y_{g,a} - x_{g,b}\right)^2} \tag{5.5}$$

where w_g is the weight factor of the record *g* used to weight the squared differences between the generated and historical standardized data, and *m* is the total number of records in the study area. Equal weights were used, with $w_g \geq 0$ and $\sum w_g = 1$, because of the standardization implemented for the data before the comparison. Each of the *b* values of $d_{b,a}$ for the data generated in year *a* obtained with Eq. (5.5) are used to sort the $x_{g,b}$ in ascending order. The first *k* values of $x_{g,b}$ with the smallest values of $d_{b,a}$ are selected, and the probability p_h of choosing one of them is defined as:

$$p_h = \frac{1/h}{\sum_{i=1}^{k} 1/i} \tag{5.6}$$

where *h* is the ranking position in ascending order. Afterwards one of the $x_{g,b}$ is randomly selected using p_h. The heuristic approach proposed by Lall and Sharma (1996) and adopted by Rajagopalan and Lall (1999) and Yates et al. (2003) suggests that $k = \sqrt{L}$, with *L* = number of years in the historical record. For this study *L* = 35 years, and thus $k \approx 6$. Finally, there is a correction of climate variables of the selected year $x_{g,b}$, by multiplication and addition in the case of precipitation and temperature

respectively, so that the chosen year fits the annual generated data y_g, just as in Greene et al. (2012). Note that other disaggregation alternatives that allow changes at the intra-annual scale (e.g. changes in the number of rainy days or in the intensity of precipitation) can also be used, such as the method proposed by Thober et al. (2014).

5.3.2. HYDROLOGICAL MODELING

The Water Evaluation and Planning (WEAP) system (Yates et al., 2005a, b) was used for the hydrologic modelling in this study. WEAP uses climate information as input to generate streamflow in a semi-distributed scale. In the model, elevation bands are defined and used as hydrological units where climate, soil, topography, surface water hydrology and land use characteristics are specified. A WEAP model already set up and calibrated using historical monthly rainfall-runoff data for the Limarí River Basin by Vicuña et al. (2011; 2012) was available. The model was re-calibration focused on the most recent years (1985 – 2011), which was validated using data from early years (1969 – 1984). Chadwick et al. (2018b) provide more details about this calibration of the WEAP model.

5.3.3. PERFORMANCE INDEXES

The performance assessment of the reservoirs system requires the definition of a satisfactory and unsatisfactory state. The system is considered to be in a satisfactory state when the water allocation goal (D^t) is met. If in a certain time step D^t is not satisfied, the system falls into an unsatisfactory state referred to as a failure. For the purpose of this study we assume that the demand does not change due to changes in factors affected by climate change (i.e. for example, we neglect changes in irrigation needs due to potential modifications in evapotranspiration rates caused by changes in

temperature, or changes in land-use practices). With this definition, an under the current operation rule, the Paloma system is on failure when the water allocation is below $D^t = \sum_{j=1}^{M} \alpha_j^t$. Note, that for the constant and progressive reduction of the water allocation goals scenarios, the value of D^t changes, hence the RRV indexes will change accordingly. The performance of the Paloma system is evaluated under the future climate projections for the period 2011-2100 using the reliability, resilience and vulnerability indexes proposed by Hashimoto et al. (1982) and widely used in the literature (e.g., Bayazit and Ünal, 1990; Moy et al, 1986; Fowler et al, 2003; Kim and Kaluarachchi, 2009; Kjeldsen and Rosbejerg, 2004; Schaefli et al. 2007; Srinivasan and Philipose, 1996, 1998; Steinscheider and Brown 2012; Goharian et al., 2017; Zhang et al., 2017; Alameddine et al., 2018).

Reliability (*Rel*) measures how often the system fails. This index is calculated as the percentage of time that the system can meet D in the *n* years under evaluation.

$$Rel = 1 - \frac{\sum_{t=1}^{n} Z_t}{n} \tag{5.7}$$

where Z_t counts the number of years at failure:

$$Z_t = \begin{cases} 0 & \text{if} \sum_{j=1}^{M} O_j^t = D^t \\ 1 & \text{if} \sum_{j=1}^{M} O_j^t < D^t \end{cases} \tag{5.8}$$

where *t* is the year from 1 up to *n*, the last year of the analysis.

Resilience (*Res*) is a measure of how fast the system recovers once it has failed. It is computed as:

$$Res = \frac{\sum_{t=1}^{n} W_t}{\sum_{t=1}^{n} Z_t} \tag{5.9}$$

where W_t equals 1 each time step in which the system passes from failure to success and 0 if it stays on failure. Hence, $\sum_{t=1}^{n} W_t \leq \sum_{t=1}^{n} Z_t$, which implies a *Res* range between 0 (no recovery from failure or always in failure) to 1 (immediate recovery from failure or never in failure).

Vulnerability is the index measuring the damage caused by a failure. In fact, several indexes have been used for this purpose (Kjeldsen and Rosbejerg, 2004). Following the approach by Srinivasan and Philipose (1996; 1998), we calculated two indexes for vulnerability: (1) the maximum vulnerability or maximum water deficit ($MaxV$) as used by Moy et al. (1986) and the average vulnerability or average water deficit ($AvgV$). They are given by:

$$MaxV = max\left(\frac{v^t}{D^t}\right) \tag{5.10}$$

where

$$v^t = D^t - \sum_{j=1}^{M} O_j^t \geq 0 \tag{5.11}$$

$$AvgV = \frac{\sum_{t=1}^{n} \frac{v^t}{D^t}}{n} \tag{5.12}$$

Note that in Eq. (5.10) and (5.12), both vulnerabilities are standardized by *D*. Just as the other indexes, $MaxV$ and $AvgV$ range between 0 and 1.

Finally, we also use the standardized average outflow (*OF*) as an additional index in our analysis, which measures the mean percentage of water that is allocated

by the reservoir system compared to the water allocation goal D^t. *OF* ranges between 0 and 1and is given by:

$$OF = \frac{\sum_{t=1}^{n} \frac{\sum_{j=1}^{M} O_j^t}{D^t}}{n} \tag{5.13}$$

5.3.4. WATER ALLOCATION GOALS

As the stream flow volume for the Limarí river basin is expected to decrease with time due to the climate change (Vicuña et al. 2011; 2012), in addition to assess the performance of the current (i.e. historical) allocation goal, two adaptation strategies are also evaluated: (1) a single constant reduction of the water allocation goal, and (2) a progressive reduction in time of the water allocation goal.

Historical Water Allocation Goal

The historical water allocation goal implies using the values of α and r determined by Ferrer et al. (1978) in Eq. (5.4), which are constant in time, having a water allocation goal $D^t = \sum_{j=1}^{M} \alpha_j^t = 320\ Mm^3$.

Constant Reduction of the Water Allocation Goal

In this adaptation strategy a single fixed reduction in the water allocation goal is implemented for the entire future period (2011-2100) to maintain the stationary historical reliability for each RCP scenario. This is achieved by having $\alpha_j^t = 240 \cdot R$, $40 \cdot R$ and $40 \cdot R$ Mm^3 for the Paloma, Recoleta and Cogotí reservoirs respectively, where R is a reduction factor that is constant in time. Hence, the water allocation goal is constant but smaller than the historical and corresponds to $D^t = \sum_{j=1}^{M} \alpha_j^t = 320 \cdot R\ Mm^3$. Finally, to assure restraining the water allocation, the restrain factor r^t also changes as follows:

$$r^t = \begin{cases} 0.5 & \text{if } D^t \geq 0.5 \cdot RB \\ \dfrac{D^t}{RB} & \text{if } D^t < 0.5 \cdot RB \end{cases} \quad (5.14)$$

Progressive Reduction of the Water Allocation Goal

In this adaptation strategy, a linearly increasing reduction of the water allocation goal is implemented through time, starting at the initial year t_0 (2011) until the final year t_f (2100). Again, the objective is to maintain the stationary historical reliability for each RCP scenario. In this strategy $\alpha_j^t = 240 \cdot R^t$, $40 \cdot R^t$ and $40 \cdot R^t$ Mm^3 for the Paloma, Recoleta and Cogotí reservoirs respectively, where R^t is a progressive reduction factor that is given by:

$$R^t = \frac{R^{t_f} - 1}{t_f - t_0} \cdot t + 1 - \left(\frac{R^{t_f} - 1}{t_f - t_0}\right) \cdot t_0 \quad (5.15)$$

where R^{t_f} is the final progressive reduction factor calibrated to obtain the desired constant reliability through time. In this case the water allocation is time dependent (D^t) and progressively reduces according to $D^t = \sum_{j=1}^{M} \alpha_j^t = 320 \cdot R^t \, Mm^3$. Hence, the restrain factor is also time dependent (r^t), and is given by Eq. (5.15).

5.4. RESULTS AND DISCUSSION

Table 5-1 summarizes the average performance of the Paloma system obtained using the 200-synthetic series for each one of the five scenarios (i.e., stationary climate and the four RCPs), for the historical allocation goal and the two adaptation strategies. The high reliability, outflows and maximum vulnerability, and low resilience in the stationary scenario shows that current operation rule, was designed to maximize the water allocation, restricted to a certain reliability, without considering other indexes. Because of the expected future water reduction, each one of the performance indexes

using the historical water allocation strategy worsens progressively under the different RCP scenarios, compared to the stationary scenario. Interestingly, for the historical water allocation goal the worsening in the performance of the systems under the RCP 2.6 scenario measured by every index as compared to the stationary scenario is bigger than when comparing the changing in the performance between the RCP 2.6 and 8.5 scenarios.

Table 5-1: Average performance of the Paloma system measured by the indexes of reliability, resilience, maximum and average vulnerability, and outflows, under the three different water allocation goals, for the stationary historical scenario and the four RCP scenarios.

Scenario	Historical Water Allocation Goal				
	Reliability	Resilience	$MaxV$	$AvgV$	Out Flows
Stationary	0.726	0.366	0.719	0.297	0.916
RCP 2.6	0.591	0.292	0.787	0.362	0.843
RCP 4.5	0.560	0.276	0.795	0.384	0.816
RCP 6.0	0.552	0.274	0.800	0.378	0.818
RCP 8.5	0.502	0.241	0.828	0.423	0.775
Scenario	Constant Reduced Water Allocation Goal				
	Reliability	Resilience	$MaxV$	$AvgV$	Out Flows
RCP 2.6	0.726	0.332	0.576	0.179	0.943
RCP 4.5	0.726	0.333	0.503	0.166	0.941
RCP 6.0	0.726	0.325	0.491	0.151	0.948
RCP 8.5	0.726	0.297	0.464	0.157	0.942
Scenario	Progressive Reduction of the Water Allocation Goal				
	Reliability	Resilience	$MaxV$	$AvgV$	Out Flows
RCP 2.6	0.726	0.327	0.655	0.223	0.935
RCP 4.5	0.726	0.315	0.632	0.211	0.937
RCP 6.0	0.726	0.316	0.618	0.200	0.942
RCP 8.5	0.726	0.299	0.609	0.201	0.942

Table 5-2: Calibrated values of the constant reduction factor (***R***) and the progressive reduction factor ($\boldsymbol{R^{t_f}}$) to maintain the stationary historical reliability for each RCP scenario.

Scenario	R	R^{t_f}
RCP 2.6	0.705	0.388
RCP 4.5	0.618	0.223
RCP 6.0	0.614	0.220
RCP 8.5	0.508	0.040

The values of the constant reduction factor (R) and the final progressive reduction factor (R^{t_f}) calibrated to obtain the stationary historical reliability of 0.726 are listed for the four RCP scenarios in Table 5-2. The constant reduction strategy designed to maintain the reliability of the stationary scenario (Table 5-1) also improves the performance of every index, except for the resilience, which slightly decreases from 0.366 to 0.332. Nevertheless, a significant reduction in the water allocation is produced. In fact, the standardized outflow index improves as there is a reduction in the water allocation (D^t). Even for the less severe RCP 2.6 scenario a 29.5% reduction (i.e. 1 – R in Table 5-2) in the water allocation is required to maintain the reliability. Furthermore, a 49.2% reduction in the water allocation is needed to maintain this level of reliability under RCP 8.5. On the other hand, Table 5-2 shows that adopting the progressive water allocation strategy implies reductions in the water allocation of 61.2% and 96% by year 2100 under scenarios RCP 2.6 and 8.5 respectively. Thus, the progressive reduction strategy requires a smaller initial reduction than the constant reduction, but a much greater reduction at the end of the century. Obtaining almost the same values of R and R^{t_f} for RCPs 4.5 and 6.0, indicate that the adaptation measurement that a decision-maker should implement between those scenarios is the same. Nevertheless, one should also analyze the uncertainty of the results associated

with the scenario, as Chadwick et al. (2018b) shows the RCPs with the biggest uncertainty for the study basin, are RCP 4.5 and 6.0.

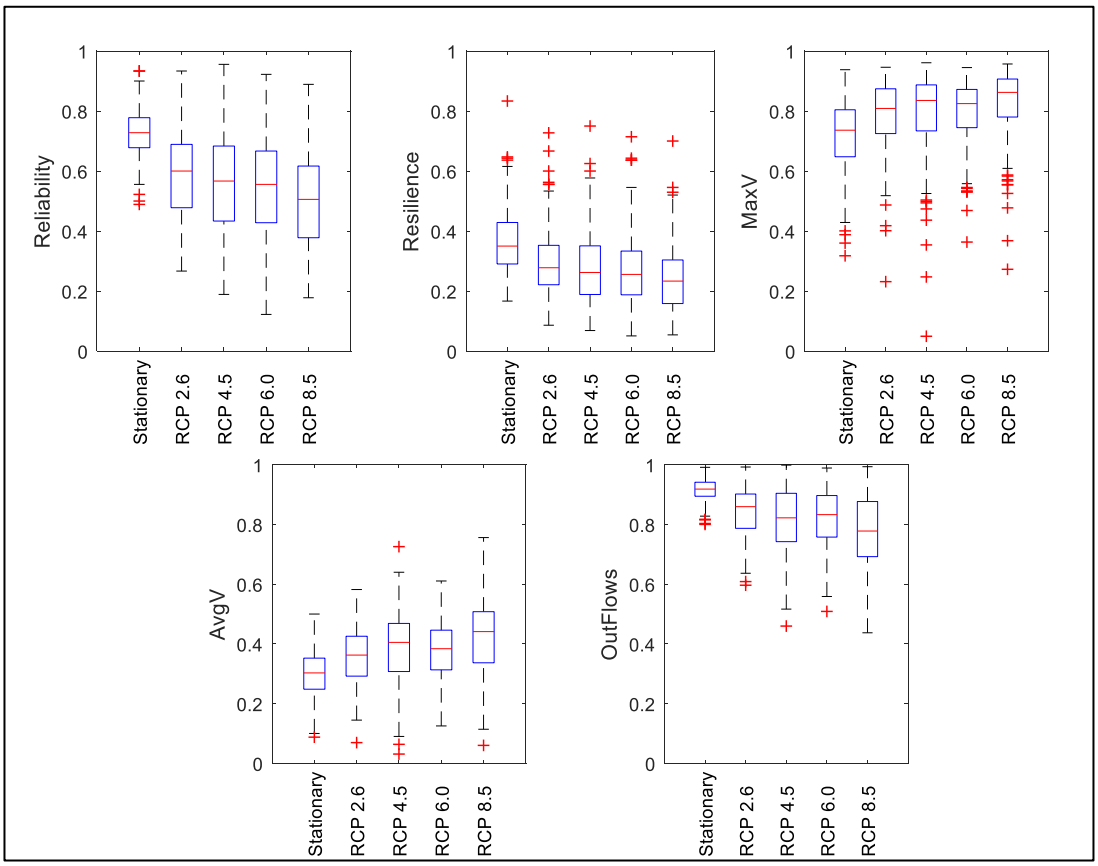

Figure 5-2: Boxplot for the indexes of reliability, resilience, maximum and average vulnerability, and standardized average outflow when considering the historical water allocation goal strategy.

To better understand the performance of the reservoirs' system beyond the average, Fig. 5-2, 5-3 and 5-4 compare the range of values of the performance indexes under all the climate scenarios for the historical, constant reduction and progressive reduction of the water allocation goal, respectively. Under the historical water allocation, the median performance for the four RCP scenarios is worse than for the stationary scenario according to all the indexes (Fig. 5-2). Nonetheless, for all the RCP scenarios the value of the indexes for some of the realizations may be as good as for

the stationary scenario. Note also that the range of indexes values under the historical allocation for the different RCP scenarios is larger than for the stationary scenario, particularly for the reliability and the standardized average outflow. The dispersion on the performance indexes in Fig. 5-2 is mostly due to the uncertainty coming from the GCMs and, to a less extent, that coming from the RCPs. This result is in agreement with Chadwick et al. (2018b), who showed a GCM-induced uncertainty larger than that from the RCPs. Nevertheless, the performance indexes showed in Fig. 5-2 are overall better than those reported by Chadwick et al. (2018b), because they utilized a commonly used quantile mapping bias correction that typically alter the GCM trends, as explained by Maurer and Priece (2014). This difference illustrates the potential impact of traditional downscaling methods that do not guarantee the preservation of GCMs statistical attributes.

Both the constant (Fig. 5-3) and the progressive (Fig. 5-4) reduction of the water allocation goal considerably improve the performance of the reservoir system. In particular, there is a reduction both in the maximum and the average vulnerability, as well as an improvement in the standardized average outflow. In fact, the values of this last metric become quite constant, and better than for the case of the historical allocation, regardless the RCP scenario. Nonetheless, neither of the strategies reduces the reliability range as compared to the historical allocation goal in any of the four RCP scenarios. The overall performance of the reservoir under both adaptation strategies is quite similar, with the vulnerability indexes being the ones for which more differences are identified. Indeed, there is an overall larger reduction in the maximum vulnerability associated with the constant water allocation reduction strategy, although a larger variability for this index across the different RCPs is also observed.

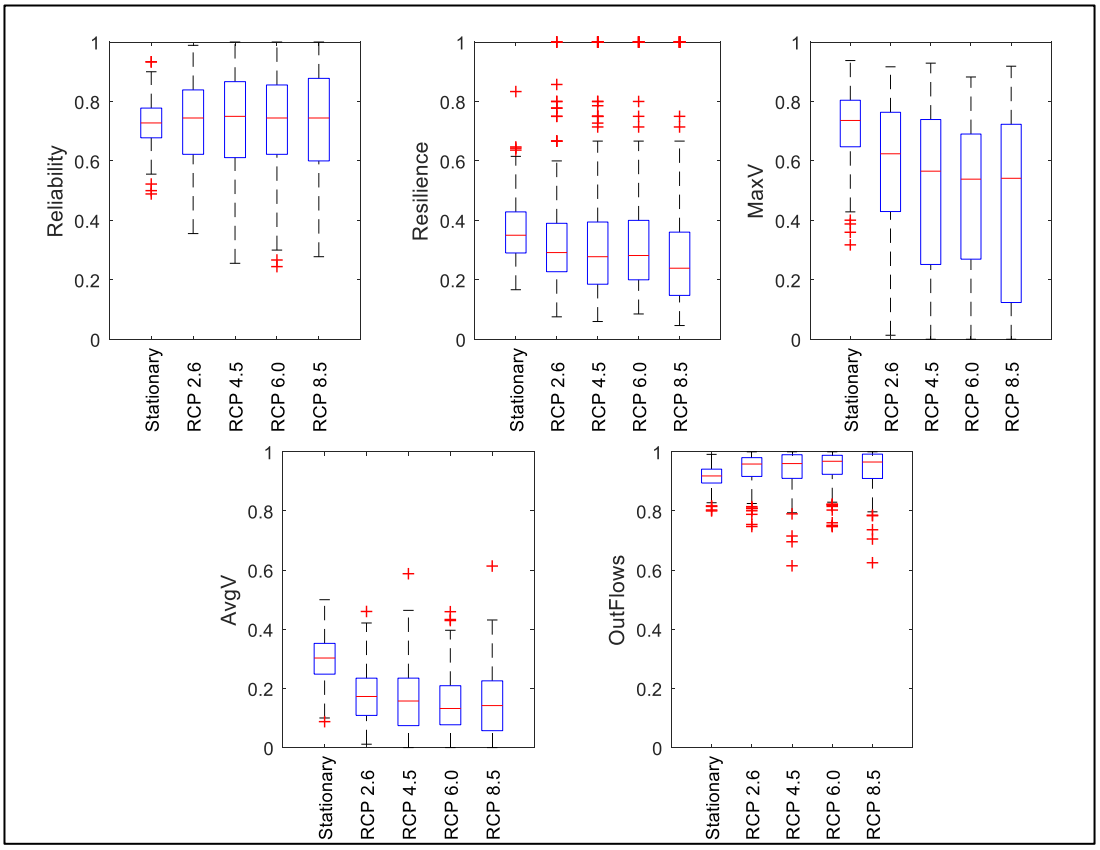

Figure 5-3: Boxplot for the indexes of reliability, resilience, maximum and average vulnerability, and standardized average outflow when considering the constant reduction of water allocation goal strategy.

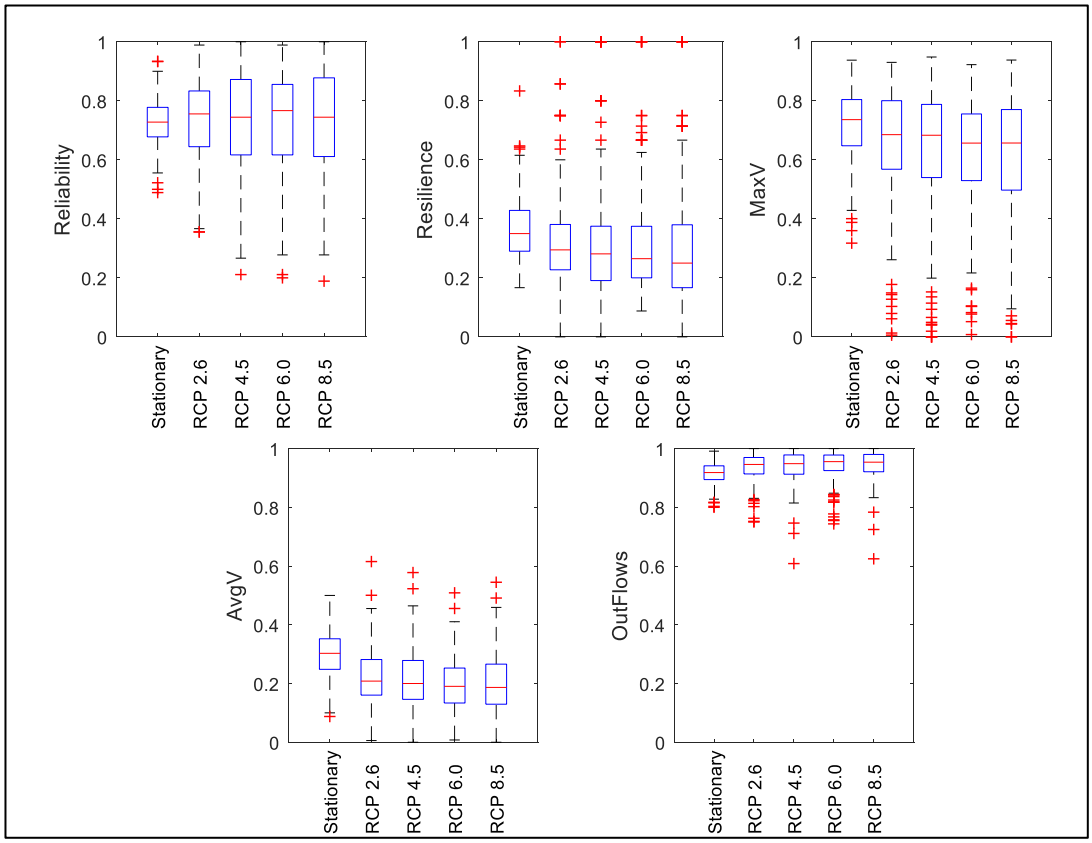

Figure 5-4: Boxplot for the indexes of reliability, resilience, maximum and average vulnerability, and standardized average outflow when considering the progressive reduction of water allocation goal strategy.

The previous results summarize the average performance for the entire future period (2011-2100). To better understand the performance of the reservoir system across time, Fig. 5-5 compares the dynamics of different impact measurements calculated from the 200 synthetic realizations for each year and climate scenario. The three water allocation goals through time are presented in millions of m^3 (Mm^3) on the first column, while the other columns show the different impacts measurements: (1) the mean number of failures as a percentage of the 200 synthetic realizations of each one of the five scenario (second column); (2) the mean failure indicating the average water scarcity for each year, of the 200 synthetic realizations per scenario, which is

standardized by between 0 and 1, by dividing by D^t(third column); and (3) the mean water allocation, which is the average water allocated for each year in the 200 synthetic realizations per scenario, which is also standardized by between 0 and 1 by dividing by D^t (fourth column). The historical water allocation goal of 320 Mm^3 (Fig. 5-5a) must be reduced to 225 Mm^3, 198 Mm^3, 196 Mm^3 and 162 Mm^3 for RCP 2.6, 4.5, 6.0 and 8.5, respectively (Fig. 5-5e) under the constant reduction strategy. On the other hand, the progressive reduction of the water allocation implies a linear reduction starting from the historical value of 320 Mm^3 up to values of 124 Mm^3, 71 Mm^3, 70 Mm^3 and 13 Mm^3 by year 2100, under the RCP 2.6, 4.5, 6.0 and 8.5 scenarios, respectively (Fig. 5-5i).

If the historical water allocation strategy is maintained, the number of failures at the beginning of the study period (2011) is similar for the five climate scenarios (Fig. 5-5b). As climate changes through time, the number of failure constantly increase, leading to failure in 70% of the realizations under RCP 8.5 by year 2100. This percentage of failure is only 25% under the stationary scenario (Fig. 5-5b). These results are similar also for the mean standardized failure and the mean standardized water allocation metrics, which systematically worsens trough time (Fig. 5-5c and 5-5d).

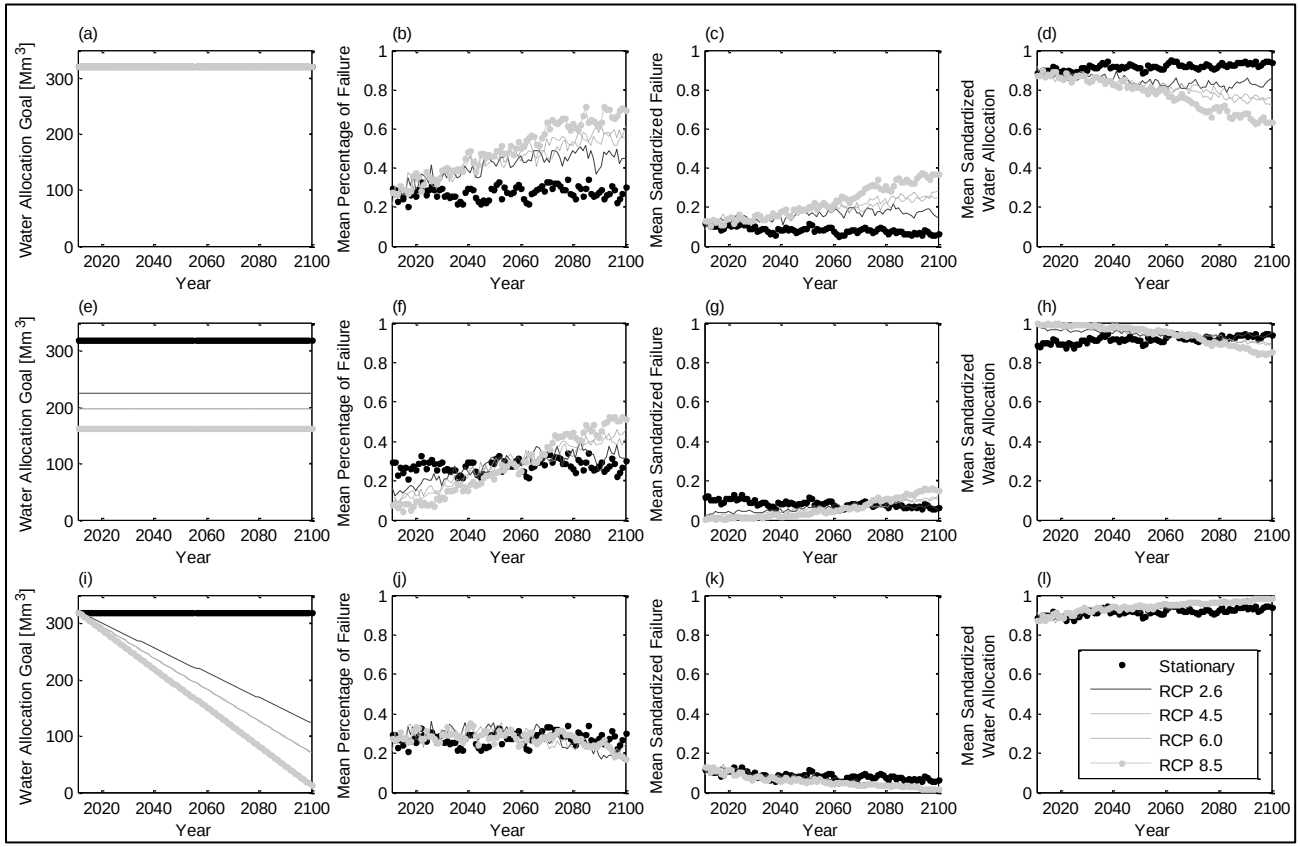

Figure 5-5: Impacts in terms of the percentage of failures (second column), the mean standardized level of failures (third column) and the mean standardized water allocation (fourth column) under the different climatic scenarios of the historical (first row), constant reduction (second row) and progressive reduction (third row) water allocation goal. The first column shows the temporal evolution of the water allocation goal associated with each strategy.

By adopting a constant reduction of the water allocation to maintain the historical reliability under the different RCP scenarios, failures are almost non-existent in year 2011 (Fig. 5-5f). After this year, the number of failures constantly increase to eventually exceed the number obtained for the stationary climate by 2060. Both the mean standardized failure (Fig. 5-5g) and the mean standardized water allocation (Fig. 5-5h) also behave in a similar manner. Both impact measurements reflect a performance better than for the stationary climate at the beginning of the study period but become worse by year 2060 up to 2100. Finally, the progressive reduction of the water allocation maintains the number of failures almost constant in time for the five climate scenarios (Fig. 5-5j). On the other hand, both the mean standardized failure (Fig. 5-5k) and the mean standardized water allocation (Fig. 5-5l) slightly improves with time for the RCP. Nonetheless, these improvements implied a reduction of 60 to 95% in the water allocation depending on the RCP scenario (Table 5-2); which illustrate the complex future this river basin and their stakeholders will likely face. Considering the magnitude of the reductions in water allocation to maintain the percentage of failure constant, to change the paradigm by increasing water usage efficiency and using alternative sources of water, as recommended by Gleick (2000), might not be enough. Some uncertainties are not considered in this analysis, such as the uncertainty of the hydrological model or in expected land-use scenarios, and future studies should analyze them to see if the abovementioned results still hold.

5.5. CONCLUSION

This work evaluates two reservoir system operation strategies to cope with water scarcity in a drying basin due to climate change. The two strategies are designed

to maintain the stationary historical reservoir reliability, these strategies are: a constant and a progressive reduction of the water allocation goal. Both strategies are compared against maintaining the historical water allocation goal. The methodology is applied to the Paloma Reservoir System located in the Limarí River basin, a semiarid Mediterranean basin in Chile, which is getting drier with climate change. The following conclusions are emphasized:

- The difference in the reservoir performance between the stationary scenario and RCP2.6 is bigger than the difference between RCP 2.6 and 8.5, regardless of the performance index or allocation goal strategy. The GCMs project that even for the less severe climate change scenario, there are severe changes expected in the Limarí hydroclimatic conditions, such as an expected reduction of a 60% in the available water under RCP 2.6.
- A single constant reduction in the water allocation goal at the beginning of the study period almost completely eliminates failures, while at the end of the study period the reservoir system is expected to fail more than the stationary historical one, regardless of the climate change scenario.
- The uncertainty of future climate projections is too big to establish the optimal progressive water reduction rate with a high degree of certainty. Despite of this, a progressive reduction over time of the water allocation allows maintaining constant the level of failure trough time. Nonetheless, this reduction also implies a significant reduction in the water to be allocated to the water users in the basin, illustrating the complex future expected for this basin.

Because for the Limarí river basin a drier future is consistently predicted by the GCMs, a progressive adaptation strategy seems to be a good strategy for the

management of the reservoir system. However, such strategy may not necessarily be the best option in other locations with different climate projections. Further research is needed to narrow the uncertainty related to climate change projections to properly calibrate the progressive adaptation strategy here proposed. Regardless the big uncertainty in the analysis, one can conclude that new water infrastructure and improvements in water efficiency are not enough to maintain the current reliability of the system. Thus, severe water allocation reductions are also needed. Most certainly the solution will have to be related to new sources of water, such as desalination, and a big reduction in the allocated water. These changes will certainly not only have a great economic impact in the region, but it will affect the ecosystem as well.

Some relevant aspects to be considered in future research are (1) the analysis of uncertainty associated with the hydrological model, (2) the consideration of future changes in the water demand caused by climate change, (3) the explicit evaluation of more sophisticated reservoir operation rules and water allocation goals, and (4) the explicit incorporation of the time of emergence evaluated in chapter 4 into climate change adaptation plans.

6. CHAPTER 6: SUMMARY, CONCLUSIONS AND RECOMMENDATIONS

This research has explored the General Circulation Models (GCMs) induced uncertainty in different steps of climate change impact studies and proposes methodologies to cope with these uncertainties and consider its impact over hydraulic systems, particularly reservoir systems. The most relevant result is the proposed methodology that combines both the information of a group of GCMs as well as the local climate information to generate future climate time series of data for climate change impact studies. Moreover, this methodology was used in two problems of great interest: (1) the identification of the time of emergence of climatic variables at local scales, and (2) the assessment of climate change impacts over the future performance of a reservoir system, as well as adaptation strategies to cope with these impacts.

The first hypothesis of this work (the uncertainty induced by the GCMs and their realizations significantly alters the results of a climate change impact study) was validated by means of analyzing the impact of climate change-induced uncertainty on the operation of large reservoirs, by assessing and quantifying the relative contribution of the GCM's, their realizations and RCP scenarios to the overall uncertainty. From this validation the following conclusions are obtained:

- The main contribution to the overall uncertainty in the performance comes from the GCMs, particularly for the early future. This uncertainty is larger than that from the RCPs and can cause significant changes in the assessment of the reservoir performance.
- The intra-GCMs (i.e. several realizations of a single GCM) uncertainty is comparable to the inter-GCM (i.e. among GCMs) uncertainty. This is a relevant

issue as multiple GCM realizations are generally not considered when studying climate change impacts on water systems.

- Counterintuitively, the uncertainty associated with the GCMs differ for different RCPs. Overall, there is more uncertainty associated with scenarios RCP 4.5 and RCP 6.0, followed by RCP 8.5, while the uncertainty for RCP 2.6 was the minimum. Additional studies are needed to determine whether this result holds for other locations.
- As expected, a strong correlation between the performance indexes and the percentage of change of precipitation simulated by the GCMs (*PC*) was found. Hence, to reduce the uncertainty of the reservoir system performance, the *PC* uncertainty must be reduced.
- Given the non-linear relationships among the RRV indexes, they provide complementary and relevant information about the current operation rule under different climate conditions. Only the standardized average outflow can be ignored, due to its strong correlation with reliability and average vulnerability.

The second hypothesis of this work (the climate generated by statistically merging the changes in precipitation and temperature from a group GCM and local statistics gives the same results as statistically generating climate from each GCM projection of the group used individually) was validated by the means of developing an approach more suitable to cope with GCM uncertainty when dealing with climate change studies at the basin scale. From this validation the following conclusions are obtained:

- The proposed method that generates climate by merging GCM statistics, with local climate statistics outperforms other commonly used downscaling and/or bias correction approaches.
- Results obtained using GCM pre- and post-analysis are very similar. On average there is less than a 0.4% difference between the probabilities of future years below different precipitation thresholds estimated with both methods.
- Using 5 to 10 trend percentiles obtained from the GCM pre-analysis is clearly better than using the single trend of the median GCM ensemble, as in the last case the uncertainty or discrepancy among the group of GCM is not formally taken into account. The GCM pre-analysis has the advantage of building GCM ensembles that incorporate not only the mean or median, but also the entire range of climate projections of a group of GCM.
- The GCM pre-analysis is able to simulate accurately the percentiles of the mean and the standard deviation of the temperature and precipitation of a group of GCM. The percentiles of the skewness and coefficient of variation are less well represented.

The third hypothesis of this work (it is possible to identify at a basin scale the time at which the climate change emerges, by using GCM projections and local climate statistics) was validated by means of proposing a methodology to estimate the time of emergence at local scales, considering both GCMs outputs and basin climatic conditions. From this validation the following conclusions are obtained:

- It is possible to identify local time of emergence with the methodology proposed in this study.

- The ToE for precipitation is identified first in the Maule, then the Maipo and finally in the Limarí. These results are related to the local climate coefficient of variation, as the higher the variation is, the later the ToE occurs. The relationship between the ToE and the coefficient of variation may not hold for other cases because the ToE also depends on the strength of the climate signal.
- The trend percentile chosen to detect the ToE has a significant impact over the year detected.

The fourth hypothesis of this work (a dynamic water allocation goal is better than a single modification of the water allocation goal on a drying basin due to climate change) was validated by means of evaluating the impact of progressive changes in climate over reservoir performance measured by performance indexes, and possible adaptation strategies to cope with this impact. From this validation the following conclusions are obtained:

- The difference in the reservoir performance between the stationary scenario and RCP2.6 is bigger than the difference between RCP 2.6 and 8.5, regardless of the performance index or allocation goal strategy. The GCMs project that even for the less severe climate change scenario, severe changes are expected for the Limarí hydroclimatic conditions, such as a reduction of a 60% in the available water under RCP 2.6.
- A single constant reduction over the water allocation goal at the beginning of the study period almost completely eliminates failures, while at the end of the study period the reservoir system is expected to fail more than under the stationary historical climate, regardless of RCP scenario.

- The uncertainty of future climate projections is too big to establish the optimal progressive water reduction rate with a high degree of certainty. Despite of this, a progressive reduction over time of the water allocation allows maintaining constant the level of failure trough time. Nonetheless, this reduction also implies a significant reduction in the water to be allocated to the water users in the basin, illustrating the complex future expected for this basin.

Future research is needed to answer some open questions associated with this dissertation. In addition to extent the application of the method here proposed to identify the local time of emergence for climatic variables to other locations in Chile and elsewhere, it is of relevance to study the feasibility of detecting the time of emergence in river flows discharges by coupling the approach here presented with a hydrological model. Also, future studies should explicitly evaluate incorporating the time of emergence in the adaptation strategies to climate change. Regarding our finding related to the assessment of adaptation strategies in the operation of reservoir, it is suggested to study in detail the potential application of the continuously changing water allocation goals here proposed, and the implication of other type of uncertainty in the assessment, particularly the coming from hydrological modeling uncertainty. Finally, potential applications of the developed methods among stake holders, water users and decision makers should be evaluated.

REFERENCE

Adeloye, A.J., N.R. Nawaz and M. Montaseri, 1999. Climate Change Water Resources Planning Impacts Incorporating Reservoir Surface Net Evaporation Fluxes: A case Study. Internal Journal of Water Resources Development, 15(4): 561-581. DOI: 10.1080/07900629948763

Adeloye, A.J., B.S. Soundharajan, C.S.P. Ojha and R. Remesan, 2016. Effect of Hedging-Integrated Rule Curves on the Performance of the Pong Reservoir (India) During Scenario-Neutral Climate Change Perturbations. Water Resources Management, 30(2): 445-470. DOI: 10.1007/s11269-015-1171-z

Ahmadalipour, A., H. Moradkhani, and A. Rana, 2017. Accounting for Downscaling and Model Uncertainty in Fine-Resolution Seasonal Climate Projections over the Columbia River Basin. Climate Dynamics., 1-17, DOI: 10.1007/s00382-017-3639-4

Akhter, J., L. Das, J.K. Meher, and A. Deb, 2018. Uncertainties and Time of Emergence of Multi-Model Precipitation Projection Over Homogeneous Rainfall Zones of India. Climate Dynamics, 50(9-10): 3813-3831. DOI: 10.1007/s00382-017-3847-y

Alameddine, I., A. Fayyad, M. Abou, and M. El-Fadel, 2018. Sustainability of Basin Level Development Under a Changing Climate. International Journal of Sustainable Development and Planning, 13(3): 394-405. DOI: 10.2495/SDP-V13-N3-394-405

Ayyub, B.M. and R.H. McCuen, 2011. Probability, Statistics and Reliability for Engineers and Scientists. 639 pp., CRC Press, Boca Ratón, FL, USA.

Bayazit, M. and N.E. Ünal, 1990. Effects of Hedging on Reservoir Performance. Water Resources Research 26(4): 713-719. DOI: 10.1029/WR026i004p00713

Bhuiyan, C., R.P. Singh and F.N. Kogan, 2006. Monitoring Drought Dynamics in the Aravalli Region (India) Using Different Indices Based on Ground and Remote Sensing Data. International Journal of Applied Earth Observation and Geoinformation, 8(4), 289-302, DOI: 10.1016/j.jag.2006.03.002

Blöschl, G. and A. Montanari, 2010. Climate Change Impact-Throwing the Dice? Hydrological Processes, 24(3): 374-381. DOI: 10.1002/hyp.7574

Boisier, J.P. and P. Aceituno, 2006. Changes in Surface and Upper-Air Temperature along the Arid Coast of Northern Chile. Paper Presented at American Meteorological Society 8th International Conference on Southern Hemisphere Meteorology and Oceanograohy (ICSHMO), 24-28 April 2006, Foz do Iguaçu São José dos Campos: INPE, 227-228.

Bown, F. and A. Rivera, 2007. Climate Change and Recent Glacier Behaviour in the Chilean Lake District. Global and Planetary Change, 59(1): 79-86. DOI: 10.1016/j.gloplacha.2006.11.015

Brady, R.X., M.A. Alexander, N.S. Lovenduski and R.R. Rykaczewski, 2017. Emergent anthropogenic trends in California Current upwelling. Geophysical Research Letters, 44(10): 5044-5052. DOI: 10.1002/2017GL072945

Bras, R.L., R. Buchenan and K.C. Curry, 1983. Real Time Adaptation Closed Loop Control of Reservoir with the High Aswan Dam as a Case Study. Water Resources Research 19(1): 33-52. DOI: 10.1029/WR019i001p00033

Brekke, L.D., E.P. Maurer, J.D. Anderson, M.D. Dettinger, E.S. Townley, A. Harrison, and T. Pruitt, 2009. Assessing Reservoir Operations Risk Under Climate Change. Water Resources Research, 45(4). DOI: 10.1029/2008WR006941

Buser, C.M., H.R. Künsch, D. Lüthi, M. Wild and C. Schär, 2009. Bayesian Multi-Model Projection of Climate: Bias Assumptions and Interannual Variability. Climate Dynamics, 33(6): 849-868. DOI: 10.1007/s00382-009-0588-6

Burke, E.J. and S.J. Brown, 2008. Evaluating Uncertainties in the Projection of Future Drought. Journal of Hydrometeorology, 9(2): 292-299. DOI: 10.1175/2007JHM929.1

Carson, M., A. Köhl, D. Stammer, A.B.A. Slangen, C.A. Katsman, R.S.W. Van de Wal, J. Church, and N. White, 2016. Coastal Sea Level Changes, Observed and Projected During the 20th and 21st Century. Climatic Change, 134(1-2): 269-281. DOI: 10.1007/s10584-015-1520-1

Chadwick, C., J. Gironás, S. Vicuña, F. Meza, and J. McPhee, 2018a. Using a Statistical Pre-Analysis Approach as an Ensemble Technique for the Unbiased Mapping of GCM Changes to Local Stations. Journal of Hydrometeorology 19(9): 1447-1465. DOI: 10.1175/JHM-D-17-0198.1

Chadwick, C., J. Gironás, A. Elshorbagy, S. Vicuña, F. Meza and J. McPhee, 2018b. Assessing the role of GCM and RCP sources of uncertainty in the performance of current reservoir operation in Semiarid Chile. Journal of Hydrology (under review).

Chen, J., F.P. Brissette and R. Leconte, 2011. Uncertainty of Downscaling Methods in Quantifying the Impact of Climate Change on Hydrology. Journal of Hydrology, 401(3): 190-202. DOI: 10.1016/j-jhydrol.2011.02.020

Clark, M.P. and R.S. Pulwarty, 2003. Devising Resilient Responses to Potential Climate Change Impact. Ogmius: Newsletter of the Center for Science and Technology Policy Research, 5: 2-3.

Datta, B. and S.J. Burges, 1984. Short-Term, Single, Multiple-Purpose Reservoir Operation: Importance of Loss Function and Forecast Errors. Water Resources Reesearch 20(9): 1167-1176. DOI: 1029/WR020i009p01167

Datta, B. and M.H. Houck, 1984. A Stochastic Optimization Model for Real-Time Operation of Reservoirs Using Uncertain Forecasts. Water Resources Research 20(8): 1039-1046. DOI: 10.1029/WR020i008p01039

Demaria, E.M.C., E.P. Maurer, B. Thrasher, S. Vicuña and F.J. Meza, 2013. Climate Change Impacts on an Alpine Watershed in Chile: Do New Model Projections Change the Story? Journal of Hydrology, 502: 128-138. DOI: 10.1016/j.jhydrol.2013.08.027

DGA (Dirección Genral de Aguas), 2008. Manual de Normas y Procedimientos Para la Administración de Recursos Hídricos. http://documentos.dga.cl/ADM5016.pdf

Diaz-Nieto, J. and R.L. Wilby, 2005. A Comparison of Statistical Downscaling and Climate Change Factor Methods: Impacts on Low Flows in the River Thames, United Kingdon. Climatic Change, 69(2-3): 245-268. DOI: 10.1007/s10584-005-1157-6

Diffenbaugh, N.S. and M. Scherer, 2011. Observational and Model Evidence of Global Emergence of Permanent, Unprecedented Hear in the 20th and 21st Centuries. Climate Change, 107(3): 615-624. DOI: 10.1007/s10584-011-0112-y

Downing, T.E., L. Ringius, M. Hulme and D. Waughray, 1997. Adapting to Climate Change in Africa. Mitigation and Adaptation Strategies for Global Change 2(1): 19-44. DOI: 10.1023/B:MITI.0000004663.31074.64.

Draper, A.J. and J.R. Lund, 2004. Optimal Hedging and Carryover Storage Value. Journal of Water Resources Planning and Management 130(1): 83-87. DOI: 10.1061/(ASCE)0733-9496(2004)130:1(83)

Ehret, U., E. Zehen, V. Wulfmeyer, K. Warrach-Sagi and J. Leibert, 2012. HESS Options "Should We Apply Bias Correction to Global and Regional Climate Model Data?" Hydrology and Earth System Discussions, 9(4): 3391-3404. DOI: 10.5194/hess-16-3391-2012

Eum, H., Y. Kim and R. N. Palmer, 2011. Optimal Drought Management Using Sampling Stochastic Dynamic Programming with a Hedging Rule. Journal of Water Resources Planning and Management 137: 113-122. DOI: 10.1061/(ASCE)WR.1943-5452.0000095

Ferrer, P., E. Brown and R. Bensan, 1978. Operación del Sistema Paloma. Ministerio de Obras Públicas, Dirección General de Obras Públicas, Dirección de Riego.

Fowler, H.J., C.G. Kilsby and P.E. O'Connell, 2003. Modeling the Impacts of Climatic Change and Variability on the Reliability, Resilience and Vulnerability of a Water Resources System. Water Resources Research, 39(8). DOI: 10.1029/2002WR001778

Fowler, H.J., C.G. Kilsby, P.E. O'Connell and A. Burton, 2005. A Weather-Type Conditioned Multi-Site Stochastic Rainfall Model For the Generation of Scenarios of Climate Variability and Change. Journal of Hydrology, 308(1): 50-66. DOI: 10.1016/j.jhydrol.2004.10.021

Fowler, H.J., C.G. Kilsby and J. Stunell, 2007. Modelling the Impacts of Projected Future Climate Change on Water Resources in North-West England. Hydrology and Earth System Sciences, 11(3): 1115-1126.

Georgakakos, A.P., H. Yao, M. Kistenmacher, K.P. Georgakakos, N.E. Graham, F.Y. Cheng, C. Spencer, and E. Shamir, 2012. Value of Adaptive Water Resources Management in Northern California Under Climatic Variability and Change: Reservoir Management. Journal of Hydrology, 412: 34-46. DOI: 10.1016/j.jhydrol.2011.04.038

Giese, B.S., S.C. Urizar and N.S. Fučkar, 2002. Southern Hemisphere Origins of the 1976 Climate Shift. Geophysical Research Letters, 29(2). DOI: 10.1029/2001GL013268

Giorgi, F. and X. Bi, 2009. Time of Emergence (TOE) of GHG-Forced Precipitation Change Hot-Spots. Geophysicla Research Letters, 36(6). DOI: 10.1029/2009GL037593

Gleick, P.H., 2000. A look at twenty-first century water resources development. Water international. 25(1): 127-138. DOI: 10.1080/02508060008686804

Goharian, E., S.J. Burian, and M. Karamouz, 2017. Using Joint Probability Distribution of Reliability and Vulnerability to Develop a Water System Performance Index. Journal of Water Resources Planning Management, 144(2): 04017081. DOI: 10.1061/(ASCE)WR.1943-5452.0000869

Greene, A.M., M. Hellmuth and T. Lumsden, 2012. Stochastic Decadal Climate Simulation for the Berg and Breede Water Management Areas, Western Cape Province, South Africa. Water Resources Research, 48(6). DOI: 10.1029/2011WR011152

Hagemann, S., C. Chen, J.O. Haerter, J. Heinke, D. Gerten and C. Piani, 2011. Impact of a Statisctical Bias Correction on the Projected Hydrological Changes Obtained From Three GCMs and Two Hydrology Models. Journal of Hydrometeorology 12(4): 556-578. DOI: 10.1175/2001JHM1336.1

Hallegatte, S., 2009. Strategies to Adapt to an Uncertain Climate Change. Global Environmental Change, 19(2): 240-247. DOI: 10.1016/j.gloenvcha.2008.12.003

Harrington, L.J., D.J. Frame, E.M. Fischer, E. Hawkins, M. Joshi, and C.D. Jones, 2016. Poorest Countries Experience Earlier Anthropogenic Emergence of Daily Temperature Extremes. Environmental Research Letters, 11(5): 055007. DOI: 10.1088/1748-9326/11/5/055007/meta

Hashimoto, T., J.R. Stedinger and D.P. Loucks, 1982. Reliability, Resiliency, and Vulnerability Criteria for Water Resources System Performance Evaluation. Water Resources Research 18(1):14-20. DOI: 10.1029/WR018i001p00014

Hawkins, E. and R Sutton, 2011. The Potential to Narrow Uncertainty in Projections of Regional Precipitation Change. Climate Dynamics, 37(1-2): 407-418. DOI: 10.1007/s00382-010-0810-6

Hawkins, E. and R. Sutton, 2012. Time of Emergence of Climate Signal. Geophysical Research Letters, 39(1). DOI: 10.1029/2011GL050087

Hay, L.E., R.L. Wilby, and G.H. Leavesley, 2000. A Comparison of Delta Change and Downscaled GCM Scenarios for three Mountainous Basins in the United States. Journal of the American Water Resources Association, 36(2): 387-397, DOI: 10.1111/j.1752-1688.2000.tb04276.x

Henson, S.A., C. Beaulieu, T. Ilyina, J.G. John, M. Long, R. Séférian, J. Tjiputra, and L. Sarmiento, 2017. Rapid Emergence of Climate Change in Environmental

Drivers of Marine Ecosystems. Nature Communications, 8: 14682. DOI: 10.1038/ncomms14682

Hotelling, H. and M.R. Pabst, 1936. Rank Correlation and Test of Significance Involving no Assumption of Normality. The Annals of Mathematical Statistics, 7(1): 29-43. DOI: 10.1214/aoms/1177732543

Jain, S.K., 2014. Investigating Parameters of Two-Point Policy for Operating a Storage Reservoir. ISH Journal of Hydraulic Engineering (ahead of print), 1-9. DOI: 10.1080/09715010.2013.848608

Keller, K.M., F. Joos and C.C. Raible, 2014. Time of Emergence of Trends in Ocean Biogeochemestry. Biogeosciences, 11(13): 3647-3659. DOI: 10.5194/bg-11-3647-2014

Khan, S., H.F. Gabriel and T. Rana, 2008. Standard Precipitation Index to Track Drought and Assess Impact of Rainfall on Watertables in Irrigation Areas. Irrigation and Drainage Systems, 22(2): 159-177. DOI:10.1007/s10795-008-9049-3

Kim, U. and J.J. Kaluarachchi, 2009. Climate Change Impacts on Water Resources in the Upper River Basin, Ethiopia. JAWRA Journal of the American Water Resources Association, 45(6): 1361-1378. DOI: 10.1111/j.1752-1688.2009.00369.x

King, A.D., M.T. Black, S.K. Min, E.M. Fischer, D.M. Mitchell, L.J. Harrington, and S.E. Perkins-Kirkpatrick, 2016. Emergence of Heat Extremes Attributable to Anthropogenic Influences. Geophysical Research Letters, 43(7): 3438-3443. DOI: 10.1002/2015GL067448

King, A.D., M.G. Donat, E.M. Fischer, E. Hawkins, L.V. Alexander, D.J. Karoly, A.J. Dittus, S.C. Lewis, and S.E. Perkins, 2015. The Timing of Anthropogenic Emergence in Simulated Climate Extremes. Environmental Research Letters, 10(9): 094015. DOI: 10.1088/1748-9326/10/9/094015/meta

Kiparsky, M., A. Milman, and S. Vicuña, 2012. Climate and Water: Knowledge of Impacts to Action on Adaptation. Annual Review of Environment and Resources, 37: 163-194. DOI: 10.1146/annurev-environ-050311-093931

Kjeldsen, T.R. and D. Rosbjerg, 2004. Choice of Reliability, Resilience and Vulnerability Estimators for Risk Assessments of Water Resources Systems. Hydrological Sciences Journal, 49(5). DOI: 10.1623/hysj.49.5.755.55136

Kundzewicz, Z.W. and J. Kindler, 1995. Multiple Criteria for Evaluation of Reliability Aspects of Water Resources Systems. IAHS Publications-Series of Proceeding and Reports-Intern Association Hydrological Sciences, 231: 217-224.

Lall, U. and C.W. Miller, 1988. An Optimization Model for Screening Multipurpose Reservoir Systems. Water Resources Research 24(7): 953-968. DOI: 10-1029/WR024i007p00953

Lall, U. and A. Sharma, 1996. A Nearest Neighbor Bootstrap for Resampling Hydrologic Time Series. Water Resources Research, 32(3): 679-693. DOI: 10.1029/95WR02966

Lee, D., S.K. Min, C. Park, M.S. Suh, J.B. Ahn, D.H. Cha, D.K. Lee, S.Y. Hong, S.C. Park, and H.S. Kang, 2016. Time of Emergence of Anthropogenic Warming Signals in the Northeast Asia Assessed from Multi-Regional Climate Models. Asia-Pacific Journal of Atmospheric Sciences, 52(2): 129-137. DOI: 10.1007/s13143-016-0014-z

Lehner, F., C. Deser, and L. Terray, 2017. Toward a New Estimate of "Time of Emergence" of Anthropogenic Warming: Insights from Dynamical Adjustment and a Large Initial-Condition Model Ensemble. Journal of Climate, 30(19): 7739-7756. DOI: 10.1175/JCLI-D-16-0792.1

Leng, G., M. Huang, N. Voisin, X. Zhang, G.R. Asrar and L.R. Leung, 2016. Emergence of new hydrologic regimes of surface water resources in the conterminous United States under future warming. Environmental Research Letters, 11 (11): 114003. DOI: 10.1088/1748-9326/11/11/114003

Liang, X., D.P. Lettenmaier, E.F. Wood, and S.J. Burges, 1994. A Simple Hydrologically Based Model of Land Surface Water and Energy Fluxes for General Circulation Models. Journal of Geophysical Research: Atmospheres, 99: 14415–28. DOI: 10.1029/94JD00483

Liang, X., E.F. Wood, and D.P. Lettenmaier, 1996. Surface Soil Moisture Parameterization of the VIC-2L Model: Evaluation and Modification. Global and Planetary Change, 13: 195–206. DOI: 10.1016/0921-8181(95)00046-1

Lettenmaier, D.P., A.W. Wood, R.N. Palmer, E.F. Wood and E. Stakhiv, 1999. Water Resources Implications of Global Warming: A US Regional Perspective. Climate Change, 43(3): 536-579. DOI: 10.1023/A:1005448007910

Lopez, H., R. West, S. Dong, G. Goni, B. Kirtman, S.K. Lee, and R. Atlas, 2018. Early Emergence of Anthropogenically Forced Heat Waves in the Western United States and Great Lakes. Nature Climate Change, 1. DOI: 10.1038/s41558-018-0116-y

Lyu, K., X. Zhang, J.A. Church, A.B. Slangen and J. Hu, 2014. Time of Emergence for Regional Sea-Level Change. Nature Climate Change, 4(11):1006. DOI: 10.1038/NCLIMATE2397

Mahlstein, I., G. Hegerl and S. Solomon, 2012a. Emerging local warming signals in observational data. Geophysical Research Letters, 39(21). DOI: 10.1029/2012GL053952

Mahlstein, I., R. Knutti, S. Solomon and R.W. Portmann, 2011. Early Onset of Significant Local Warming in Low Latitude Countries. Enviromental Research Letters, 6(3): 034003. DOI: 10.1088/1748-9326/6/3/034009

Mahlstein, I., R.W. Portmann, J.S. Daniel, S. Solomon, and R. Knutti, 2012b. Perceptible Changes in Regional Precipitation in a Future Climate. Geophysical Research Letters, 39(5). DOI: 10.1029/2011GL050738

Massey, Jr.F.J., 1951. The Kolmogorov-Smirnov Test for Goodness of Fit. Journal of the American Statistical Association, 46(253): 68-78. DOI: 10.1080/01621459.1951. 10500769

Matonse, A.H., D.C. Pierson, A. Frei, M.S. Zion, A. Anandhi, E. Schneiderman and B. Wright, 2013. Investigating the Impact of Climate Change on New York City's Primary Water Supply. Climate Change, 116(3-4): 437-456. DOI: 10.1007/s10584-0120515-4

Maurer, E.P., 2007. Uncertainty in Hydrological Impacts of Climate Change in the Sierra Nevada, California, Under Two Emission Scenarios. Climate Change 82: 309-325. DOI: 10.1007/s10584-006-9180-9

Maurer, E.P., J.C. Adam and A.W. Wood, 2009. Climate Model Based Consensus on the Hydrological Impacts of Climate Change to the Rio Lampa Basin of Central

America. Hydrology and Earth System Sciences, 13: 183-194. DOI: 10.5194/hessd-5-3099-2008

Maurer, E.P. and D.W. Pierce, 2014. Bias Correction Can Modify Climate Model Simulated Precipitation Changes without Adverse Effect on the Ensemble Mean. Hydrology and Earth System Sciences, 18(3): 915-925. DOI: 10.5194/hess-18-915-2014

Merz, R., J. Parajka and G. Blöschl, 2011. Time Stability of Catchment Model Parameters: Implications for Climate Impact Analyses. Water Resources Research, 47(2). DOI: 10.1029/2010WR009505

Meza, F.J., D.S. Wilks, L. Gurovich and N. Bambach, 2012. Impacts of Climate Change on Irrigated Agriculture in the Maipo Basin, Chile: Reliability of Water Rights and Changes in the Demand for Irrigation. Journal of Water Resources Planning and Management, 138(5): 421-430. DOI: 10.1061/(ASCE)WR.1943-5452.0000216

McKee, T.B., N.J. Doesken and J. Kleist, 1993, January. The Relationship of Drought Frequency and Duration to Time Scale. In: Proceedings of the 8th Conference on Applied Climatology. 17(22): 179-183. Boston, MA: American Meteorological Society.

Milly, P.C.D., J. Betancourt, M. Falkenmark, R.M. Hirsch, Z.W. Kundzewicz, D.P. Lettenmaier, and R.J. Stouffer, 2008. Stationarity Is Dead: Whither Water Management? Science, 319(1): 573-574. DOI: 10.1126/science.1151915

Milly, P.C.D., J. Betancourt, M. Falkenmark, R. M. Hirsch, Z.W. Kundzewicz, D.P. Lettenmaier, R.J. Stouffer, M.D. Dettinger and V. Krysanova, 2015. On

Critiques of “Stationarity is Dead: Whither Water Management?” Water Resources Research, 51(9): 7785-7789. DOI: 10.1002/2015WR017408

Minville, M., F. Brissette and R. Leconte, 2008. Uncertainty of the Impact of Climate Change on the Hydrology of a Nordic Watershed. Journal of Hydrology, 358(1): 70-83. DOI: 10.1016/j.jhydrol.2008.05.033

Mondal, M.S. and S.A. Wasimi, 2007. Evaluation of Risk-Related Performance in Water Management for the Ganges Delta of Bangladesh. Journal of Water Resources Planning and Management, 133(2): 179-187. DOI: 10.1061/(ASCE)0733-9496(2007)133:2(179)

Mondal, M.S., J.U. Chowdhury and M.R. Ferdous, 2010. Risk-Based Evaluation for Meeting Future Water Demand of the Brahmaputra Floodplain within Bangladesh. Water Resources Management, 24(5): 853-869. DOI: 10.1007/s11269-009-9475-5

Montecinos, A., and P. Aceituno, 2003. Seasonality of the ENSO-related Reinfall Variability in Central Chile and Associated Circulation Anomalies. Journal of Climate, 16(2): 281-296. DOI: 10.1175/1520-0442(2003)016<0281:SOTERR>2.0.CO;2

Mora, C., A.G. Frazier, R.J. Longman, R.S. Dacks, M.M. Walton, E.J. Tong, J.J. Sanchez, L.R. Kaiser, Y.O. Stender, J.M. Anderson, C.M. Ambrosino, I. Fernandez-Silva, L.M. Giuseffi, and T.W. Giambelluca, 2013. The Projected Timing of Climate Departure from Recent Variability. Nature, 502(7470): 183. DOI: 10.1038/nature12540

Moss, R.H., J.A. Edmonds, K.A. Hibbard, M.R. Manning, S.K. Rose, D.P. VanVuuren, T.R. Carter, S. Emori, M. Kainuma, T. Kram, G.A. Meehl, J.F.B.

Mitchell, N. Nakicenovic, K. Riahi, S.J. Smith, R.J. Stouffer, A.M. Thomson, J.P. Weyant and T.J. Wilbanks, 2010. The Next Generation of Scenarios for Climate Change Research and Assessment. Nature, 436(7282): 747-756. DOI: 10.1038/nature08823

Moy, M., J.L. Cohon and C.S. ReVelle, 1986. A Programming Model for Analysis of the Reliability, Resilience, and Vulnerability of a Water Supply Reservoir. Water Resources Research 22(4): 489-498. DOI: 10.1029/WR022i004p00489

Muir, L.C., J.N. Brown, J.S. Risbey, S.E. Wijffels and A.S. Gupta, 2013. Determining the Time of Emergence of the Climate Change Signal at Regional Scale. CAWCR Res. Lett, 10: 8-19.

Myers, D., 1994. Spatial Interpolation: an Overview. Geoderma, 62(1): 17-28. DOI: 10.1016/0016-7061(94)90025-6

Nash, J. and J.V. Sutcliffe, 1970. River Flow Forecasting Trough Conceptual Models Part I – A Discussion of Principles. Journal of Hydrology, 10(3): 282-290. DOI: 10.1016/0022-1694(70)90255-6

Nguyen, T.H., S.K. Min, S. Paik, and D. Lee, 2018. Time of Emergence in Regional Precipitation Changes: an Updated Assessment Using the CMIP5 Multi-Model Ensemble. Climate Dynamics, 1-15. DOI: 10.1007/s00382-018-4073-y

Obeysekera, J. and J.D. Salas, 2013. Quantifying the Uncertainty of Design Floods Under Nonstationary Conditions. Journal of Hydrologic Engineering, 19(7): 1438-1446. DOI: 10.1061/(ASCE)He.1943-5584.0000931

Ouyang, F., H. Lü, Y. Zhu, J. Zhang, Z. Yu, X. Chen and M. Li, 2014. Uncertainty Analysis of Downscaling Method in Assessing the Influence of Climate Change

on Hydrology. Stochastic Environmental Research and Risk Assessment, 28: 991-1010. DOI: 10.1007/s00477-013-0796-9

Pierce, D.W., D.R. Cayan, E.P. Maurer, J.T. Abatzoglou and K.C. Hegewisch, 2015. Improved Bias Correction Techniques for Hydrological Simulations of Climate Change. Journal of Hydrometeorology, 16(6): 2421-2442. DOI: 10.1175/JHM-D-14-0236.1

Rajagopalan, B. and U. Lall, 1999. A k-nearest neighbor simulation for daily precipitation and other weather variables. Water Resources Research, 35(10): 3089-3101. DOI: 10.1029/1999WR90028

Read, L.K., and R.M. Vogel, 2015. Reliability, Return Periods, and Risk Under Nonstationarity. Water Resources Research, 51(8): 6381-6398. DOI: 10.1002/2015WR017089

Reclamation, 2014. Downscaled CMIP3 and CMIP5 Climate and Hydrology Projections: Release of Hydrology Projections, Comparison with Preceding Information, and Summary of User Needs U.S. Department of the Interior, Bureau of Reclamation, Technical Services Center, Denver,CO 110 pp.

Rosenblüth, B., H.A. Fuenzalida and P. Aceituno, 1997. Recent Temperature Variations Southern South America. International Journal of Climatology, 17: 67-85. DOI: 10.1002/(SICI)1097-0088(199701)17:1<67::AID-JOC>3.0.CO;2-G

Salas, J.D., B. Rajagopalan, L. Saito and C. Brown, 2012. Special Section on Climate Change and Water Resources: Climate Nonstationarity and Water Resources Managemente. Journal of Water Resources Planning and Management, 138: 385-388. DOI: 10.1061/(ASCE)WR.1943-5452.0000279

Salas, J.D. and J. Obeysekera, 2013. Revisiting the Concepts of Return Period and Risk for Nonstationary Hydrologic Extreme Events. Journal of Hydrologic Engineering, 19(3): 554-568. DOI: 10.1061/(ASCE)HE.1943-5584.0000820

Samadi, S., G.J. Carbone, M. Mahdavi, F. Sharifi and M.R. Bihamta, 2013. Statistical Downscaling of River Runoff in a Semi-Arid Catchment. Water Resources Management, 27(1): 117-136. DOI: 10.1007/s11269-0170-6

Schaefli, B., B. Hingray and A. Musy, 2007. Climate Change and Hydropower Production in the Swiss Alps: Quantification of Potential Impacts and Related Modelling Uncertainties. Hydrology and Earth System Sciences Discussions, 11(3): 1191-1205.

Schlef, K.E., S. Steinschneider, and C.M. Brown, 2017. Spatiotemporal Impacts of Climate and Demand on Water Supply in the Apalachicola-Chattahoochee-Flint Basin. Journal of Water Resources Planning Management, 144(2): 05017020. DOI: 10.1061/(ASCE)WR.1943-5452.0000865

Serinaldi, F. and C.G. Kilsby, 2015. Stationarity is Undead: Uncertainty Dominates the Distribution of Extremes. Advances in Water Resources, 77: 17-36. DOI: 10.1016/j.advwaters.2014.12.013

Sharma, D., A.D. Gupta, and M.S. Babel, 2007. Spatial Disaggregation of Bias-Corrected GCM Precipitation for Improved Hydrologic Simulation: Ping River Basin, Thailand. Hydrology and Earth System Sciences, 11(4): 1373-1390. DOI: 10.5194/hess-11-1373-2007

Shi, H., J. Chen, K. Wang, and J. Niu, 2018. A New Method and a New Index for Identifying Socioeconomic Drought Events Under Climate Change: A Case

Study of the East River Basin in China. Science of the Total Environment, 616-617: 363-375. DOI: 10.1016/j.scitotenv.2017.10.321

Shiau, J.T., 2009. Optimization of Reservoir Hedging Rules Using Multiobjective Genetic Algorithm. Journal of Water Resources Planning and Management 135(5): 355-363. DOI: 10.1061/(ASCE)0733-9496(2009)135:5(355)

Shiau, J.T., 2011. Analytical Optimal Hedging With Explicit Incorporation of Reservoir Release and Carryover Storage Targets. Water Resources Research 47(1). DOI: 10.1029/2010WR009166

Shih, J.S. and C. ReVelle, 1994 Water-Supply Operations during Drought: Continuous Hedging Rule. Journal of Water Resources Planning and Management 120: 613-629. DOI: 10.1061/(ASCE)0733-9496(1994)120:5(613)

Shih, J.S. and C. ReVelle, 1995 Water-Supply Operations during Drought: A Discrete Hedging Rule. European Journal of Operational Research, 82: 163-175. DOI: 10.1016/0377-2217(93)E0237-R

Shortridge, J., T. Aven and S. Guikema, 2017. Risk Assessment Under Deep Uncertainty: A Methodological Comparison. Reliability Engineering & System Safety, 159: 12-23. DOI: 10.1016/j.ress.2016.10.017

Simonovic, S.P. and M.A. Marino, 1982. Reliability Programing in Reservoir Management 3. System of Multipurpose Reservoir. Water Resources Research, 18(4): 735-743. DOI: 10.1029/WR018i004p00735

Sinha, A., B.V. Rao and C.H. Bischof, 1999. Nonlinear Optimization Model for Screening Multipurpose Reservoir Systems. Journal of Water Resources Planning and Management, 125: 299-233. DOI: 10.1061/(ASCE)0733-9496(1999)125:4(229)

Smitha, P.S., B. Narasimhan, K.P. Sudheer, H. Annamalai, 2018. An Improved Bias Correction Method of Daily Rainfall Data Using a Sliding Window Technique for Climate Change Impact Assessment. Journal of Hydrology, 556: 100-118. DOI: 10.1016/j.jhydrol.2017.11.010

Soundharajan, B.S., A.J. Adeloye and R. Remsan, 2016. Evaluating the Variability in Surface Water Reservoir Planning Characteristics During Climate Change Impact Assessment. Journal of Hydrology, 538: 625-639. DOI: 10.1016/j.jhydrol.2016.04.051

Srinivasan, K. and M.C. Philipose, 1996. Evaluation and Selection of Hedging Policies Using Stochastic Reservoir Simulation. Water Resources Management 10(3): 163-188. DOI: 10.1007/BF00424201

Srinivasan, K. and M.C. Philipose, 1998. Effect of Hedging on Over-Year Reservoir Performance. Water Resources Management, 12(2): 95-120. DOI: 10.1023/A:1007936115706

Stedinger, J.R., B.F. Sule and D.P. Lockus, 1984. Stochastic Dynamic Programming Models for Reservoir Operation Optimization. Water Resources Research, 20(11): 1499-1505. DOI: 10.1029/WR020i011p01499

Stedinger, J.R. and V.W. Griffis, 2011. Getting From Here to Where? Flood Frequency Analysis and Climate. Journal of the American Water Resources Association, 47(3): 506-513. DOI: 10.1111/j.1752-1688.2011.00545.x

Steinschneider, S. and C. Brown, 2012. Dynamic Reservoir Management with Real-Option Risk Hedging as a Robust Adaptation to Nonstationary Climate. Water Resources Research, 48(5). DOI: 10.1029/2011WR011540

Steinschneider, S., R. McCrary, S. Wi, K. Mulligan, L.O. Mearns, and C. Brown, 2015a. Expanded Decision-Scaling Framework to Select Robust Long-Term Water-System Plans Under Hydroclimatic Uncertainties. Journal of Water Resources Planning Management, 141(11): 04015023. DOI: 10.1061/(ASCE)WR.1943-5452.0000536

Steinschneider, S., S. Wi, and C. Brown, 2015b. The Integrated Effects of Climate and Hydrologic Uncertainty on Future Flood Risk Assessments. Hydrological Processes 29(12): 2823-2839. DOI: 10.1002/hyp.10409

Sui, Y., X. Lang and D. Jiang, 2014. Time of Emergence of Climate Signals Over Chine Under RCP4.5 Scenario. Climate Change, 125(2): 265-276. DOI: 10.1007/s10584-014-1151-y

Sun, F., M.L. Roderick, W.H. Lim and G.D. Farquhar, 2011. Hydroclimatic Projections for the Murray-Darling Based on an Ensemble Derived From Intergovernmental Panel on Climate Change AR4 Climate Models. Water Resources Research, 47(12). DOI: 10.1029/2010WR009829

Taylor, K.E., R.J. Stouffer and G.A. Meehl, 2012. An Overview of CMIP5 and the Experiment Design. Bulletin of the American Meteorological Society, 93(4): 485-498. DOI: 10.1175/BAMS-D-11-00094.1

Teng, J., J. Vaze, F.H. Chiew, B. Wang and J.M. Perraud, 2012. Estimating the Relative Uncertainties Sourced From GCMs and Hydrological Models in Modeling Climate Change Impact on Runoff. Journal of Hydrometeorology, 13(1): 122-139. DOI: 10.1175/JHM-D-11-058.1

Teutschbein, C. and J. Seibert, 2010. Regional Climate Models for Hydrological Impact Studies at the Catchment Scale: A Review of Recent Modeling

Strategies. Geography Compass, 4(7): 834-860. DOI: 10.1111/j.1749-8198.2010.00357.x

Thober, S., J. Mai., and M Zink, 2014. Stochastic Temporal Disaggregation of Monthly Precipitation for Regional Gridded Data Sets. Water Resources Research, 50(11): 8714-8735. DOI: 10.1002/2014WR015930

Trenberth, K.E., 1990. Recent Observed Interdecadal Climate Change in the Northern Hemisphere. Bulleting of the American Meteorigical Society, 71(7): 988-993. DOI: 10.1175/1520-0477(1990)071<0988:ROICCI>2.0.CO;2

Trenberth, K.E. and D.P. Stepaniak, 2001. Indices of el Niño Evolution. Journal of Climate, 14(8): 1697-1701. DOI: 10.1175/1520-0442(2001)014<1697:LIOENO>2.0.CO;2

University of Washington, 2015. Time of Emergence of Climate Change Signals in the Puget Sound Basin Project. Report Prepared for the US EPA Seattle WA by Amy Snover and Eric Salathé.

VanRheenen, N.T., A.W. Wood, R.N. Palmer and D.P. Lettermaier, 2004. Potential Implications of PCM Climate Change Scenario for Sacramento-San Joaquin River Basin Hydrology and Water Resources. Climate Change, 62(1-3): 189-216. DOI: 10.1023/B:CLIM.0000013686.97342.55

Vicuña, S. and J.A. Dracup, 2007. The Evolution of Climate Change Impact Studies on Hydrology and Water Resources in California. Climatic Change, 82(3-4): 327-350. DOI: 10.1007/s10584-006-9207-2

Vicuña, S., J.A. Dracup, J.R. Lund, L.L. Dale, and E.P. Maurer, 2010. Basin-scale Water System Operations with Uncertain Future Climate Conditions:

Methodology and Case Studies. Water Resources Research, 46(4). DOI: 10.1029/2009WR007838

Vicuña, S., R.D. Garreaud and J. McPhee, 2011. Climate Change Impacts on the Hydrology of a Snowmelt Driven Basin in Semiarid Chile. Climate Change, 105: 469-488. DOI:10.1007/s10584-011-0301-8

Vicuña, S., J. McPhee and R.D. Garreaud, 2012. Agriculture Vulnerability to Climate Change in a Snowmelt-Driven Basin in Semiarid Chile. Journal of Water Resources Planning and Management, 138: 431-441. DOI: 10.1061/(ASCE)WR.1943-5452.0000202

Vogel, R.M., C. Yaindl and M. Walter, 2011. Nonstationarity: Flood Magnification and Recurrence Reduction Factors in the United States. Journal of the American Water Resources Association, 47(3): 464-474. DOI: 10.1111/j.1752-1688.2011.00541.x

Walton, D.B., A. Hall, N. Berg, M. Schwartz, and F. Sun, 2017. Incorporating Snow Albedo Feedback into Downscaled Temperature and Snow Cover Projections for California's Sierra Nevada. Journal of Climate, 30: 1417-1438. DOI: 10.1175/JCLI-D-16-0168.1

Whateley, S., and C. Brown, 2016. Assessing the Relative Effects of Emissions, Climate Means, and Variability on Large Water Supply Systems. Geophysical Research Letters. 43(21). DOI: 10.1002/2016GL070241

Whetton, P., K. Hennessy, J. Clarke, K. Mclnnes and D. Kent, 2012. Use of Representative Climate Futures in Impact and Adaptation Assessment. Climatic Change, 115(3-4): 433-442. DOI: 10.1007/s10584-012-0471-z

Wilby, R.L. and S. Dessai, 2010. Robust Adaptation to Climate Change. Weather, 65(7), 180-185. DOI: 10.1002/wea.543

Wood, A.W., E.P. Maurer, A. Kumar and D.P. Lettenmaier, 2002. Long-Range Experimental Hydrological Forecasting for the Eastern United States. Journal of Geophysical Research: Atmospheres, 107 (D20). DOI: 10.1029/2001JD000659

Wood, A.W., L.R. Leung, V. Sridhar and D.P. Lettenmaier, 2004. Hydrological Implications of Dynamical and Statistical Approaches to Downscaling Climate Model Outputs. Climate Change, 62(1-3): 189-216. DOI: 10.1023/B:CLIM.0000013685.99609.9e

Yates, D., S. Gangopadhyay, B. Rajagopalan and K. Strzepek, 2003. A Technique for Generating Regional Climate Scenario Using Nearest-Neighbor Algorithm. Water Resources Research, 39(7). DOI: 10.1029/2002WR0017769

Yates, D., J. Sieber, D. Purkey and A. Huber-Lee, 2005a. WEAP21-A Demand-, Priority-, and Preference-Driven Water Planning Model: Part 1: Model Characteristics. Water International, 30(4): 487-500. DOI: 10.1080/02508060508691893

Yates, D., D. Purkey, J. Sieber, A. Huber-Lee and H. Galbraith, 2005b. WEAP21-A Demand-, Priority-, and Preference-Driven Water Planning Model: Part 2: Aiding Freshwater Ecosystem Service Evaluation. Water International 30(4): 501-512. DOI: 10.1080/0250806508691894

Yoo, J., 2009. Maximization of Hydropower Generation through the Application of a Linear Programming Model. Journal of Hydrology, 376: 182-187. DOI: 10.1016/j.jhydrol.2009.07.026

Yung, B.B., B.A. Tolson and D.H. Burn, 2011. Risk Assessment of a Water Supply System under Climate Variability: a Stochastic Approach, Canadian Journal of Civil Engineering, 38(3): 252-262. DOI: 10.1139/L10-132

Zhang, C., B. Xu, Y. Li, and G. Fu, 2017. Exploring the Relationships among Reliability, Resilience, and Vulnerability of Wager Supply Using Many-Objective Analysis. Journal of Water Resources Planning Management, 143(8): 04017044. DOI: 10.1061/(ASCE)WR.1943-5452-0000787

APPENDIX A: PERCENTAGE OF CHANGE OF THE RAW GCM

GCMs used in the study and the corresponding Percentage of Change (*PC*) of precipitation for different RCPs without downscaling.

Table A1: GCM list and their precipitation change percentage.

Number	GCM	Realization	RCP 2.6	RCP 4.5	RCP 6.0	RCP 8.5
1	ACCESS1.0	r1i1p1	Na	-0.07	Na	-0.05
2	BCC-CSM1.1	r1i1p1	-0.01	-0.08	-0.07	-0.11
3.1	CanESM2	r1i1p1	-0.11	-0.17	Na	-0.22
3.2	CanESM2	r2i1p1	-0.14	-0.16	Na	-0.13
3.3	CanESM2	r3i1p1	-0.20	-0.26	Na	-0.22
3.4	CanESM2	r4i1p1	-0.02	-0.02	Na	-0.03
3.5	CanESM2	r5i1p1	0.03	-0.04	Na	-0.08
4.1	CCSM4	r1i1p1	-0.04	-0.07	-0.04	-0.08
4.2	CCSM4	r2i1p1	0.05	0.02	0.13	-0.06
4.3	CCSM4	r3i1p1	0.00	0.03	-0.01	-0.04
4.4	CCSM4	r4i1p1	-0.02	0.03	-0.02	-0.02
4.5	CCSM4	r5i1p1	0.01	0.05	0.01	-0.05
5.1	CNRM-CM5	r10i1p1	Na	Na	Na	-0.03
5.2	CNRM-CM5	r1i1p1	Na	-0.04	Na	-0.02
5.3	CNRM-CM5	r2i1p1	Na	Na	Na	-0.01
5.4	CNRM-CM5	r4i1p1	Na	Na	Na	-0.03
5.5	CNRM-CM5	r6i1p1	Na	Na	Na	-0.08
6.1	CSIRO-Mk3.6.0	r10i1p1	-0.15	-0.21	-0.24	-0.35
6.2	CSIRO-Mk3.6.0	r1i1p1	0.02	0.02	-0.02	-0.09
6.3	CSIRO-Mk3.6.0	r2i1p1	-0.22	-0.38	-0.33	-0.33
6.4	CSIRO-Mk3.6.0	r3i1p1	-0.14	-0.15	-0.10	-0.29
6.5	CSIRO-Mk3.6.0	r4i1p1	-0.15	-0.18	-0.21	-0.30
6.6	CSIRO-Mk3.6.0	r5i1p1	-0.17	Na	-0.29	-0.24
6.7	CSIRO-Mk3.6.0	r6i1p1	-0.05	-0.03	-0.08	-0.23
6.8	CSIRO-Mk3.6.0	r7i1p1	-0.24	-0.29	-0.25	-0.37
6.9	CSIRO-Mk3.6.0	r8i1p1	-0.10	-0.32	-0.31	-0.35
6.10	CSIRO-Mk3.6.0	r9i1p1	-0.16	-0.23	-0.24	-0.30
7	FGOALS-g2	r1i1p1	-0.06	-0.08	Na	-0.19
8	GFDL-CM3	r1i1p1	-0.17	-0.23	-0.21	-0.22
9	GFDL-ESM2G	r1i1p1	-0.19	-0.30	-0.28	-0.37
10	GFDL-ESM2M	r1i1p1	-0.14	-0.24	-0.29	-0.34
11.1	GISS-E2-R	r1i1p1	0.06	0.05	0.10	0.10
11.2	GISS-E2-R	r2i1p1	Na	0.06	Na	Na
11.3	GISS-E2-R	r3i1p1	Na	0.11	Na	Na
11.4	GISS-E2-R	r4i1p1	Na	0.07	Na	Na
11.5	GISS-E2-R	r5i1p1	Na	0.16	Na	Na
12	INM-CM4	r1i1p1	Na	0.04	Na	0.02

Table A1: (Continued)

Number	GCM	Realization	RCP 2.6	RCP 4.5	RCP 6.0	RCP 8.5
13.1	IPSL-CM5A-LR	r1i1p1	Na	-0.24	-0.23	-0.32
13.2	IPSL-CM5A-LR	r2i1p1	Na	-0.24	Na	-0.37
13.3	IPSL-CM5A-LR	r3i1p1	Na	-0.27	Na	-0.38
14	IPSL-CM5A-MR	r1i1p1	-0.26	-0.30	Na	-0.39
15	MIROC5	r1i1p1	-0.07	-0.16	-0.11	-0.18
16	MIROC-ESM	r1i1p1	-0.21	-0.29	-0.27	-0.38
17	MIROC-ESM-CHEM	r1i1p1	-0.19	-0.21	-0.23	-0.32
18.1	MPI-ESM-LR	r1i1p1	-0.04	-0.21	Na	-0.28
18.2	MPI-ESM-LR	r2i1p1	-0.01	-0.19	Na	-0.25
18.3	MPI-ESM-LR	r3i1p1	-0.14	-0.14	Na	-0.30
19	MRI-CGCM3	r1i1p1	-0.02	0.00	Na	-0.05
20	NorESM1-M	r1i1p1	-0.08	-0.08	-0.04	-0.09

Note: Na corresponds to GCM and RCP combinations that were not available or not used for this study.

APPENDIX B: GENERATION OF CORRELATED DATA

To preserve the spatial correlation and the correlation between temperature and precipitation, we use the correlation matrix of the historical annual data to generate correlated uniform random numbers u [0-1]. Using $y = {F_Y}^{-1}(u, \theta)$ we obtain random values of temperature and precipitation in each station that preserve the observed correlation. Random uniform numbers are produced using a Vector Autoregressive Model VAR(0), although a VAR(1) model can also be used in case temporal correlation were to be considered. Indeed a VAR(1) model was tested in the application here reported, but results are not presented as autocorrelation is not statistically significant for annual observed data. In the implementation of the VAR(0) model correlated random numbers following a standardized normal distribution are first generated (step 1), and subsequently transformed into uniformly distributed correlated values, using the correlation matrix for space transformation described by Hotelling and Pabst (1936) (step 2). In particular, in step 1 we apply the Cholesky factorization of the correlation matrix in the normal space to transform uncorrelated to correlated normally distributed random values. In step 2 the inverse normal distribution transforms these numbers into uniform correlated values.

Table B1: Meteorological stations in the Limarí basin measuring Precipitation (P) and Temperature (T).

Station	Variable	Elevation (m)	Latitude	Longitude
Pabellón	P	1,920	30º 24' 12" S	70º 33' 08" W
Las Ramadas	P, T	1,380	31º 01' 11" S	70º 35' 11" W
Tascadero	P	1,230	31º 00' 58" S	70º 40' 28" W
Cogotí 18	P	840	31º 05' 12" S	70º 57' 08" W
Recoleta Embalse	P	350	30º 30' 36" S	71º 06' 07" W
Paloma Embalse	P, T	320	30º 41' 48" S	71º 02' 18" W
El Tomé	P	420	30º 49' 12" S	70º 58' 08" W
Punitaqui	P	280	30º 49' 35" S	71º 15' 37" W
Ovalle DGA	P	220	30º 36' 12" S	71º 12' 08" W

Table B2: Comparison between observed (Obs) and simulated annual statistics using the annual climate generator (Gen) for precipitation (P) and temperature (T) gauges in the Limarí basin.

	Pabellon	Las Ramadas	Tascadero	Cogotí 18	Recoleta Embalse	Paloma Embalse	El Tomé	Punitaqui	Ovalle DGA	Las Ramadas	Paloma Embalse
Variable	P (mm)	P (mm)	P (mm)	P (mm)	P (mm)	P (mm)	P (mm)	P (mm)	P (mm)	T(°C)	T(°C).
Mean (Gen)	162.5	340.9	299.8	192.7	110.4	139.3	173.3	170.5	110.4	16.25	17.22
Mean (Obs)	163.0	341.5	300.4	192.6	110.1	139.1	173.2	170.3	109.8	16.25	17.22
Std. Dev. (Gen)	103.5	208.9	202.2	132.9	81.3	100.9	124.0	134.8	78.7	0.55	0.34
Std. Dev. (Obs)	104.4	209.8	203.5	133.0	80.9	100.7	123.9	134.6	78.0	0.54	0.34
A. Corr*. (Gen)	0.94	1.00	0.98	0.92	0.89	0.92	0.94	0.92	0.88	-0.42	0.32
A. Corr*. (Obs)	0.94	1.00	0.98	0.93	0.89	0.92	0.94	0.92	0.88	-0.43	0.33

* Annual correlation (A. Corr.) is computed between annual precipitation in Las Ramadas gauge and the rest of the rain gauges and temperature measurements in the basin

To verify the method, we tested it in replicating stationary annual climate of nine precipitation stations and two temperature stations located in the Limarí basin (Table B1). We generated 10,000 years of stationary annual precipitation and temperature correlated data from the stations listed in Table B1, to obtain the results presented in Table B2. As shown in Table B2, the proposed method successfully replicates the mean, standard deviation and correlation among precipitation and temperature in the different stations.

APPENDIX C: GENERAL CIRCULATION MODELS USED IN CHAPTER 3

Table C1: General Circulation Models (GCMs) used in this study.

Number	GCM Name	GCM Realization
1	ACCESS1.0	r1i1p1
2	BCC-CSM1.1	r1i1p1
3	CanESM2	r1i1p1
4	CanESM2	r2i1p1
5	CanESM2	r3i1p1
6	CanESM2	r4i1p1
7	CanESM2	r5i1p1
8	CCSM4	r1i1p1
9	CCSM4	r2i1p1
10	CCSM4	r3i1p1
11	CCSM4	r4i1p1
12	CCSM4	r5i1p1
13	CNRM-CM5	r10i1p1
14	CNRM-CM5	r1i1p1
15	CNRM-CM5	r2i1p1
16	CNRM-CM5	r4i1p1
17	CNRM-CM5	r6i1p1
18	CSIRO-Mk3.6.0	r10i1p1
19	CSIRO-Mk3.6.0	r1i1p1
20	CSIRO-Mk3.6.0	r2i1p1
21	CSIRO-Mk3.6.0	r3i1p1
22	CSIRO-Mk3.6.0	r4i1p1

Number	GCM Name	GCM Realization
23	CSIRO-Mk3.6.0	r5i1p1
24	CSIRO-Mk3.6.0	r6i1p1
25	CSIRO-Mk3.6.0	r7i1p1
26	CSIRO-Mk3.6.0	r8i1p1
27	CSIRO-Mk3.6.0	r9i1p1
28	FGOALS-g2	r1i1p1
29	GFDL-CM3	r1i1p1
30	GFDL-ESM2G	r1i1p1
31	GFDL-ESM2M	r1i1p1
32	GISS-E2-R	r1i1p1
33	INM-CM4	r1i1p1
34	IPSL-CM5A-LR	r1i1p1
35	IPSL-CM5A-LR	r2i1p1
36	IPSL-CM5A-LR	r3i1p1
37	IPSL-CM5A-MR	r1i1p1
38	MIROC5	r1i1p1
39	MIROC-ESM	r1i1p1
40	MIROC-ESM-CHEM	r1i1p1
41	MPI-ESM-LR	r1i1p1
42	MPI-ESM-LR	r2i1p1
43	MPI-ESM-LR	r3i1p1
44	MRI-CGCM3	r1i1p1
45	NorESM1-M	r1i1p1

APPENDIX D: GENERAL CIRCULATION MODELS USED IN CHAPTER 4 AND 5

Table D1: General Circulation Models (GCM) and RCP scenarios used in this study.

	GCM Name	Realization	RCP 2.6	RCP 4.5	RCP 6.0	RCP 8.5
1	ACCESS1.0	r1i1p1		x		x
2	BCC-CSM1.1	r1i1p1	x	x	x	x
3	CanESM2	r1i1p1	x	x		x
4	CanESM2	r2i1p1	x	x		x
5	CanESM2	r3i1p1	x	x		x
6	CanESM2	r4i1p1	x	x		x
7	CanESM2	r5i1p1	x	x		x
8	CCSM4	r1i1p1	x	x	x	x
9	CCSM4	r2i1p1	x	x	x	x
10	CCSM4	r3i1p1	x	x	x	x
11	CCSM4	r4i1p1	x	x	x	x
12	CCSM4	r5i1p1	x	x	x	x
13	CNRM-CM5	r10i1p1				x
14	CNRM-CM5	r1i1p1		x		x
15	CNRM-CM5	r2i1p1				x
16	CNRM-CM5	r4i1p1				x
17	CNRM-CM5	r6i1p1				x
18	CSIRO-Mk3.6.0	r10i1p1	x	x	x	x
19	CSIRO-Mk3.6.0	r1i1p1	x	x	x	x
20	CSIRO-Mk3.6.0	r2i1p1	x	x	x	x
21	CSIRO-Mk3.6.0	r3i1p1	x	x	x	x
22	CSIRO-Mk3.6.0	r4i1p1	x	x	x	x
23	CSIRO-Mk3.6.0	r5i1p1	x		x	x
24	CSIRO-Mk3.6.0	r6i1p1	x	x	x	x
25	CSIRO-Mk3.6.0	r7i1p1	x	x	x	x
26	CSIRO-Mk3.6.0	r8i1p1	x	x	x	x
27	CSIRO-Mk3.6.0	r9i1p1	x	x	x	x
28	FGOALS-g2	r1i1p1	x	x		x
29	GFDL-CM3	r1i1p1	x	x	x	x
30	GFDL-ESM2G	r1i1p1	x	x	x	x
31	GFDL-ESM2M	r1i1p1	x	x	x	x
32	GISS-E2-R	r1i1p1	x	x	x	x
33	GISS-E2-R	r2i1p1		x		
34	GISS-E2-R	r3i1p1		x		
35	GISS-E2-R	r4i1p1		x		

Table D1: (Continued)

	GCM Name	Realization	RCP 2.6	RCP 4.5	RCP 6.0	RCP 8.5
36	GISS-E2-R	r5i1p1		x		
37	INM-CM4	r1i1p1		x		x
38	IPSL-CM5A-LR	r1i1p1		x	x	x
39	IPSL-CM5A-LR	r2i1p1		x		x
40	IPSL-CM5A-LR	r3i1p1		x		x
41	IPSL-CM5A-MR	r1i1p1	x	x		x
42	MIROC5	r1i1p1	x	x	x	x
43	MIROC-ESM	r1i1p1	x	x	x	x
44	MIROC-ESM-CHEM	r1i1p1	x	x	x	x
45	MPI-ESM-LR	r1i1p1	x	x		x
46	MPI-ESM-LR	r2i1p1	x	x		x
47	MPI-ESM-LR	r3i1p1	x	x		x
48	MRI-CGCM3	r1i1p1	x	x		x
49	NorESM1-M	r1i1p1	x	x	x	x